

**ANALYSIS OF DAIMLER-CHRYSLER / EUROPEAN
RADIATED EMISSIONS TESTING SETUP FOR
MODULES**

By

Christopher Mark Coleman

A THESIS

Submitted to
Michigan State University
in partial fulfillment of the requirements
for the degree of

MASTER OF SCIENCE

Department of Electrical Engineering

1999

ABSTRACT

ANALYSIS OF DAIMLER-CHRYSLER / EUROPEAN RADIATED EMISSIONS TESTING SETUP FOR MODULES

By

Christopher Mark Coleman

Electromagnetic compatibility testing standards and regulations have become commonplace in industry. In order to ensure that one electronic device does not interfere with the functional behavior of another, governments and other agencies impose regulations on the radiated electromagnetic emissions of electronic devices. In the automotive industry, the Comité International Spécial Des Perturbations Radioélectriques (CISPR) organization regulates the allowable radiated emissions from an electronic module to be used in automobiles sold in Europe. A specific testing setup is required by CISPR to perform the regulatory measurements. This thesis presents a numerical model of the testing setup that can be used to predict the effects of altering the testing setup on the measurements of a module's radiated emissions. The numerical model is compared to an experimental setup constructed at MSU which also models the CISPR measurement setup. This experimental setup will help verify the numerical model's ability to predict the effects of varying certain physical parameters of the testing setup.

Copyright by
Christopher Mark Coleman
1999

For my Parents

ACKNOWLEDGMENTS

I wish to thank fellow graduate student and friend Mike Havrilla for his help and support given during my research. Without him, I would not have been able to perform the measurements and calibration techniques essential to this research. His enthusiasm and unending quest for knowledge are also a constant reminder of my reasons for staying in graduate school.

I wish also to thank Dr. E.J. Rothwell for his friendship and help as a thesis advisor. Dr. D.P. Nyquist also was a great source of ideas and answers throughout my research. I also thank Dr. Leo Kempel for being a part of my thesis committee.

I want to thank Ahmet Kizilay for his help with using \LaTeX and his thesis style files. With his help, countless hours of thesis formatting have been saved.

I am grateful to the National Science Foundation. Their funding made work on this thesis possible.

A special thanks needs to be given to Dave Schilling, Greg Brooks, Ponniah Illivarison, Andrew Xiong, Tom Livernois, Poul Anderson, Norman Welsh, and the other employees at Daimler-Chrysler who dedicated their time to help me with this project.

Most of all, I would like to thank my fiancée Johnna for her support throughout this thesis. She has helped me from crossing the edge of insanity many times in the recent past. Johnna will be happier that this thesis is finally complete than I am.

TABLE OF CONTENTS

LIST OF TABLES	ix
LIST OF FIGURES	x
CHAPTER 1	
Introduction	1
1.1 Overview	1
1.2 NSF GOALI Project	3
1.3 MSU / Daimler-Chrysler Interaction	3
CHAPTER 2	
Project Description	4
2.1 Overview	4
2.2 CISPR EMC Requirements	4
2.3 Daimler-Chrysler’s Testing Setup at Auburn Hills	6
2.4 Goal of Thesis Research	8
CHAPTER 3	
Numerical Modeling	10
3.1 Overview	10
3.2 Numerical Electromagnetics Code (NEC)	10
3.3 Geometry	12
3.4 Procedure	15
3.4.1 Z to S -Parameter Conversion	18
3.5 Typical Numerical Results	20
CHAPTER 4	
Experimental Work	33
4.1 Overview	33
4.2 Description of Experimental Setup	33
4.2.1 Method 1: Transformer Included in the S -Parameter Measurements	37
4.2.2 Method 2: Transformer Calibrated out of the Measurements	37
4.2.3 Method 3: Measurement with No Transformer Balun	39
4.3 Comparison of Experimental Setup to CISPR 25 Requirements and Numerical Model	42

4.4	Typical Experimental Results	43
CHAPTER 5		
	Results and Analysis	53
5.1	Overview	53
5.2	Comparison of Measurement Methods	53
5.2.1	Method 1: Transformer Included in the S -Parameter Measurements	54
5.2.2	Method 2: Transformer Calibrated out of the Measurements	64
5.2.3	Method 3: Measurement with No Transformer Balun	74
5.3	Comparison of Measured Results to Numerical Results	84
5.3.1	Results for a Wire Harness Location of $d = 5$ cm	84
5.3.2	Results for a Wire Harness Location of $d = 15$ cm	93
5.3.3	Results for a Wire Harness Location of $d = 20$ cm	102
5.3.4	Numerical Results for All Wire Positions	111
5.4	Conclusions	118
CHAPTER 6		
	Conclusion	121
APPENDIX A		
	NEC Grid Generator Program	124
A.1	Overview	124
A.2	Explanation of Program	124
A.3	Source Code for <code>cmst1</code>	127
APPENDIX B		
	Additional Fortran Programs	143
B.1	Overview	143
B.2	Z-Parameter Calculation Program	143
B.3	Source Code for <code>zparmake</code>	144
B.4	Z-Parameter to S-Parameter Conversion and Data Processing Program	148
B.5	Source Code for <code>sparconv</code>	150
B.6	Phase Correction Program	158
B.7	Source Code for <code>sphase</code>	159
APPENDIX C		
	NEC Input Code	161
C.1	NEC Input Code	161

BIBLIOGRAPHY 170

LIST OF TABLES

Table 2.1	Lengths labeled in Figure 2.2.	8
-----------	--	---

LIST OF FIGURES

Figure 2.1	Diagram of the CISPR 25 radiated emissions module testing setup.	6
Figure 2.2	Diagram of Testing Setup at CTC.	9
Figure 3.1	Diagram of system modeled in NEC.	13
Figure 3.2	Diagram of table sections.	14
Figure 3.3	Terminal plane definitions and locations of V_n and I_n for a linear two port network.	15
Figure 3.4	Terminal plane definitions and locations of a_n and b_n for a linear two port network.	19
Figure 3.5	Magnitude of S_{11} ($d = 10$ cm) found using NEC.	23
Figure 3.6	Phase of S_{11} ($d = 10$ cm) found using NEC.	24
Figure 3.7	Magnitude of S_{21} (or S_{12}) ($d = 10$ cm) found using NEC.	25
Figure 3.8	Phase of S_{21} (or S_{12}) ($d = 10$ cm) found using NEC.	26
Figure 3.9	Magnitude of S_{22} ($d = 10$ cm) found using NEC.	27
Figure 3.10	Phase of S_{22} ($d = 10$ cm) found using NEC.	28
Figure 3.11	Magnitude of S_{11} for an isolated table-wire harness antenna and the table-antenna system.	29
Figure 3.12	Phase of S_{11} for an isolated table-wire harness antenna and the table-antenna system.	30
Figure 3.13	Magnitude of S_{22} for an isolated dipole and the table-antenna system.	31
Figure 3.14	Phase of S_{22} for an isolated dipole and the table-antenna system.	32
Figure 4.1	Diagram of experimental setup at Michigan State University.	34
Figure 4.2	Diagram of cable and adaptor arrangement for measurement method 1.	38
Figure 4.3	Diagram of cable and adaptor arrangement for measurement method 2.	40
Figure 4.4	Diagram of cable and adaptor arrangement for measurement method 3.	41
Figure 4.5	Measured magnitude of S_{11} ($d = 10$ cm).	45
Figure 4.6	Measured phase of S_{11} ($d = 10$ cm).	46
Figure 4.7	Measured magnitude of S_{21} (in dB) ($d = 10$ cm).	47
Figure 4.8	Measured phase of S_{21} ($d = 10$ cm).	48
Figure 4.9	Measured magnitude of S_{12} (in dB) ($d = 10$ cm).	49

Figure 4.10	Measured phase of S_{12} ($d = 10$ cm).	50
Figure 4.11	Measured magnitude of S_{22} ($d = 10$ cm).	51
Figure 4.12	Measured phase of S_{22} ($d = 10$ cm).	52
Figure 5.1	Magnitude of S_{11} ($d = 10$ cm) using method 1.	56
Figure 5.2	Phase of S_{11} ($d = 10$ cm) using method 1.	57
Figure 5.3	Magnitude of S_{21} (in dB) ($d = 10$ cm) using method 1.	58
Figure 5.4	Phase of S_{21} ($d = 10$ cm) using method 1.	59
Figure 5.5	Magnitude of S_{12} (in dB) ($d = 10$ cm) using method 1.	60
Figure 5.6	Phase of S_{12} ($d = 10$ cm) using method 1.	61
Figure 5.7	Magnitude of S_{22} ($d = 10$ cm) using method 1.	62
Figure 5.8	Phase of S_{22} ($d = 10$ cm) using method 1.	63
Figure 5.9	Magnitude of S_{11} ($d = 10$ cm) using method 2.	66
Figure 5.10	Phase of S_{11} ($d = 10$ cm) using method 2.	67
Figure 5.11	Magnitude of S_{21} (in dB) ($d = 10$ cm) using method 2.	68
Figure 5.12	Phase of S_{21} ($d = 10$ cm) using method 2.	69
Figure 5.13	Magnitude of S_{12} (in dB) ($d = 10$ cm) using method 2.	70
Figure 5.14	Phase of S_{12} ($d = 10$ cm) using method 2.	71
Figure 5.15	Magnitude of S_{22} ($d = 10$ cm) using method 2.	72
Figure 5.16	Phase of S_{22} ($d = 10$ cm) using method 2.	73
Figure 5.17	Magnitude of S_{11} ($d = 10$ cm) using method 3.	76
Figure 5.18	Phase of S_{11} ($d = 10$ cm) using method 3.	77
Figure 5.19	Magnitude of S_{21} (in dB) ($d = 10$ cm) using method 3.	78
Figure 5.20	Phase of S_{21} ($d = 10$ cm) using method 3.	79
Figure 5.21	Magnitude of S_{12} (in dB) ($d = 10$ cm) using method 3.	80
Figure 5.22	Phase of S_{12} ($d = 10$ cm) using method 3.	81
Figure 5.23	Magnitude of S_{22} ($d = 10$ cm) using method 3.	82
Figure 5.24	Phase of S_{22} ($d = 10$ cm) using method 3.	83
Figure 5.25	Magnitude of S_{11} ($d = 5$ cm) using method 2.	85
Figure 5.26	Phase of S_{11} ($d = 5$ cm) using method 2.	86
Figure 5.27	Magnitude of S_{21} (in dB) ($d = 5$ cm) using method 2.	87
Figure 5.28	Phase of S_{21} ($d = 5$ cm) using method 2.	88
Figure 5.29	Magnitude of S_{12} (in dB) ($d = 5$ cm) using method 2.	89

Figure 5.30	Phase of S_{12} ($d = 5$ cm) using method 2.	90
Figure 5.31	Magnitude of S_{22} ($d = 5$ cm) using method 2.	91
Figure 5.32	Phase of S_{22} ($d = 5$ cm) using method 2.	92
Figure 5.33	Magnitude of S_{11} ($d = 15$ cm) using method 2.	94
Figure 5.34	Phase of S_{11} ($d = 15$ cm) using method 2.	95
Figure 5.35	Magnitude of S_{21} (in dB) ($d = 15$ cm) using method 2.	96
Figure 5.36	Phase of S_{21} ($d = 15$ cm) using method 2.	97
Figure 5.37	Magnitude of S_{12} (in dB) ($d = 15$ cm) using method 2.	98
Figure 5.38	Phase of S_{12} ($d = 15$ cm) using method 2.	99
Figure 5.39	Magnitude of S_{22} ($d = 15$ cm) using method 2.	100
Figure 5.40	Phase of S_{22} ($d = 15$ cm) using method 2.	101
Figure 5.41	Magnitude of S_{11} ($d = 20$ cm) using method 2.	103
Figure 5.42	Phase of S_{11} ($d = 20$ cm) using method 2.	104
Figure 5.43	Magnitude of S_{21} (in dB) ($d = 20$ cm) using method 2.	105
Figure 5.44	Phase of S_{21} ($d = 20$ cm) using method 2.	106
Figure 5.45	Magnitude of S_{12} (in dB) ($d = 20$ cm) using method 2.	107
Figure 5.46	Phase of S_{12} ($d = 20$ cm) using method 2.	108
Figure 5.47	Magnitude of S_{22} ($d = 20$ cm) using method 2.	109
Figure 5.48	Phase of S_{22} ($d = 20$ cm) using method 2.	110
Figure 5.49	Numerical magnitudes of S_{11} for all wire harness positions.	112
Figure 5.50	Numerical phases of S_{11} for all wire harness positions.	113
Figure 5.51	Numerical magnitudes of S_{21} for all wire harness positions.	114
Figure 5.52	Numerical phases of S_{21} for all wire harness positions.	115
Figure 5.53	Numerical magnitudes of S_{22} for all wire harness positions.	116
Figure 5.54	Numerical phases of S_{22} for all wire harness positions.	117

CHAPTER 1

INTRODUCTION

1.1 Overview

Electromagnetic compatibility (EMC) has become an important area of electrical engineering in industry. Testing standards and regulations imposed by governments and other agencies have forced companies to pay close attention to the electromagnetic properties of their products. One of the regulated properties is the radiated electromagnetic energy from an electronic device. Most products sold in the United States must comply with radiated emissions standards set by the Federal Communications Commission (FCC) [1]. Automobiles manufactured in the United States are one group of products that are not regulated by the FCC because of an exemption given by the FCC. However, automobiles manufactured in the United States are subject to regulations from the Comité International Spécial Des Perturbations Radioélectriques (CISPR) organization if they are to be sold in Europe.

In order to comply with the CISPR regulations, the Daimler-Chrysler Corporation has dedicated a semi-anechoic chamber to employ the testing method outlined in the CISPR 25 document describing radiated electromagnetic emissions [2]. The testing setup measures the radiated emissions from an electronic module such as a radio, anti-lock brake system, etc. to be used in an automobile. One of the concerns of Daimler-Chrysler is the possible effect of currents on a wire harness used to control the electronic modules during the test on the measured radiated emissions. This thesis investigates the effect of possible currents on the harness by developing a numerical model of the testing setup and comparing the model to an experimental arrangement built at Michigan State University (MSU) similar to the one specified by the CISPR 25 document.

This thesis is organized as follows. First, a brief explanation of the NSF GOALI project which funded the research for this thesis will be given in Section 1.2 of this chapter. Following that will be a discussion of the MSU / Chrysler interaction formed through this project.

The remainder of this thesis is divided into several chapters. Chapter 2 will give a description of the research project performed for this thesis. This will include an overview of the CISPR organization's EMC requirements found in Section 2.2, a description of Chrysler's CISPR testing facility found in Section 2.3, and an explanation of the research important for Chrysler and others attempting to meet the CISPR requirements. The goal of this research project will then be discussed in 2.4.

Chapter 3 is devoted to the numerical modeling of the CISPR testing arrangement. Section 3.2 will explain how the Numerical Electromagnetics Code (NEC) will be used to model the CISPR setup. Section 3.3 will then explain the exact geometry which was modeled with NEC. Typical numerical results are then given in Section 3.5.

The experimental portion of this research is dealt with in Chapter 4. A description of the experimental setup constructed at MSU is found in Section 4.2. A comparison of the experimental setup to both the numerical model and the CISPR regulation testing setup is given in Section 4.3. Typical experimental results are then given in Section 4.4.

Next, Chapter 5 will give a presentation of all the numerical and experimental results, as well as a comparison of the results. Section 5.2 will compare the results using the three different measurement methods used for the experimental work done for this thesis. Section 5.3 will then compare the remaining measured results with the numerical results. Conclusions drawn from the numerical and measured data will then be presented in Section 5.4.

After the conclusion of the thesis in Chapter 6, the Fortran based NEC grid generating program written for this thesis is included and explained in Appendix A.

Three other Fortran programs were written for this research and are discussed in Appendix B. The NEC input code generated from the grid generating program can be found in Appendix C.

1.2 NSF GOALI Project

The research completed for this thesis project was funded by the National Science Foundation (NSF). The NSF Grant Opportunities for Academic Liaison with Industry (GOALI) program helped fund the development of an electromagnetic compatibility course to be taught at Michigan State University. The program was set up to foster an interaction between industry and academia. The funding enabled graduate research assistants from MSU to help design the EMC course with the advice and expertise from industry by the Daimler-Chrysler Corporation. As well as the course development, the funding allowed some of the graduate students to perform research guided by both Daimler-Chrysler's industry expertise and MSU's academic experience.

1.3 MSU / Daimler-Chrysler Interaction

As discussed in the previous section, funding through the NSF GOALI project fostered an interaction between MSU's Department of Electrical Engineering and the Daimler-Chrysler Corporation. Through this interaction, industry experts from the Electrical / Electronic Systems Compatibility (EESC) group at Daimler-Chrysler identified a research project in the area of electromagnetic compatibility suitable for a thesis. The professors at MSU then guided the research for this thesis to ensure that it fit the academic mold required for a Master of Science thesis. Thus this thesis was influenced both by industry and academia in the hope that it will be both practical and scholarly.

CHAPTER 2

PROJECT DESCRIPTION

2.1 Overview

In the automobile industry, electronic modules such as car radios, anti-lock brake controllers, cruise controllers, trip computers, etc., are tested to determine if they will behave properly in their electromagnetic environment. This is important for the safety of the automobile and its passengers as well as the reputation of the company and the satisfaction of its customers. Electronic modules must not radiate electromagnetic energy above acceptable levels or they might interfere with other electronic devices. Thus, organizations such as CISPR decide what levels of radiation are acceptable and then regulate the allowable radiated emissions from products using specific testing methods. Companies such as Daimler-Chrysler must then test their products to determine if they meet the requirements set by the organizations or government agencies. As briefly discussed in Chapter 1, this thesis investigates CISPR's regulatory testing method itself by developing a numerical model of the testing setup to compare to an experimental setup constructed at MSU.

This chapter will discuss the goal of the research performed for this thesis. First an introduction to the CISPR organization and its requirements will be given in Section 2.2. Then an explanation of the testing setup available for radiated emissions testing at Daimler-Chrysler will be discussed in 2.3. Finally, the goal of this thesis will be discussed in Section 2.4.

2.2 CISPR EMC Requirements

Most automobile modules such as radios, instrument clusters, anti-lock brake systems, etc., are connected to a wire harness that contains power lines and bus or communication lines during normal operation. To operate these modules in the same

functional environment as they are operated in an automobile, these lines must be connected to the module during a test. Electromagnetic energy coupled to these wires has the capability of radiating. The shape and length of the wire harness will directly influence the efficiency of this radiation. The radiated electromagnetic fields from the wire harness might be received by the measurement antenna and interpreted as measured radiated emissions from the module. This would be somewhat misleading, since the origin of the emissions would then lie in the coupling of the energy to the wire harness. Thus the situation is really a conducted emissions problem.

Because the lines leading to the module are necessary for the module's operation, they cannot be removed for a radiated emissions test. Therefore the CISPR 25 document imposes requirements on the location of the module and the wire harness to standardize the measurement setup. A diagram of the CISPR 25 radiated emissions measurement setup is shown in Figure 2.1. The DUT referenced in the figure is the Device Under Test. A module is placed in a specified location on a conducting table. The metallic test bench is located .9 m above the ground plane. The wire harness that controls the module is required to be located 10 cm back from the edge of the table, 5 cm above the table, and to be 1.5 m in length.

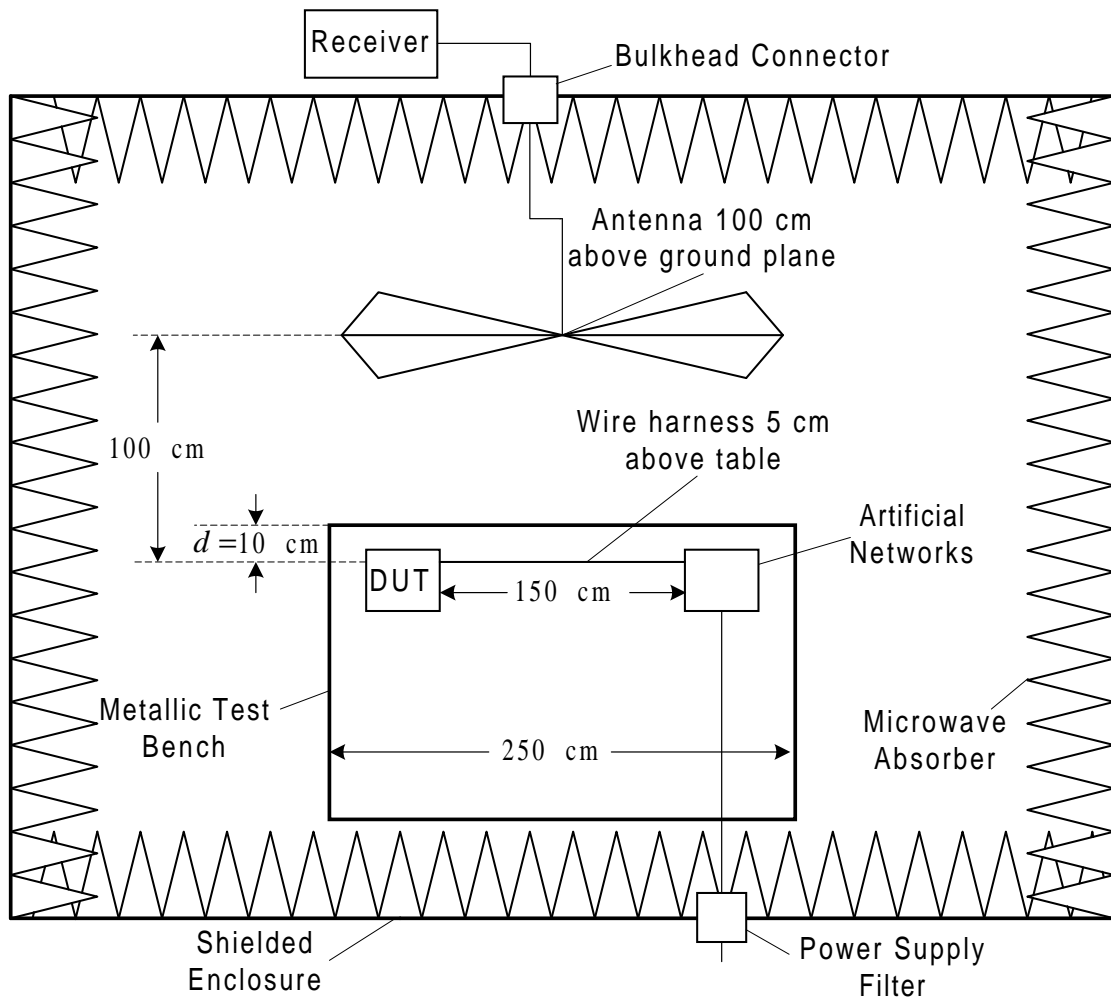


Figure 2.1. Diagram of the CISPR 25 radiated emissions module testing setup.

This measurement setup is required for any laboratory desiring to test electronic modules for compliance to CISPR 25 standards. The next section will discuss a measurement setup found in industry used to test radiated emissions from modules.

2.3 Daimler-Chrysler's Testing Setup at Auburn Hills

At the Daimler-Chrysler Technology Center (CTC) in Auburn Hills, Michigan, a measurement facility was constructed to test the radiated emissions from electronic modules. The measurement room is a semianechoic chamber located inside a shielded enclosure to prevent external electromagnetic interference. This measurement room was

originally constructed to perform measurements self-imposed by the Daimler-Chrysler Corporation, but it is now desired to use the room to perform module tests using the measurement methods outlined in the CISPR 25 documentation. The automobile industry is usually exempted from government regulations concerning electromagnetic compatibility because the automotive self-regulations are usually much stricter than those imposed by governmental regulatory agencies. However, the Daimler-Chrysler Corporation is interested in performing the CISPR 25 test as another self-regulatory testing method.

A diagram of the measurement setup at CTC is shown in Figure 2.2. The conducting table is located .9 m above the ground plane. Notice that the conducting table where the module is placed does not have the exact shape or dimensions specified in the CISPR 25 documentation. Therefore, the Systems Compatibility group at Daimler-Chrysler wishes to understand how small changes in the measurement setup will affect the measured radiated emissions from an electronic module. If the Daimler-Chrysler measurement group had a numerical model which could accurately predict the changes in measured values due to changes in the table size or shape, they could be used when interpreting the measured data. The dimensions labeled in Figure 2.2 are listed in Table 2.1.

Table 2.1. Lengths labeled in Figure 2.2.

Label	Physical dimension (meters)
l_1	7.55
l_2	1.08
l_3	1.74
l_4	1.54
l_5	4.27
l_6	3.04
l_7	1.21
l_8	0.61
l_9	0.61
l_{10}	2.35
l_{11}	2.16
l_{12}	1.20

2.4 Goal of Thesis Research

As discussed in this chapter, it would be valuable to industry to have a numerical model of the CISPR 25 radiated emissions setup to see the effects on the measurements by possible RF currents on the wire harness. This numerical model must be compared to results found by experimental measurements to test its validity. The goals of the research performed for this thesis are to develop a numerical model of the CISPR 25 radiated emissions testing setup which as closely as possible predicts experimental measurements made using a similar setup, and then determine if the numerical model can predict changes due to varying the physical parameters of the system.

A numerical model of the CISPR 25 testing setup was developed using Lawrence Livermore National Laboratory's Numerical Electromagnetics Code (NEC) at MSU. To compliment the numerical work, an experimental arrangement was also constructed in the Electromagnetics Laboratory at MSU. Using a vector network analyzer, measurements were performed to compare to the numerical results. Changes

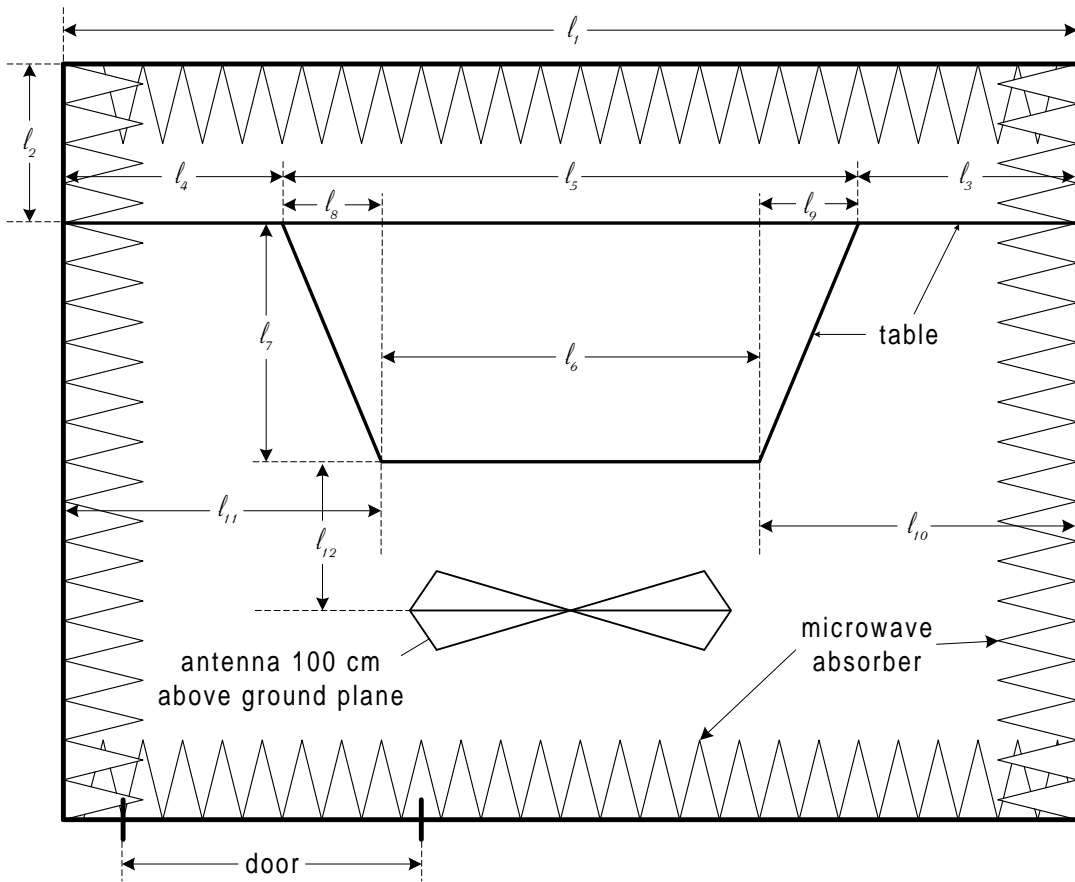


Figure 2.2. Diagram of Testing Setup at CTC.

in the distance of the wire harness to the table edge were made in both the numerical model and the experimental measurements to verify if the numerical model could accurately predict the testing setup.

CHAPTER 3

NUMERICAL MODELING

3.1 Overview

This chapter discusses the numerical modeling performed for this thesis. The goal of the numerical modeling done for this project is to find a property or quantity that can be compared to experimental measurements. As will be discussed in Chapter 4, experimental measurements have been performed with a vector network analyzer. A network analyzer measures the magnitude and phase properties of a two port electronic system and computes and displays the S -parameters of the network [3]. A scheme was developed to compute the Z -parameters of the theoretical table-antenna system using NEC as described in Section 3.4 of this chapter. These theoretical Z -parameters are then converted to S -parameters and will be compared to the measured S -parameters of the system in Chapter 5.

3.2 Numerical Electromagnetics Code (NEC)

The numerical modeling performed for this project was done with the aid of the Numerical Electromagnetics Code (NEC). NEC analyzes electromagnetic systems with a numerical solution of integral equations established from the boundary conditions associated with the electric and magnetic fields. NEC solves the integral equations numerically by the method of moments. NEC has been under development at Lawrence Livermore National Laboratory for over twenty years. Version 4.1 of NEC was used for the numerical modeling done for this project. The two manuals produced by the writers of NEC are the user's manual [4] and the program theory description manual [5].

NEC is able to calculate the currents on thin wire antenna structures due to various source excitations. One of the reasons that NEC was chosen as the numerical tool for

this project is because it can, with sufficient accuracy, model a flat surface such as the CISPR 25 testing table, thin wire antennae such as the dipole receiving antenna and the wire harness antenna, and an infinite ground plane. An infinite ground plane is modeled by modifying the Green's function in the electric field integral equation.

NEC reads geometry, excitation, and frequency information from an input file called `nec.in`. Except for the ground plane, the table and antenna system is modeled as a system of wires, with each wire split into a certain number of wire segments. NEC calculates the current on each of these segments. For accurate numerical results, the segment length needs to be smaller than about $.1\lambda$ at the highest frequency investigated, where λ is the wavelength. The frequency band that will be investigated for this project ranges from 50 MHz to 150 MHz. The geometries created for this project use one segment per wire, so each wire must satisfy this length requirement.

There is no input command in NEC for a thin finite conducting plate such as a metal table. Therefore, a wire mesh grid was created to model the table. To obtain accurate numerical results, the mesh size or the length of each wire must be smaller than about $.1\lambda$ for all frequencies analyzed.

Another requirement for accurate numerical results is imposed on the wire radius. The wire radius a is specified for each wire in NEC. Accurate results require that $2\pi a/\lambda \ll 1$ for all frequencies studied. Also, the wire radius must be much smaller than the length of the wire segment. To satisfy these criteria, a wire radius of 1 millimeter was chosen for all of the wires.

NEC-4 is provided in the form of Fortran source code by Lawrence Livermore National Laboratory. This was very important for this project because the NEC Fortran code had to be modified to create specialized current files to help in the computation of an electrical system's Z and S -parameters. The Digital Visual Fortran Optimizing Compiler (Version 6.0, Update A) was used to compile all of the Fortran programs used in this project, including NEC.

3.3 Geometry

A geometry was created using NEC to model the experimental setup. This was accomplished by using the NEC-input code generator developed for this project. This NEC-input code generator, “`cmst1`,” is described in detail in Appendix A. The NEC-input code generator creates a file named “`nec.in`” that NEC-4 uses to run the method-of-moments solution to the input file.

A diagram of the setup that was modeled in NEC is shown in Figure 3.1. Free space is assumed for the surrounding media. A flat conducting surface 2.44 m long and 1.22 m wide exists .9 m above an infinite ground plane. This table is broken into six sections as shown in Figure 3.2. This is done so that two vertical wires that touch the table can do so at the end of a segment of the table’s wires, regardless of the grid spacing. This is important so that charge can flow freely from the vertical wires on to the table. The two vertical wires are each .05 m long and connected by a 1.5 m long wire that is broken into many segments by the program `cmst1`. Each of the six sections of the table are broken up into a grid of many small wire segments so that the table appears to be a solid ground plane of finite width and length. The wire radiator above the table is placed a distance d back from the table lip and the ends of the wire are placed .5 m from both edges of the table so that the ends are equidistant from the edge of the table, as shown in Figure 3.1.

A dipole receiving antenna is placed 1.0 m away from the lip of the table at a height of 1.0 m above the ground plane. The length of the antenna was chosen such that it will be resonant in the absence of the ground plane, table, and wire radiator at the middle of the frequency band investigated. This frequency is 100 MHz. A half-wave dipole (the antenna’s full length l being a half wavelength) will be approximately resonant when

$$l \approx \frac{\lambda}{2} \tag{3.1}$$

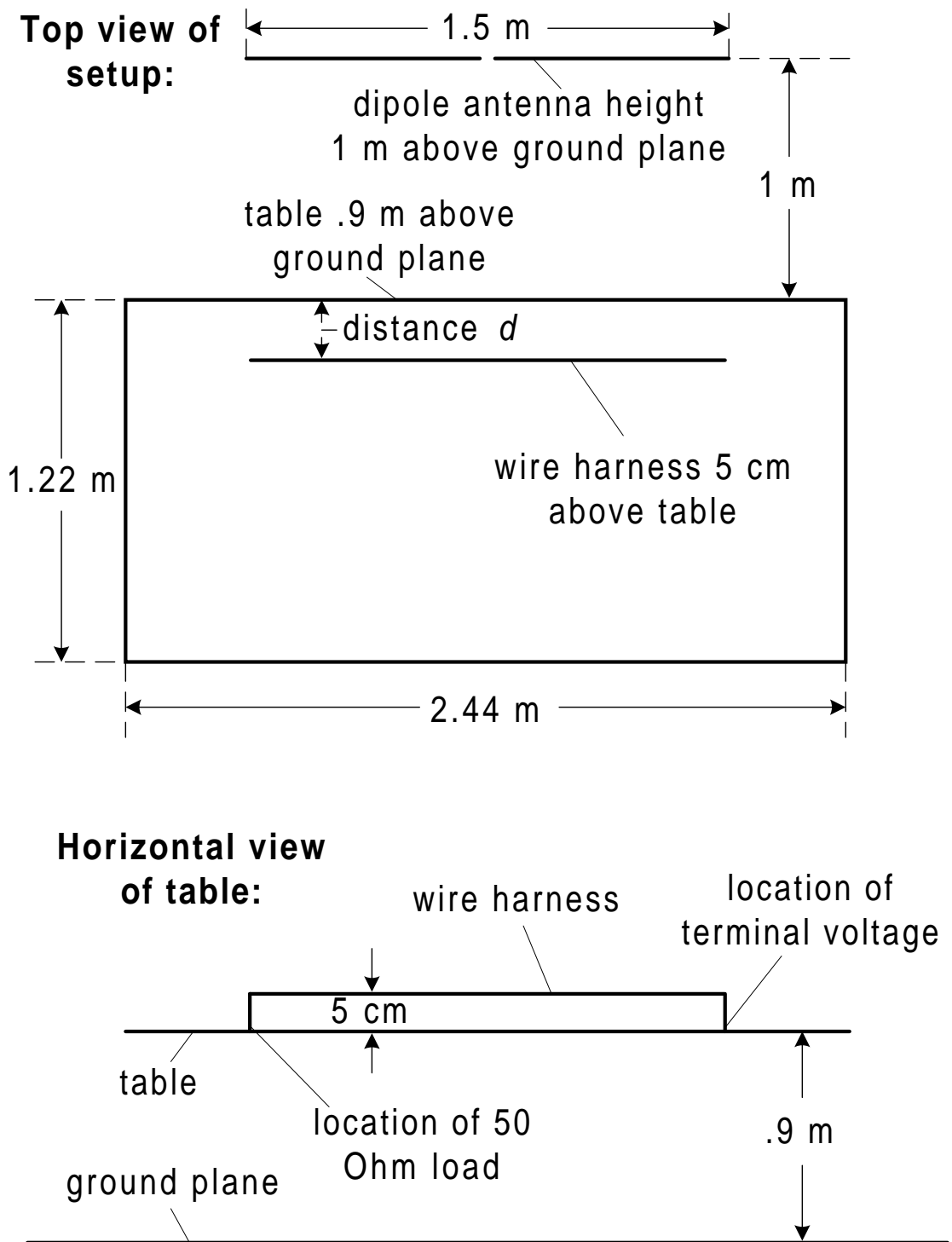


Figure 3.1. Diagram of system modeled in NEC.

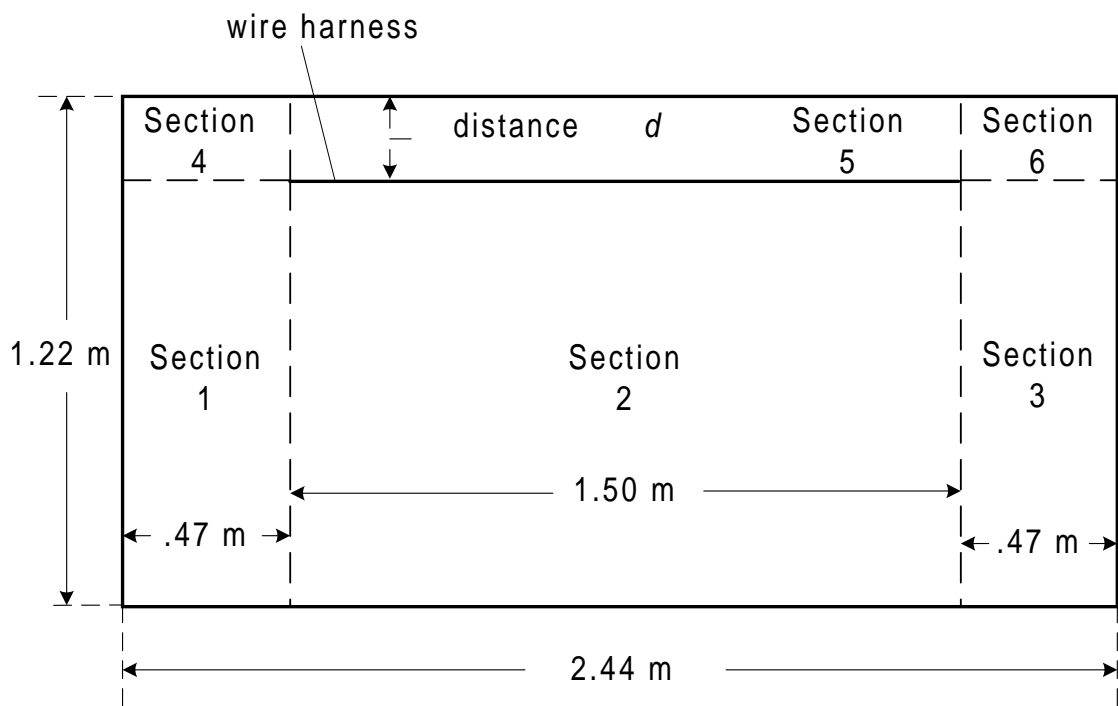


Figure 3.2. Diagram of table sections.

The resonant length is then $l = 1.5$ m. Thus the antenna should have a half-length of .75 m so that it will perform best in the middle of the frequency band. The program `cmst1` generated the NEC-4 code for this dipole antenna.

3.4 Procedure

As discussed in Section 3.1, the theoretical Z -parameters of the table-dipole antenna system are desired so that they can be converted to S -parameters and compared to measured results. Since the most easily accessible quantity from NEC is currents on wire segments, a method must be used to find the Z -parameters from the currents. The method used is presented in this section.

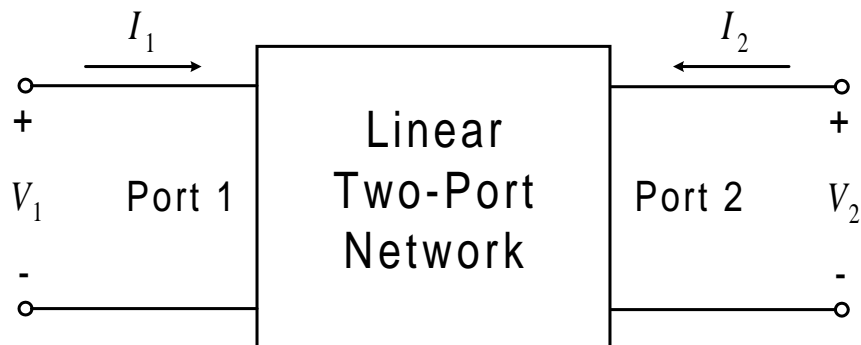


Figure 3.3. Terminal plane definitions and locations of V_n and I_n for a linear two port network.

A simple explanation of two-port networks and the Z and S -parameters is now provided. Assume that two terminal planes, or ports, can be defined in a linear electrical system. Figure 3.3 shows the location of the voltages and currents at the terminal planes or ports of a two-port electrical network. If the network is linear, the voltages can be written as a linear combination of the currents, or

$$[V] = [Z] [I] \tag{3.2}$$

where $[Z]$ is the impedance, or Z -parameter matrix of the network [6]. For a two-port network, the matrix description can be written as

$$\begin{bmatrix} V_1 \\ V_2 \end{bmatrix} = \begin{bmatrix} Z_{11} & Z_{12} \\ Z_{21} & Z_{22} \end{bmatrix} \begin{bmatrix} I_1 \\ I_2 \end{bmatrix} . \quad (3.3)$$

Expressions for the voltages V_1 and V_2 are then found to be

$$V_1 = Z_{11} I_1 + Z_{12} I_2 \quad (3.4)$$

$$V_2 = Z_{21} I_1 + Z_{22} I_2 . \quad (3.5)$$

Since the electrical network describing the table-antenna system can be assumed to be a reciprocal network, $Z_{12} = Z_{21}$ [6]. With this assumption, the voltage expressions become

$$V_1 = Z_{11} I_1 + Z_{21} I_2 \quad (3.6)$$

$$V_2 = Z_{21} I_1 + Z_{22} I_2 . \quad (3.7)$$

A method to find the Z -parameters is described as follows. Apply test voltages or currents at specific ports under certain conditions (port n opened, shorted, or loaded) and measure or calculate a resulting voltage or current due to the test excitation. The Z parameters can then be found algebraically from these measurements. For the first step, open-circuit Port 2 so that $I_2 = 0$. Then

$$V_1 = Z_{11} I_1 . \quad (3.8)$$

Next, apply a test voltage V_1 at Port 1 and calculate or measure the resulting current

I_1 . Z_{11} is then found as

$$Z_{11} = \frac{V_1}{I_1} . \quad (3.9)$$

Similarly, if Port 1 is open-circuited (implying $I_1 = 0$) and a test voltage V_2 is applied to Port 2 resulting in a measured or calculated current I_2 , then

$$Z_{22} = \frac{V_2}{I_2} . \quad (3.10)$$

Finally, to obtain Z_{21} , short circuit Port 2 to force $V_2 = 0$. Then

$$V_2 = Z_{21} I_1 + Z_{22} I_2 = 0 . \quad (3.11)$$

Apply a test voltage V_1 to Port 1, and measure or calculate the resulting currents I_1 and I_2 . Then

$$Z_{21} = -Z_{22} \frac{I_2}{I_1} . \quad (3.12)$$

Since Z_{22} was found in a previous step, Z_{21} and therefore Z_{12} are found from the above equation.

This method will now be applied to the NEC model. First, the two ports on the table-antenna system need to be defined. Port 1 is defined to be the input terminals to the wire radiator above the table. This port is taken to be the bottom wire segment in the NEC model. Port 2 is taken to be the center wire segment on the dipole receiving antenna. These port definitions are convenient because in NEC a test Voltage can be applied over a wire segment, and the current on every wire segment is calculated.

To calculate the Z -parameters numerically, NEC must be run three separate times under different port excitations and loads. The first run places a near infinite impedance (100 M Ω) at Port 2 and applies a test voltage at Port 1. Along with the normal NEC output, the file `cur_p1z2.txt` is created. This file contains the real and imaginary parts of the currents for Port 1. The currents for Port 2 are unneces-

sary because they are forced to zero due to the large impedance. Next, a second run of NEC is performed with an large impedance at Port 1 and a test voltage applied at Port 2. NEC produces the file `cur_p2z3.txt` that contains the real and imaginary currents for port 2 during this step. During the final NEC run, Port 2 is shorted, meaning there is no applied voltage or impedance loading across the Port 2 wire segment, and a test voltage is applied to Port 1. NEC produces two files for this step, `cur_p1z1.txt` and `cur_p2z1.txt`, which contain the real and imaginary currents for Port 1 and Port 2, respectively.

After the three NEC runs, the program `zparmake` reads in the port current files (`cur_p1z1.txt`, `cur_p2z1.txt`, `cur_p1z2.txt` and `cur_p2z3.txt`) and computes the Z -parameters of the two-port network using the equations derived in this section. An explanation of the Fortran code as well as the source file for the program `zparmake` can be found in Appendix B. After the Z -parameters are calculated, the program prints the real and imaginary parts of the Z -parameters to the files `z11_num.txt`, `z21_num.txt` and `z22_num.txt`.

3.4.1 Z to S -Parameter Conversion

Another program, `sparconv`, is used to convert the Z -parameter files into S -parameters so that they can be more easily compared to measured results. S -parameters relate the complex wave amplitudes that enter and exit an n -port linear network. For the n th port, the complex wave amplitude entering the port is designated as a_n , and the complex wave amplitude exiting the port is designated as b_n . A diagram of a two port linear network defining the incoming and outgoing waves can be found in Figure 3.4.

The scattering matrix, $[S]$, of this network is defined by the relation

$$[b] = [S] [a] \tag{3.13}$$

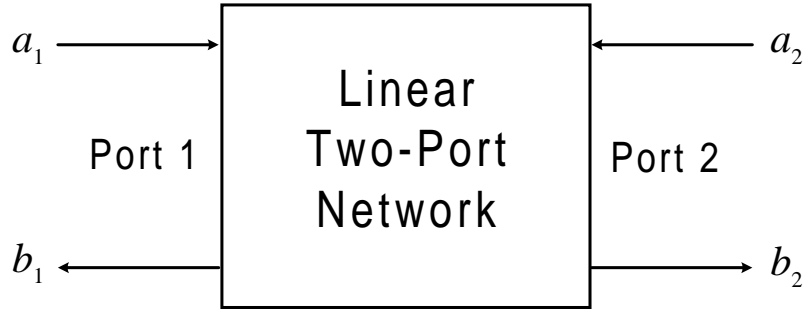


Figure 3.4. Terminal plane definitions and locations of a_n and b_n for a linear two port network.

or

$$\begin{bmatrix} b_1 \\ b_2 \end{bmatrix} = \begin{bmatrix} S_{11} & S_{12} \\ S_{21} & S_{22} \end{bmatrix} \begin{bmatrix} a_1 \\ a_2 \end{bmatrix}. \quad (3.14)$$

A full treatment relating Z -parameters to S -parameters, including the relationship between the terminal voltages and currents to the complex wave amplitudes, can be found in standard texts on microwave networks [6]. Of interest here are the formulas converting between the two sets of parameters. If the Z -parameters of a two-port network are known, the scattering matrix is found by

$$[S] = ([Z] + [U])^{-1} ([Z] - [U]) \quad (3.15)$$

where

$$[U] = \begin{bmatrix} 1 & 0 \\ 0 & 1 \end{bmatrix} \quad (3.16)$$

is the identity matrix [6]. Writing expressions for each S -parameter gives

$$S_{11} = \frac{(Z_{11} - Z_0)(Z_{22} + Z_0) - Z_{12}Z_{21}}{\Delta Z}, \quad (3.17)$$

$$S_{12} = \frac{2 Z_{12}Z_0}{\Delta Z}, \quad (3.18)$$

$$S_{21} = \frac{2 Z_{21} Z_0}{\Delta Z}, \quad (3.19)$$

and

$$S_{22} = \frac{(Z_{11} + Z_0)(Z_{22} - Z_0) - Z_{12}Z_{21}}{\Delta Z}, \quad (3.20)$$

where Z_0 is the characteristic impedance of the port and

$$\Delta Z = (Z_{11} + Z_0)(Z_{22} + Z_0) - Z_{12}Z_{21}. \quad (3.21)$$

It can be seen from equations 3.18 and 3.19 that since $Z_{12} = Z_{21}$, $S_{12} = S_{21}$.

The Fortran program `sparconv` was used to read in the numerically-calculated Z -parameter files (`z11_num.txt`, `z21_num.txt` and `z22_num.txt`), convert the Z -parameters to S -parameters, and then print out the numerically calculated S -parameters to the files `ns11.txt`, `ns21.txt`, `ns12.txt`, and `ns22.txt`. The program `sparconv` was also used to format and manipulate the measured S -parameter data. A description of the program `sparconv`, including the source code, can be found in Appendix B.

Once this method of computing the S -parameters of the NEC-modeled system was established, the S -parameters of the table-antenna system were generated for several positions of the table's wire radiator. The results are discussed in the next section.

3.5 Typical Numerical Results

Using the method discussed in Section 3.4, the S -parameters of the table-antenna system were generated numerically for several different cases. The S -parameters were calculated for $d = 5$ cm, $d = 10$ cm, $d = 15$ cm, and $d = 20$ cm where d is the distance along the table from the front lip of the table back to the elevated wire, as shown in Figure 3.1. The S -parameters were determined for each case from 50

MHz to 150 MHz in increments of 1 MHz for a total of 101 frequency points. As discussed in Section 3.4, three NEC runs were needed for each wire position to be able to determine the S -parameters of the table-antenna system.

After the S -parameters were calculated, they were imported and plotted using the Axum commercial plotting software. Typical numerical results for the magnitude and phase of the S -parameters are shown in Figure 3.5 through Figure 3.9 found in the following pages. The distance d for these plots is 10 cm.

Resonance is defined as the phenomenon where the average electric and magnetic stored energies of a system are equal [6]. This occurs for Port 1 when the input impedance looking into Port 1 is purely real. Since the input impedance looking into Port 1 when Port 2 is match terminated is

$$Z_{in} = Z_0 \frac{1 + S_{11}}{1 - S_{11}} \quad (3.22)$$

where Z_0 is the characteristic impedance at Port 1, the input impedance is purely real when the phase of S_{11} equals zero degrees.

The magnitude and phase plots for S_{11} are shown in Figure 3.5 and Figure 3.6, respectively. These plots indicate that the numerical model predicts a resonance for the table-wire harness antenna system around 91 MHz. The NEC model shows that very little signal enters Port 1 outside of a band 40 to 50 MHz wide centered at the resonant frequency. These magnitude and phase curves are plotted along with the magnitude and phase of S_{11} for a table-wire harness antenna in the absence of dipole antenna in Figure 3.11 and Figure 3.12, respectively. In the labeling for these figures, the separation corresponds to the distance between the dipole antenna and the conducting table. The 1 m separation is the normal separation investigated here, and the infinite separation is the case investigated for the isolated dipole antenna. Notice that both the magnitudes and phases of S_{11} are nearly identical for the isolated

table-wire harness case and for the complete table-antenna system.

The magnitude and phase plots for S_{21} are shown in Figure 3.7 and Figure 3.6, respectively. For this NEC model, $S_{21} = S_{12}$, so plots for S_{12} are not included as separate figures. Notice that the NEC model predicts a near linear phase over the entire band studied. The model predicts a local maximum in the magnitude of S_{21} of around -90 dB at 96 MHz.

Figure 3.9 and Figure 3.10 show the magnitude and phase plots for S_{22} where Port 2 is the input to the dipole antenna. The NEC model predicts a resonance at 95 MHz. These magnitude and phase curves are also plotted along with the magnitude and phase curves of S_{22} for an isolated dipole antenna in Figure 3.13 and Figure 3.14. For the isolated case, Port 2 is assumed to be the only port for convenience. Notice that the numerical results for both the magnitude and phase of S_{22} of an isolated dipole antenna closely match those of the dipole antenna in the complete table-antenna system.

A complete discussion and analysis of the numerically generated S -parameters for all of the wire positions can be found in Chapter 5. The next chapter will discuss the experimental portion of the research completed for this thesis project. The S -parameters of a system similar to that modeled by NEC were measured at MSU's Electromagnetics Laboratory. These measured S -parameters will be compared to the numerical results obtained using NEC in Chapter 5.

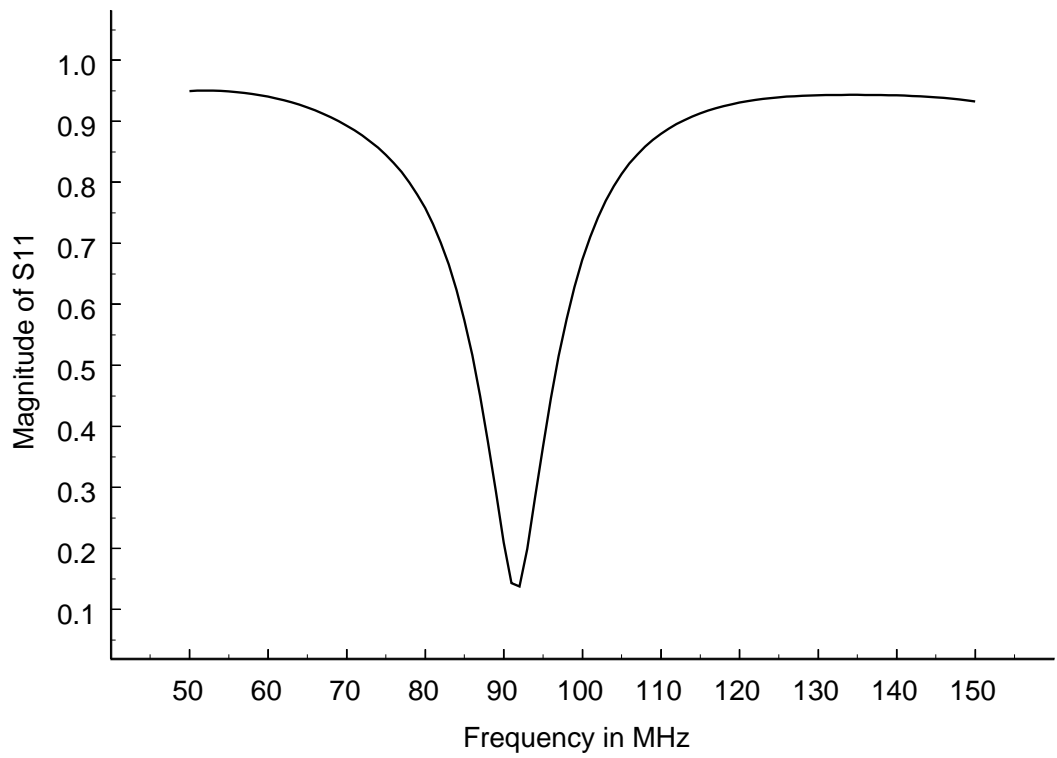


Figure 3.5. Magnitude of S_{11} ($d = 10$ cm) found using NEC.

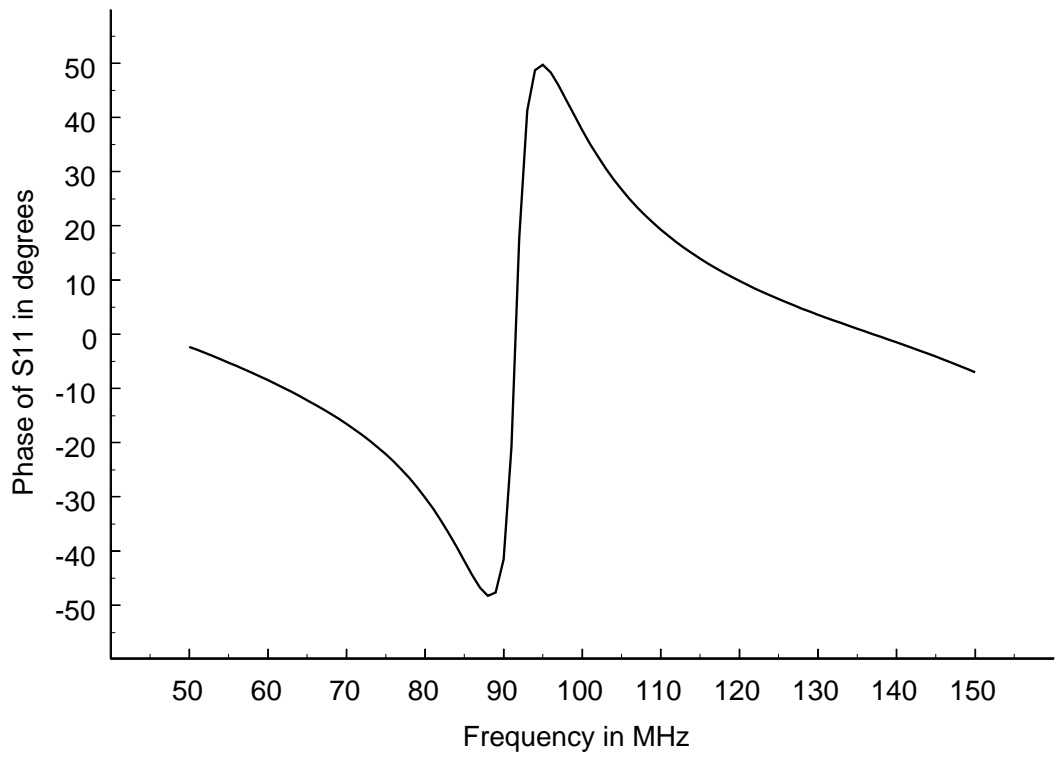


Figure 3.6. Phase of S_{11} ($d = 10$ cm) found using NEC.

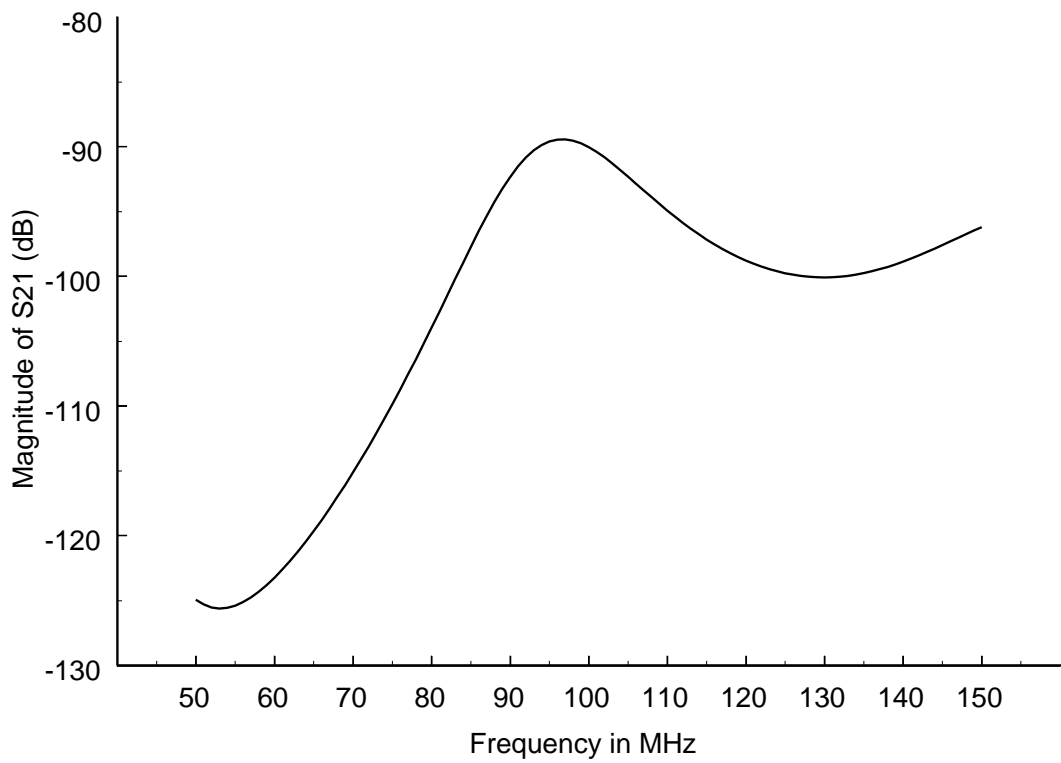


Figure 3.7. Magnitude of S_{21} (or S_{12}) ($d = 10$ cm) found using NEC.

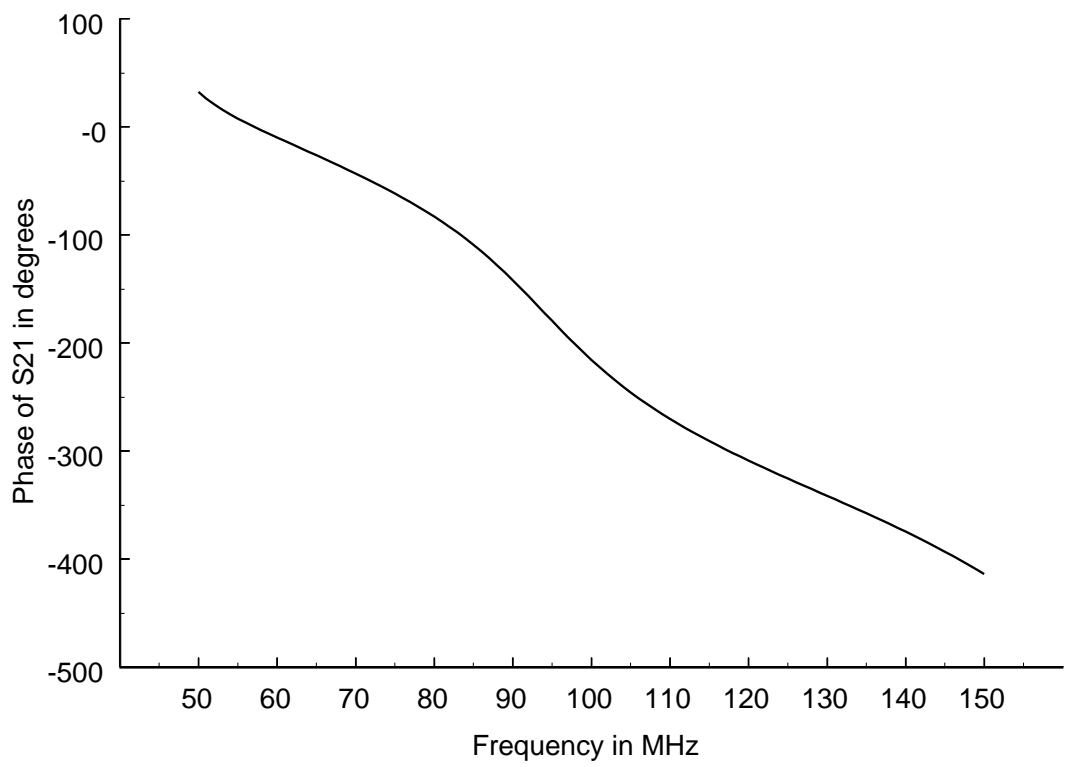


Figure 3.8. Phase of S_{21} (or S_{12}) ($d = 10$ cm) found using NEC.

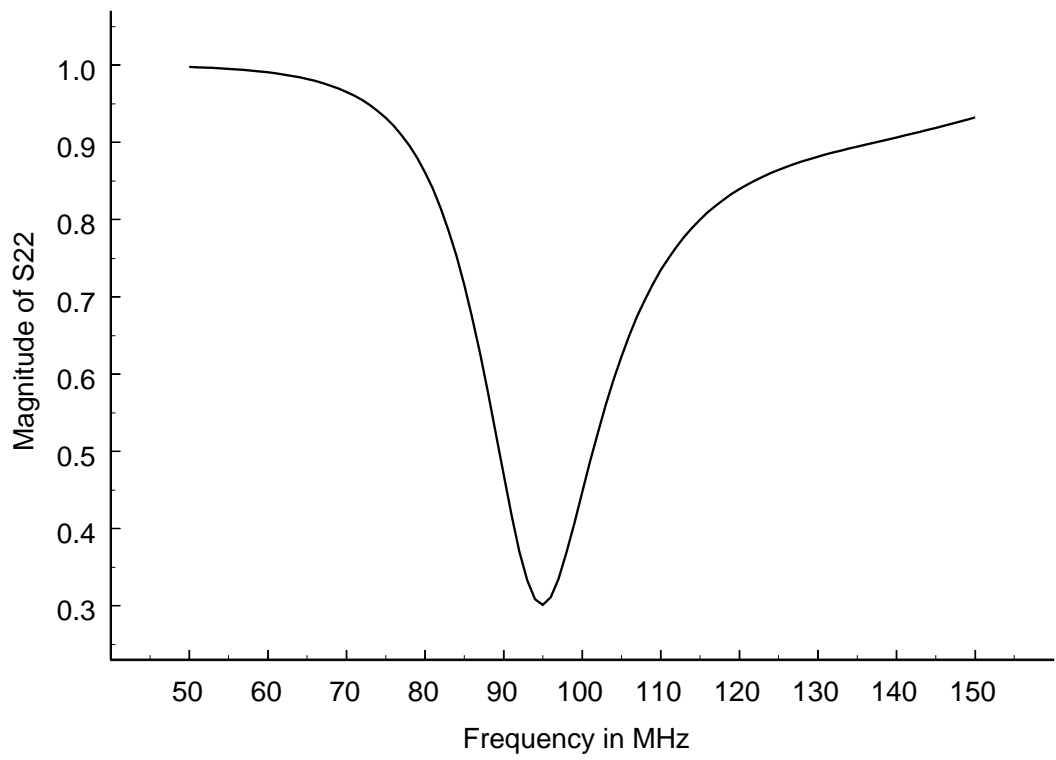


Figure 3.9. Magnitude of S_{22} ($d = 10$ cm) found using NEC.

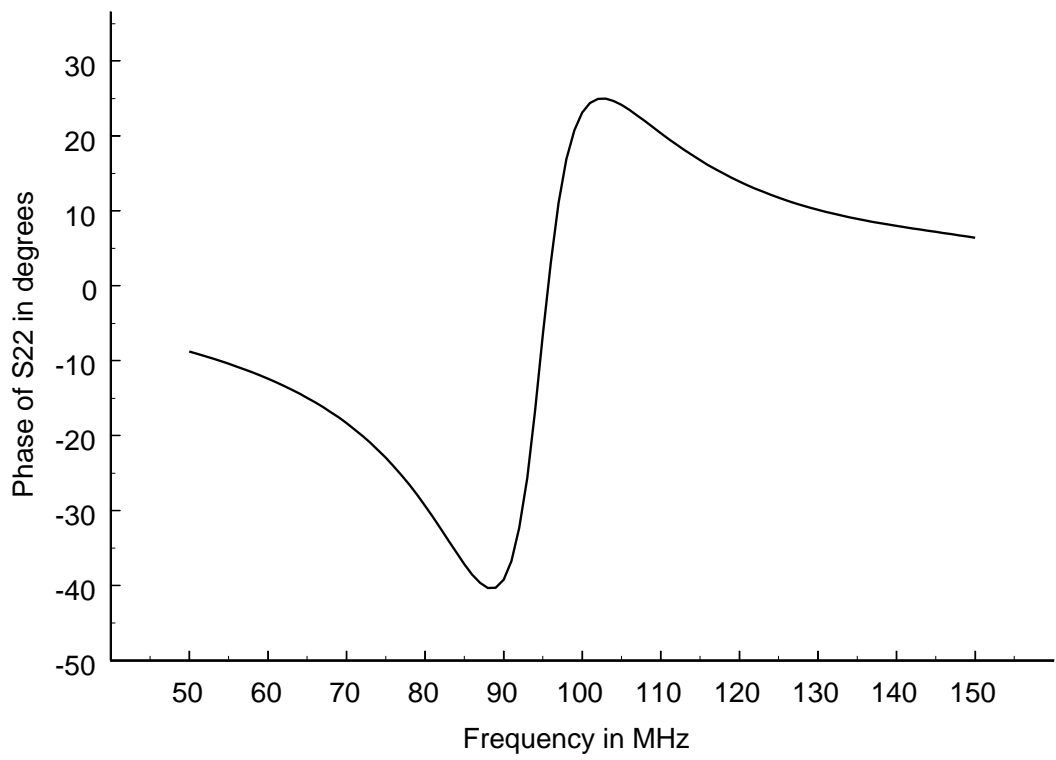


Figure 3.10. Phase of S_{22} ($d = 10$ cm) found using NEC.

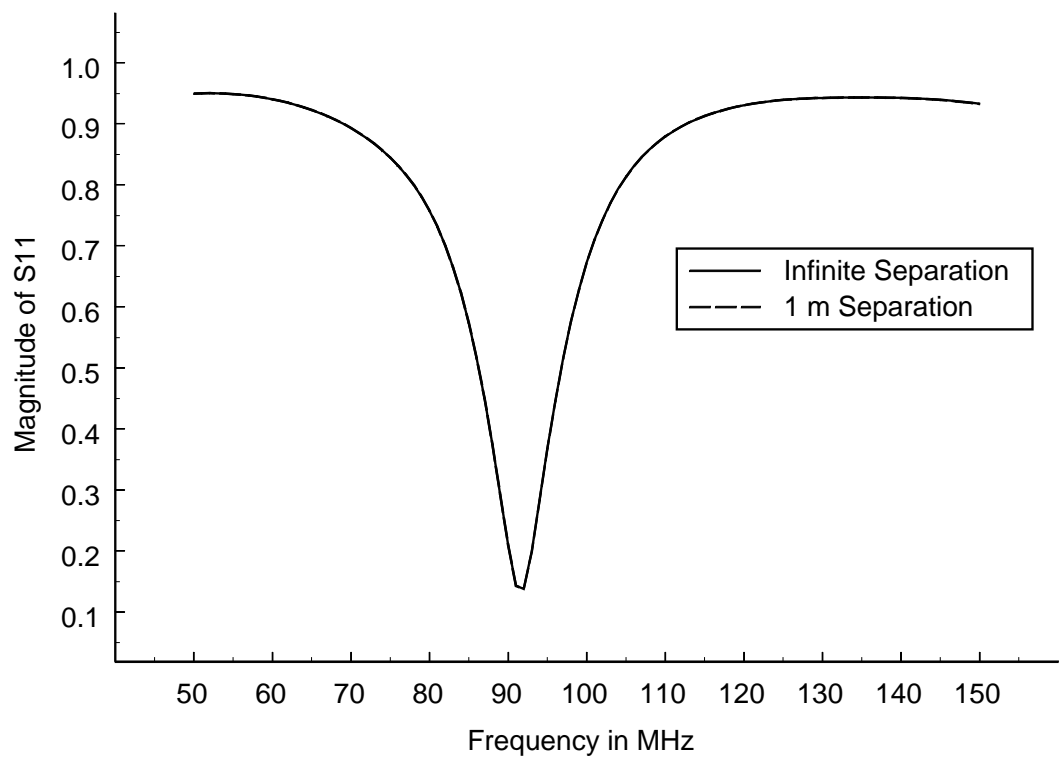


Figure 3.11. Magnitude of S_{11} for an isolated table-wire harness antenna and the table-antenna system.

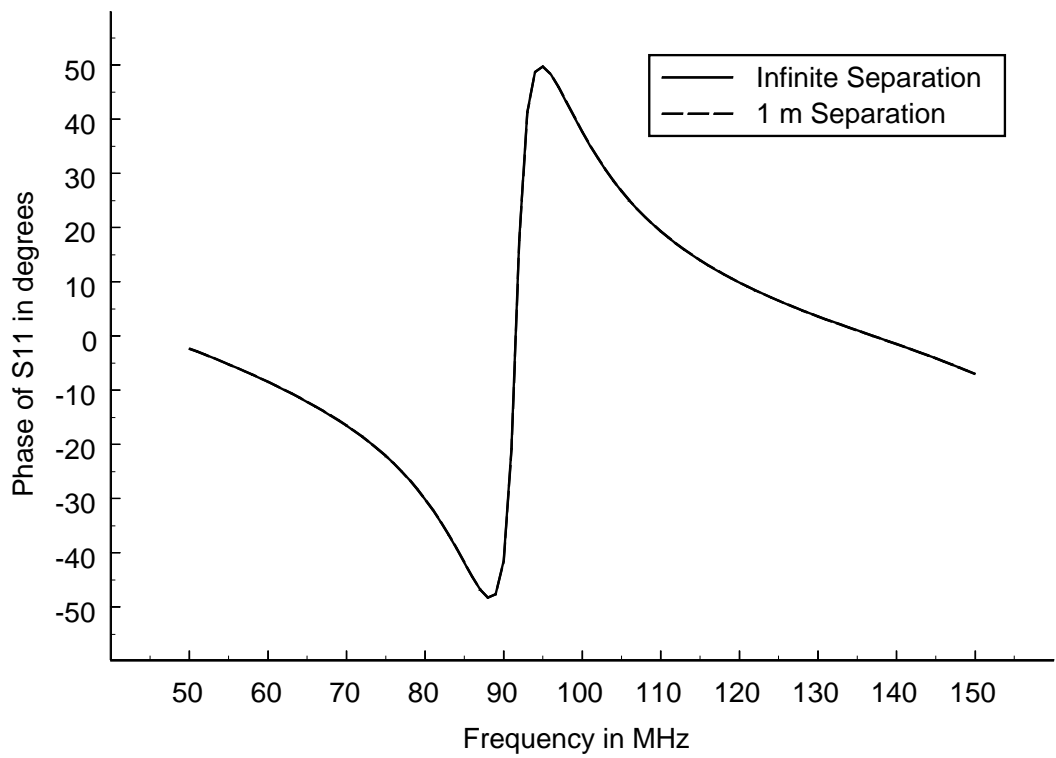


Figure 3.12. Phase of S_{11} for an isolated table-wire harness antenna and the table-antenna system.

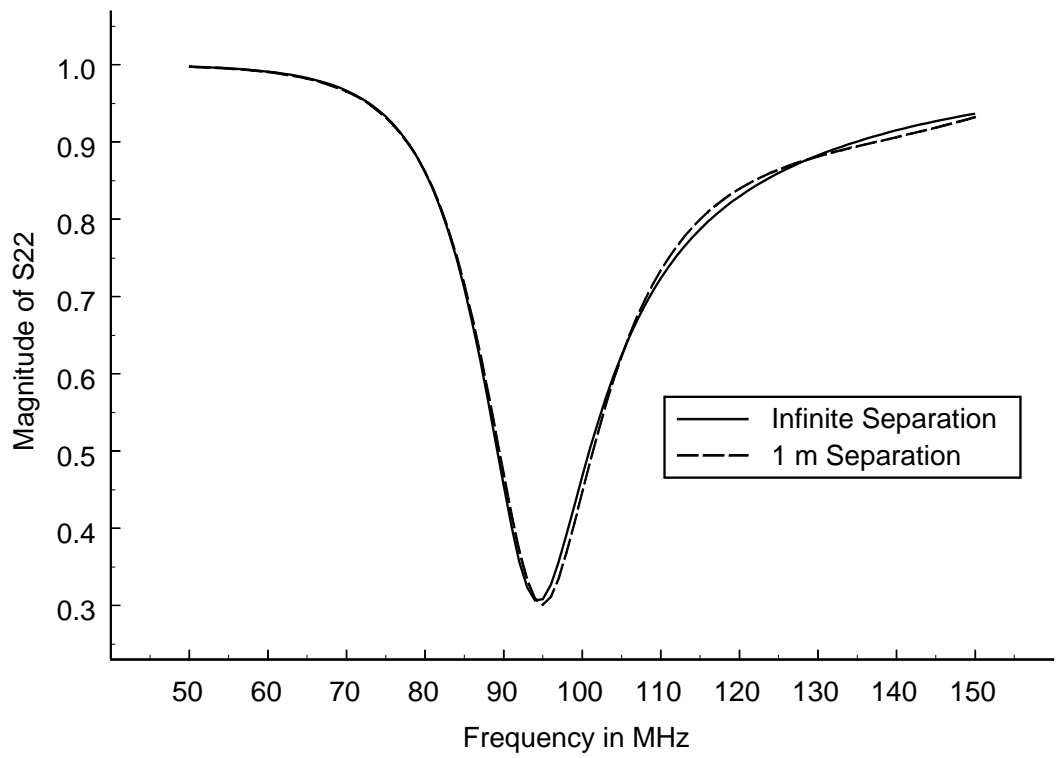


Figure 3.13. Magnitude of S_{22} for an isolated dipole and the table-antenna system.

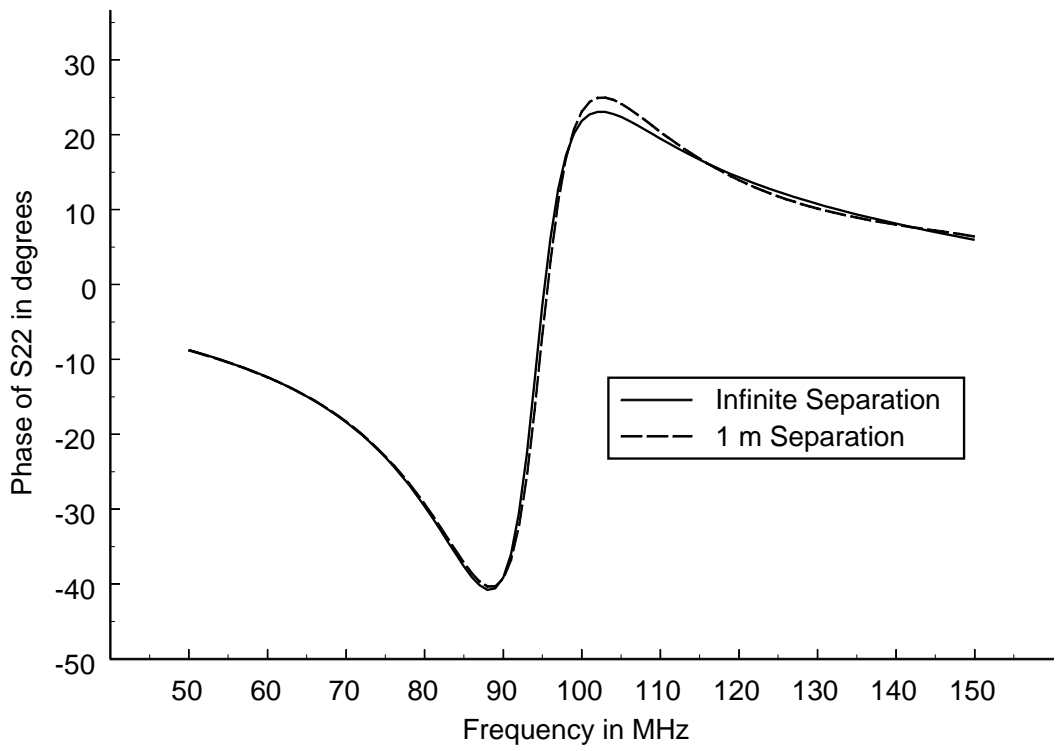


Figure 3.14. Phase of S_{22} for an isolated dipole and the table-antenna system.

CHAPTER 4

EXPERIMENTAL WORK

4.1 Overview

Experimental work was performed to compliment the numerical modeling portion of this project. A setup similar to the one modeled in Chapter 3 was constructed to verify the computer simulation. This chapter will explain the experimental work performed for this project. Section 4.2 will discuss the apparatus and measurement techniques. Next, Section 4.3 will give a description of how the experimental arrangement compares to the testing requirements laid out in CISPR 25. Finally, Section 4.4 will give some typical experimental results. A complete presentation of the experimental results, along with a comparison to the numerical results, can be found in Chapter 5.

4.2 Description of Experimental Setup

An experimental setup that closely meets the CISPR 25 requirements was constructed at the Engineering Research Complex at Michigan State University. A diagram of the setup can be found in Figure 4.1.

The Electromagnetics Laboratory at Michigan State University has access to a large ground plane (20 feet by 24 feet) where many radar and target identification experiments have been performed. This ground plane was chosen as the platform to perform this experiment. One extraneous 4 foot by 8 foot section of the ground plane was used as the conducting table top. The metal plate has a thickness of 1/8". The table dimensions are very close to those found in the CISPR 25 documentation (2.44 m actual length versus 2.5 m specified length) [2]. The width of the table used measured 1.22 m. This width is unspecified in the CISPR 25 documents.

Four wooden 4"×4" posts were cut and drilled to act as the legs for the table.

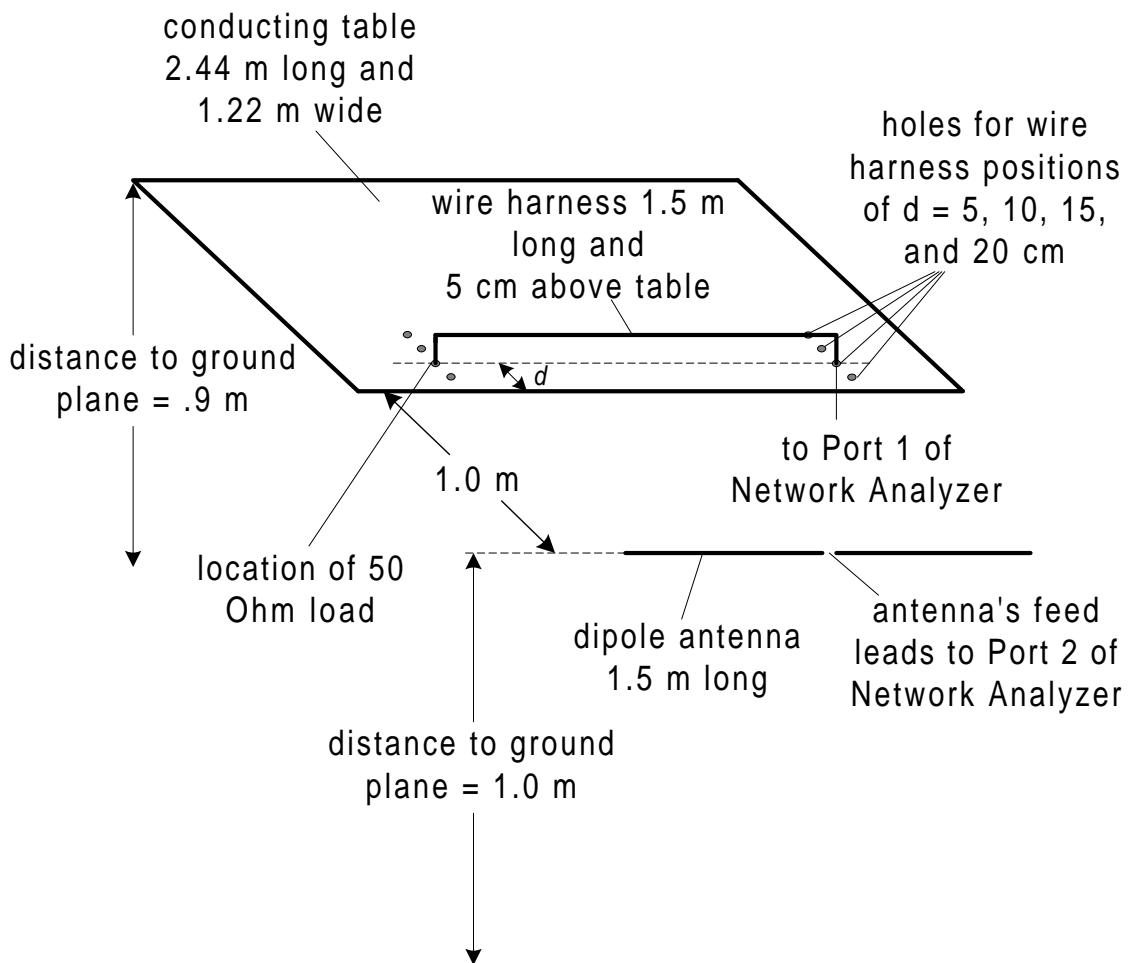


Figure 4.1. Diagram of experimental setup at Michigan State University.

The lengths of the posts were chosen such that the total height of the table measures .9 m, as specified in the CISPR 25 documentation [2]. The table top and legs were then assembled and the table was placed on top of the ground plane.

Next, a total of eight holes were drilled through the table as shown in Figure 4.1. The two holes in each of the four sets were drilled 1.5 m apart and equidistant from both the sides and the front of the table. The four sets were chosen to be spaced at 5 cm, 10 cm, 15 cm, and 20 cm back from the front edge of the table. This distance is specified in the CISPR 25 document to be 10 cm. The other distances were chosen to investigate the effect of distance on the measured S -parameters.

The holes were drilled so that a Type-N female-to-female microwave connector can be threaded from under the table until the face of the connector is flush with the table surface. This requires a 5/8"-24 tap, which calls for a pilot hole size ranging from .580" to .590" in diameter. However, a drill bit with a diameter in this range could not be found, so a 9/16" bit (.5625" diameter) was used. The holes were then expanded by using a metal file until the tap snugly fit in each hole. The holes were then hand threaded using the 5/8"-24 tap. Then two Type-N female-to-female microwave connectors were threaded into the table from the underside.

Two Type-N male center conducting pins were then taken from two unused adaptors. These pins were soldered to the ends of a thin copper wire. This wire was carefully measured to be 1.6 m long so that each pin could rest in the female center conductor of the adaptors threaded into the table and so the wire could be strung 5 cm above the table across the entire 1.5 m distance between adaptors. The wire was suspended above a conducting table by low dielectric constant Styrofoam supports.

A 50 Ω load with a male Type-N connector was connected to one of the Type-N female connectors on the underside of the table. A cable arrangement with a Type-N male connector on one end was mated with the other Type-N connector on the underside of the table. This cable would be used to provide energy to the table, wire

radiator and load arrangement.

A dipole antenna was then chosen to act as the receiving antenna for the system. This type of antenna was selected for several reasons. A dipole antenna designed to work around the 50 MHz to 150 MHz region is reasonable in physical size so that it is not too difficult to construct and set up. A broadband antenna designed to work at these low frequencies might be extremely large. A dipole antenna is very inexpensive compared to some of the broadband antennae used in industry. With limited funds, this is a major consideration. Most importantly, the dipole antenna may be modeled in NEC simply and accurately, which is of primary importance for this project. Some of the popular broadband antennae have complicated geometries and feeding arrangements which are difficult to implement in a NEC input code generator. As seen in Appendix A, the dipole antenna was simple to add to the grid-generating program developed for this project. A common TV antenna was purchased to be used as the dipole antenna with two adjustable length poles that can be set at different angles. A $300\ \Omega$ twin lead wire originally extended from the antenna's feed point. As will be discussed in the following subsections the twin lead is modified depending on which measurement method is used.

One of the difficulties of these measurements was determining a suitable feeding arrangement for the dipole receiving antenna. A well known problem exists when a coaxial line is connected directly to a dipole antenna (inner conductor to one monopole and outer conductor to the other monopole). The currents on the coaxial line have the possibility of being unbalanced under this arrangement [7]. Therefore, three different feeding and calibration methods were performed for one position of the wire radiator ($d = 10$ cm). The method producing the best result for this distance was then chosen and used to perform the measurements for the rest of the wire positions. The three methods are described in the next subsections.

4.2.1 Method 1: Transformer Included in the *S*-Parameter Measurements

Method 1 was the first antenna feed and calibration setup attempted during these measurements. First, the dipole antenna's 300 Ω twin lead was cut about two cm from the antenna's feed point. A standard 300 Ω to 75 Ω VHF / UHF TV transformer was then used to reduce the mismatch to the 50 Ω cable used in the electromagnetics laboratory and, more importantly, to act as a balun to balance the possible unbalanced currents on the cable. As shown in Figure 4.2, a series of adaptors was then used to connect the antenna to 50 Ω cable. This cable routes the energy received by the antenna back to the measurement equipment.

An HP 8510C Vector Network Analyzer (VNA) was used to make the measurements for this experiment. The cable leading from the underside of the table was connected to Test Port 1 of the VNA and the cable leading from the dipole antenna was connected to Test Port 2. An HP 85054B Type-N calibration kit was used for the calibration standards. The *S*-Parameters of the table-antenna network were then measured from 50 MHz to 150 MHz using 801 frequency points. An IF averaging factor of 128 was used, as well as a dwell time of 100 milliseconds using a stepped frequency sweep. The results of these measurements for a wire distance of $d = 10$ cm with a comparison to the numerical results are shown in Chapter 5 in Figure 5.1 through Figure 5.8. As will be discussed later, only the case where $d = 10$ cm is included in this thesis for Method 1, just to be used as a comparison to Method 2, the best measurement method.

4.2.2 Method 2: Transformer Calibrated out of the Measurements

Method 2 was the second setup used for this project's measurements, and it proved to be the most successful. Instead of allowing the transformer to be part of the measured system, the calibration plane for this method was moved as close to the receiving

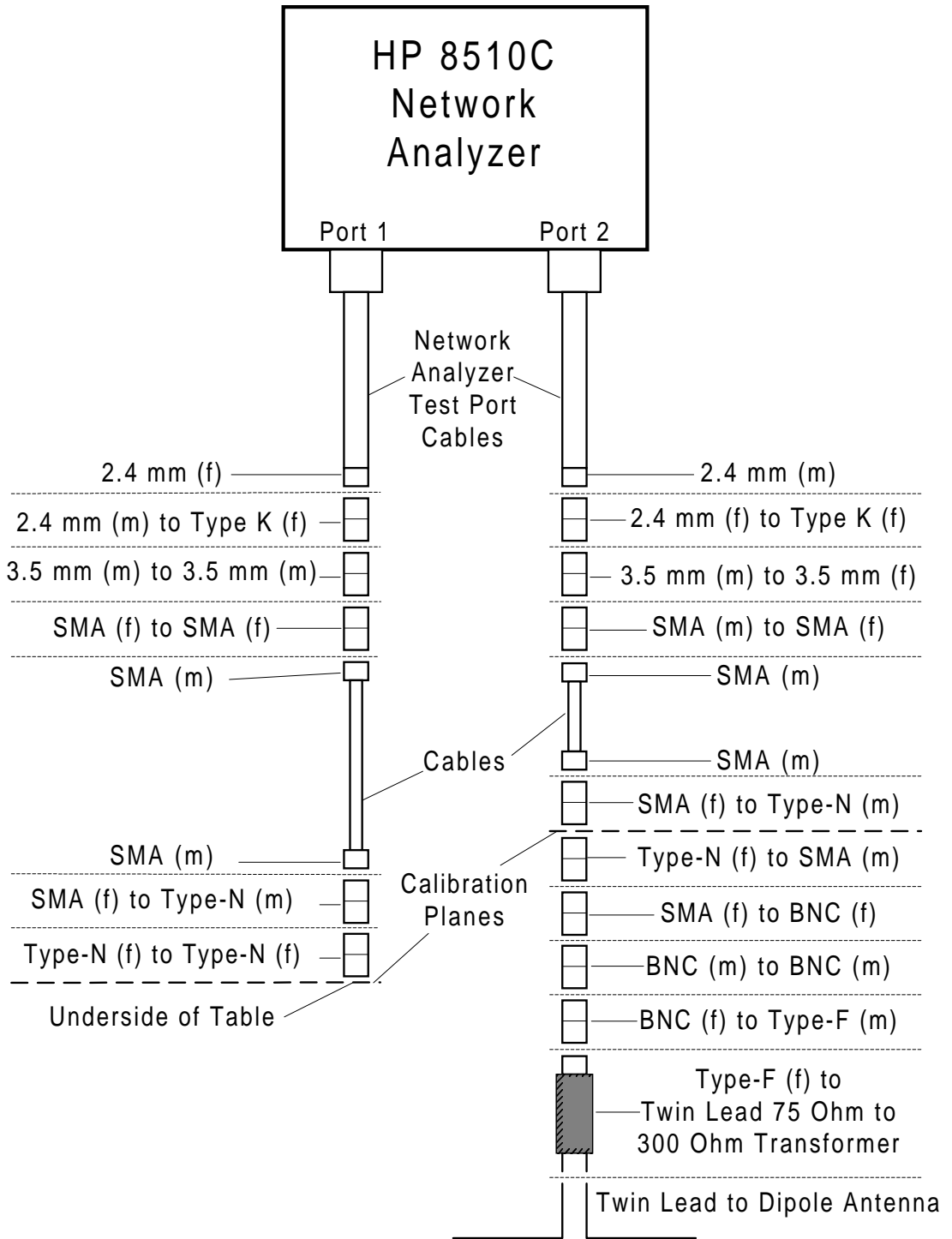


Figure 4.2. Diagram of cable and adaptor arrangement for measurement method 1.

dipole as possible. The small amount of $300\ \Omega$ transmission line that extended from the dipole antenna was completely stripped and a female BNC adaptor was soldered directly to the dipole's leads. A male BNC to female Type-N adaptor was then used so that the Type-N calibration kit could be used to establish the calibration plane at the female Type-N connector. The $300\ \Omega$ line extending from the transformer was stripped and a male Type-N connector was connected by again soldering a female BNC adaptor to the leads and using adaptors to change to a male Type-N connector. A diagram of the adaptor arrangement can be found in Figure 4.3.

The HP 8510C was again used to perform the S -parameter measurements. The results obtained using this method more closely matched the numerical results than results obtained using the other calibration methods. Typical results for this method can be found in Section 4.4. Complete results for all wire distances can be found in Chapter 5.

4.2.3 Method 3: Measurement with No Transformer Balun

Although measurements for all four wire distances were already performed using Method 2 with acceptable results, one more measurement method was performed for comparison. In the first two measurement methods, a transformer was used as a balun to balance the potentially unbalanced currents on the coaxial cable feeding the dipole antenna. As a comparison, the transformer and much of the adaptor assembly was removed from the Method 2 system and a Type-N male connector was placed at the end of the coaxial cable leading to the antenna. The system was calibrated to this male connector, and the connector was mated to the female Type-N adaptor connected to the dipole antenna. A diagram of the adaptor assembly for this measurement method is shown in Figure 4.4.

Once again the HP 8510C network analyzer was used to perform the S -parameter measurements for this measurement / calibration method. The results for the $d = 10$ cm case are shown in Figure 5.17 through Figure 5.24 found in Chapter 5. Notice

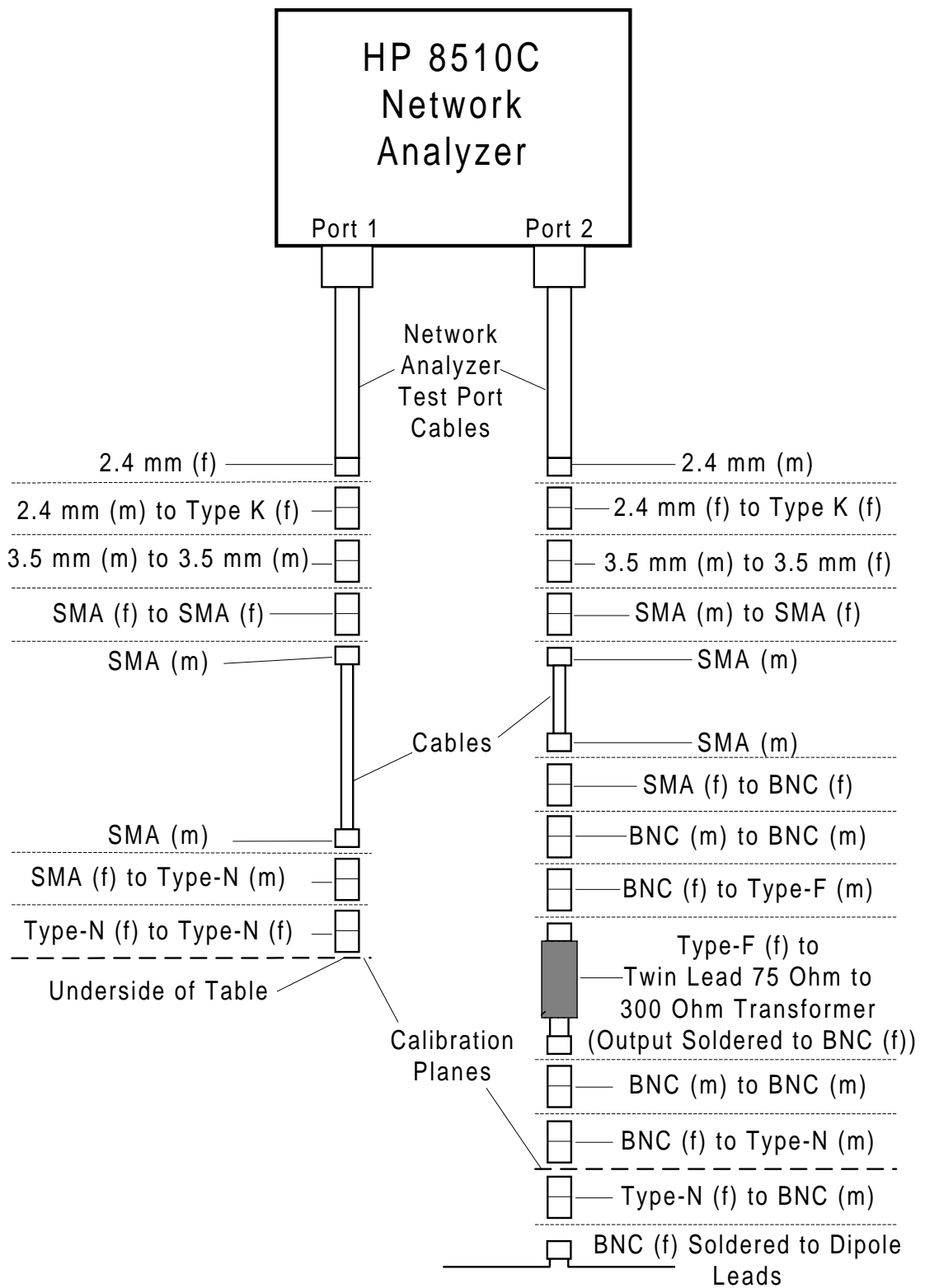


Figure 4.3. Diagram of cable and adaptor arrangement for measurement method 2.

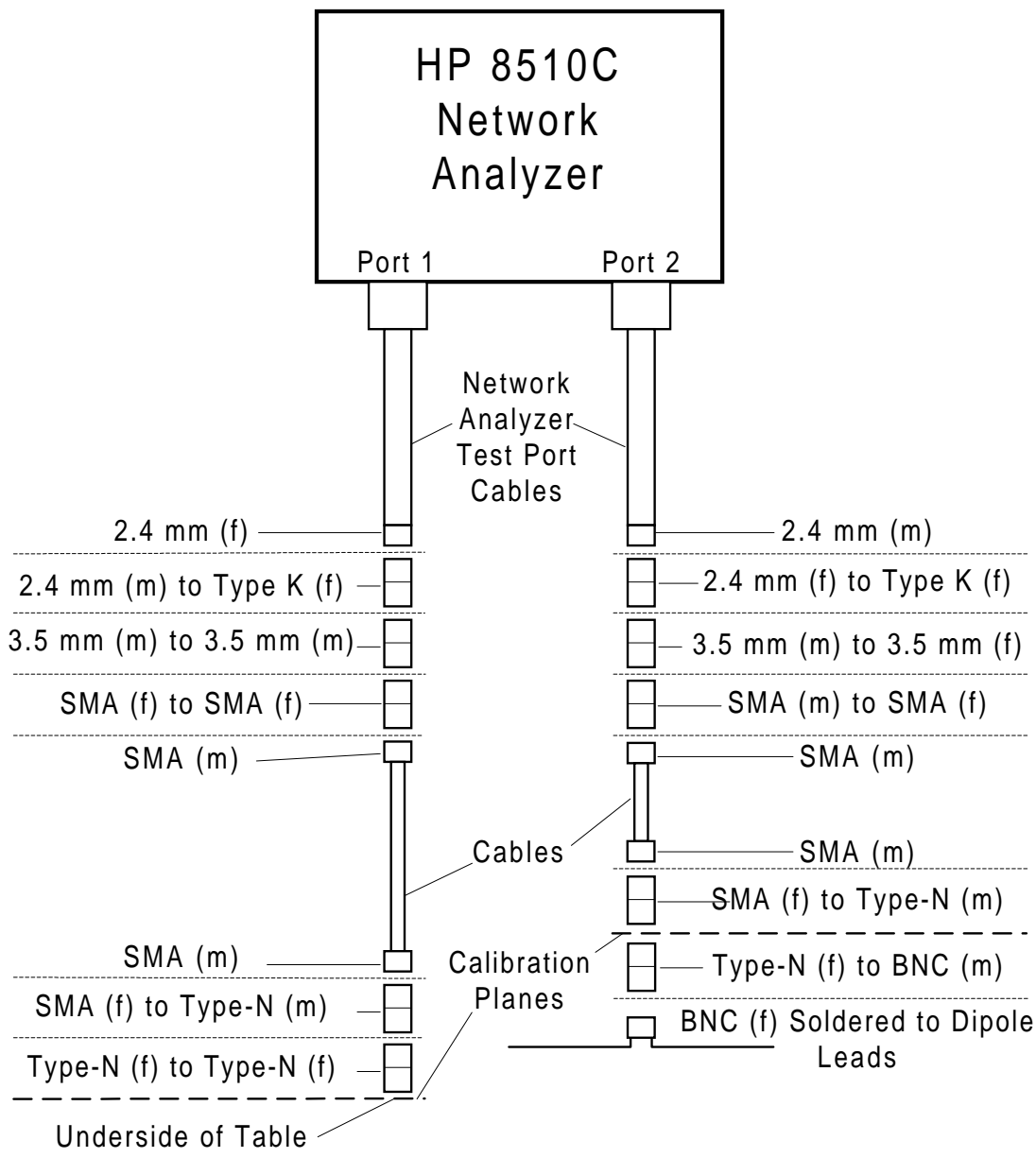


Figure 4.4. Diagram of cable and adaptor arrangement for measurement method 3.

that the results do not match the numerical results as well as those obtained using the second measurement / calibration method.

4.3 Comparison of Experimental Setup to CISPR 25 Requirements and Numerical Model

As mentioned in Chapter 2, the goal of this project was to obtain an experimental setup and a predictable numerical model that both resemble the testing setup outlined in the CISPR 25 requirements [2]. In this section, the similarities and differences will be discussed between the experimental setup, the numerical model, and the CISPR 25 requirements.

The table and wire harness radiator dimensions are very similar for the MSU experimental setup, the NEC model, and the CISPR 25 requirements. The table length for both the MSU experimental setup and the NEC model was 2.44 m. As stated previously, this is close to the 2.5 m length specified in the CISPR document. The radiating wire harness was centered left to right on the table at a distance d back from the front edge of the table and suspended 5 cm above the table in all three models or setups. The distance d specified in the CISPR document is 10 cm [2]. Measurements for the experimental setup at MSU as well as numerical modeling was performed for $d = 10$ cm, as well as 5, 15, and 20 cm. Results from the other distances were desired because they could possibly predict the effect of varying the harness' distance from the lip during a CISPR 25 test.

The distance between the receiving antenna and the table was specified to be .9 m in the CISPR 25 document. Since the wire harness distance would be varied from 5 cm to 20 cm in the numerical model and experimental setup at MSU, the .9 m distance between the antenna and the table lip was not used. Therefore, a 1 m distance was chosen for these models as shown in Figure 3.1 and Figure 4.1.

The main difference between the CISPR 25 requirements and the experimental

setup at MSU is that while the CISPR 25 documentation requires the use of a semi-anechoic chamber inside a shielded enclosure, the experimental setup at MSU was performed openly above a ground plane in a large laboratory room. Reflections from walls, the ceiling, metal cabinets, or other structures as well as external electromagnetic interference had the possibility of affecting the measurements performed at MSU. Although the electromagnetics laboratory at MSU does have an anechoic chamber, the microwave absorber on the walls is not very effective below 500 MHz, which would not be very useful for these measurements. Also, the chamber is fully anechoic, and therefore has no ground plane on the floor.

The numerical model follows the CISPR 25 guidelines more closely. No extraneous objects or structures such as walls or ceilings are included in the numerical model, which models the effect of the absorber well. No external electromagnetic interference is present in the numerical model, which resembles the effect of the shielded enclosure in the CISPR 25 requirements. The numerical model and the CISPR 25 requirements therefore have similar differences to the experimental setup at MSU. One difference between the numerical model and the CISPR 25 requirements is that an infinite ground plane exists 90 cm below the table in the numerical model, and only a ground plane as large as the semianechoic chamber is present in the CISPR 25 requirements.

4.4 Typical Experimental Results

Using the second measurement method of Section 4.2.2, S -parameter measurements were performed for all four wire distances ($d = 5, 10, 15,$ and 20 cm). Typical results are found in this section in Figure 4.5 through Figure 4.12 using $d = 10$ cm. These results will be discussed briefly in this section.

From the magnitude and phase plots of S_{11} , Figure 4.5 and Figure 4.6, respectively, it is seen that a resonance exists around 95 MHz. The measured data of the table / wire harness antenna system is very similar to the numerical data calculated in NEC

and discussed in Chapter 3. A resonance effect exists at 91 MHz in the NEC model, which is a close prediction to the measured 95 MHz value.

The magnitude and phase plots for S_{21} are shown in Figure 4.7 and Figure 4.8, respectively. These measured plots appear much more jagged as a function of frequency than their numerical counterparts found in Chapter 3. However, the general envelope of the magnitude data is similar to the numerical model, and the phase characteristics show a somewhat decreasing linear dependence. A better comparison between the measured and numerical results would be to plot both sets of data on the same figure. This is done for all wire distances in Chapter 5.

Comparing the magnitude and phase data for S_{21} (Figure 4.7 and Figure 4.8, respectively) with the data for S_{12} (Figure 4.9 and Figure 4.10, respectively), it is seen that the two sets of data are nearly identical. Therefore, the reciprocity assumptions inherent in the NEC model are supported by these measured results.

Figure 4.11 and Figure 4.12 show the magnitude and phase characteristics of the measured data for S_{22} . Notice that although the data is less smooth than the numerical results, the measured data shows a resonance at 95 MHz. This is the same result found from the NEC model.

A complete analysis of the experimental results is presented in Chapter 5. The measured results will be directly compared with those found from the NEC model discussed in Chapter 3.

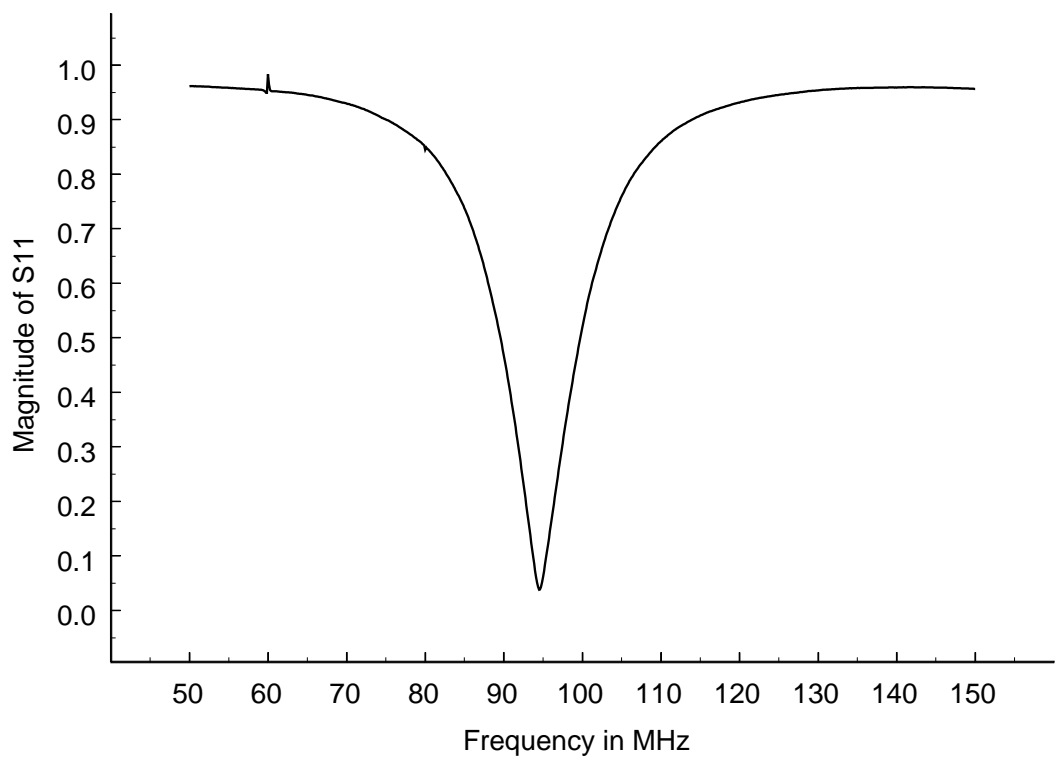


Figure 4.5. Measured magnitude of S_{11} ($d = 10$ cm).

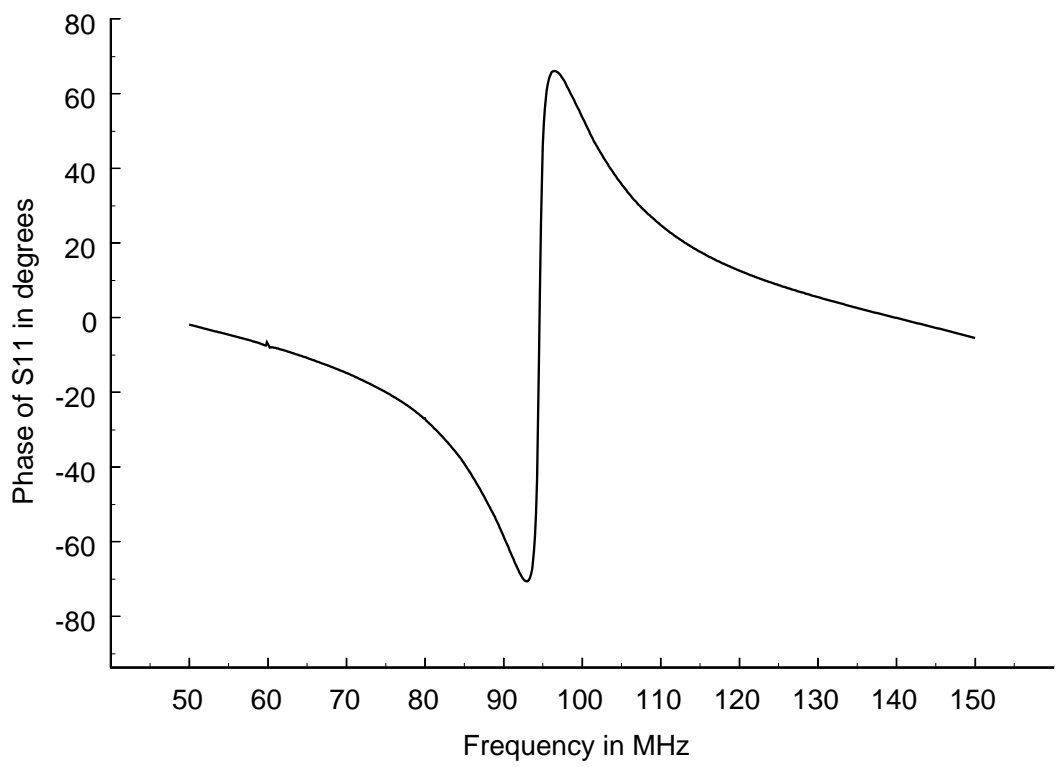


Figure 4.6. Measured phase of S_{11} ($d = 10$ cm).

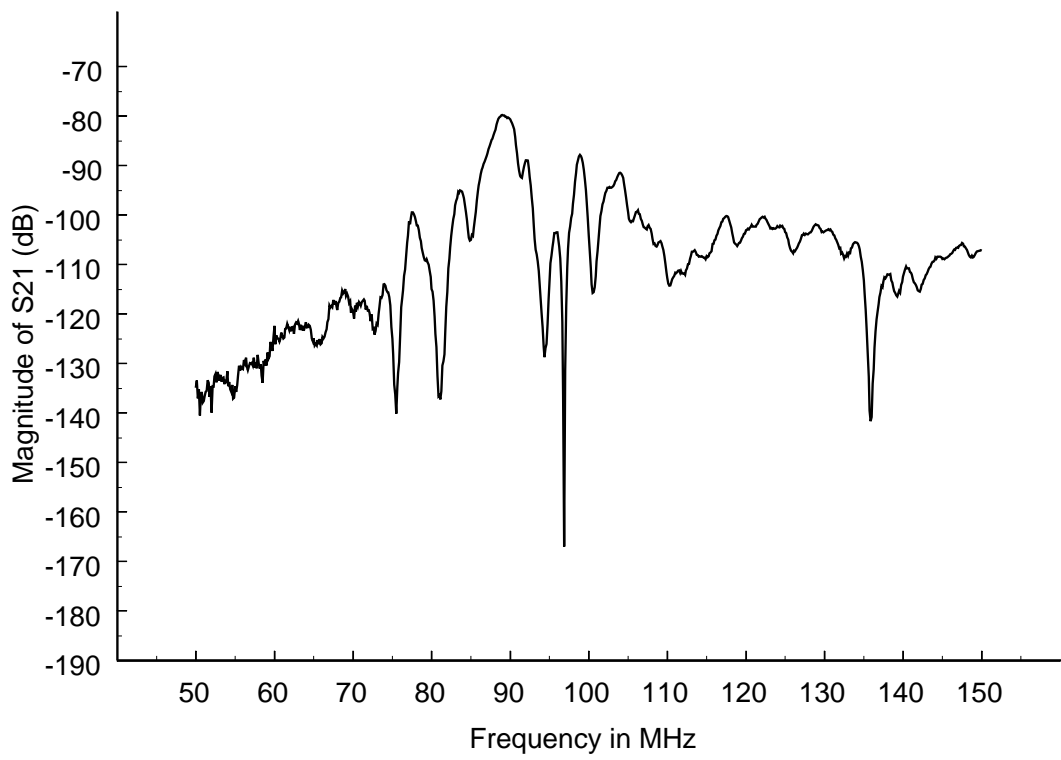


Figure 4.7. Measured magnitude of S_{21} (in dB) ($d = 10$ cm).

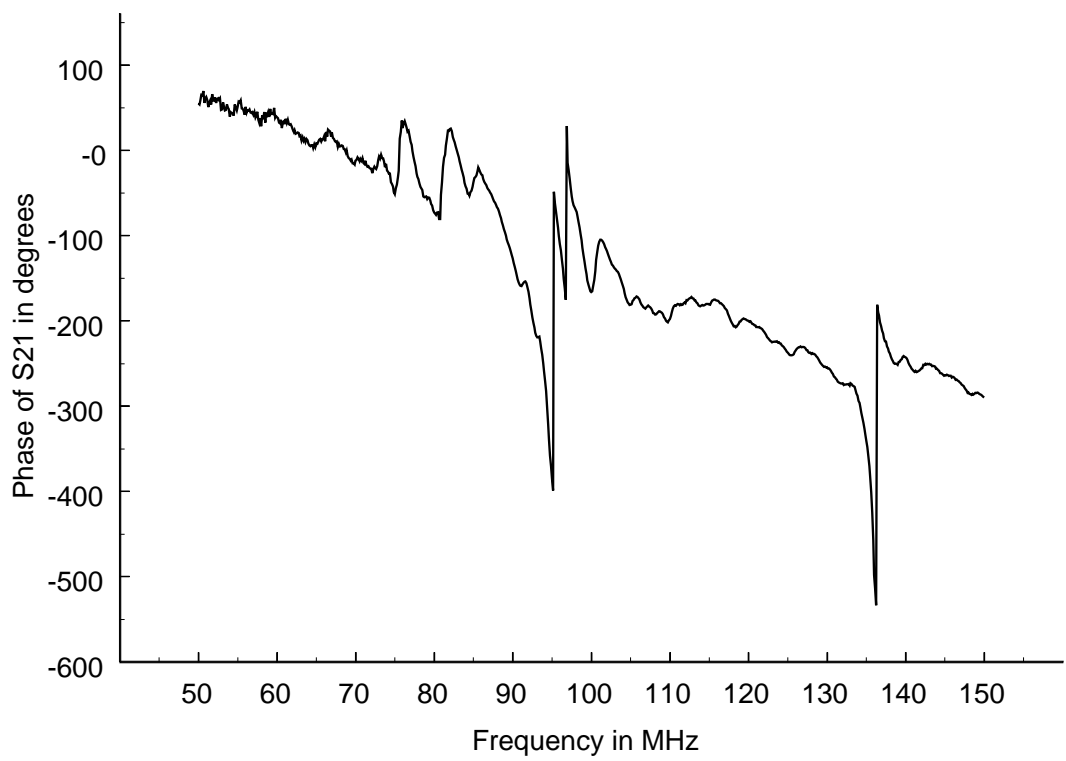


Figure 4.8. Measured phase of S_{21} ($d = 10$ cm).

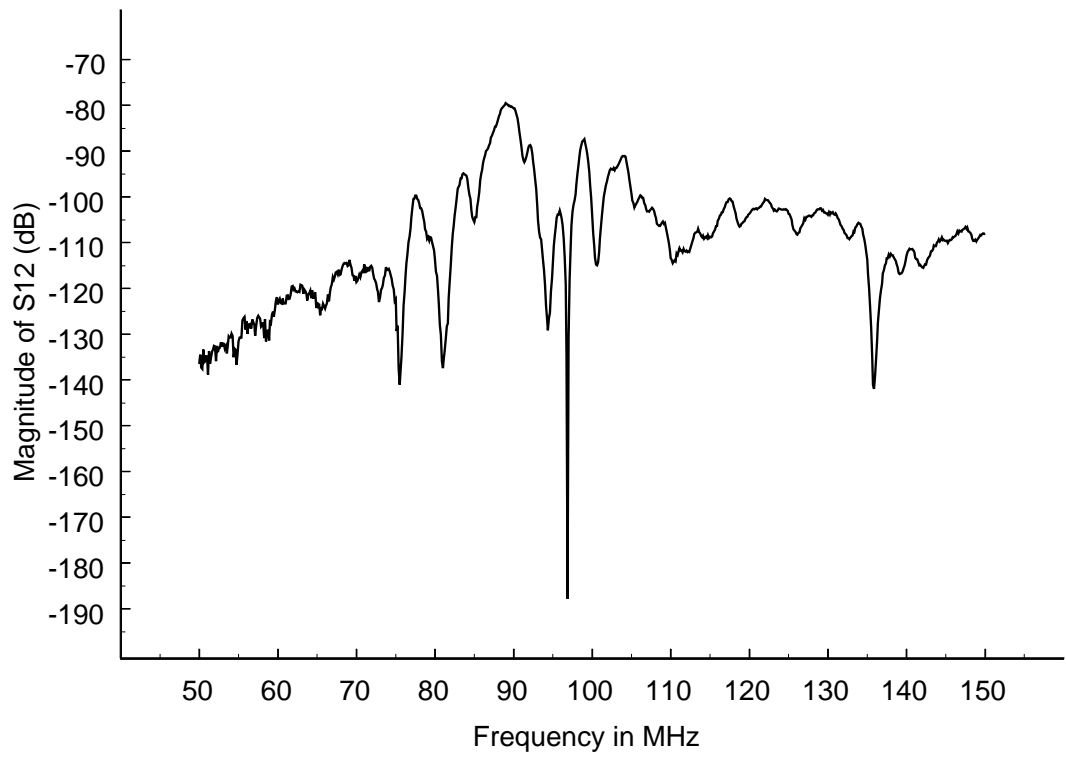


Figure 4.9. Measured magnitude of S_{12} (in dB) ($d = 10$ cm).

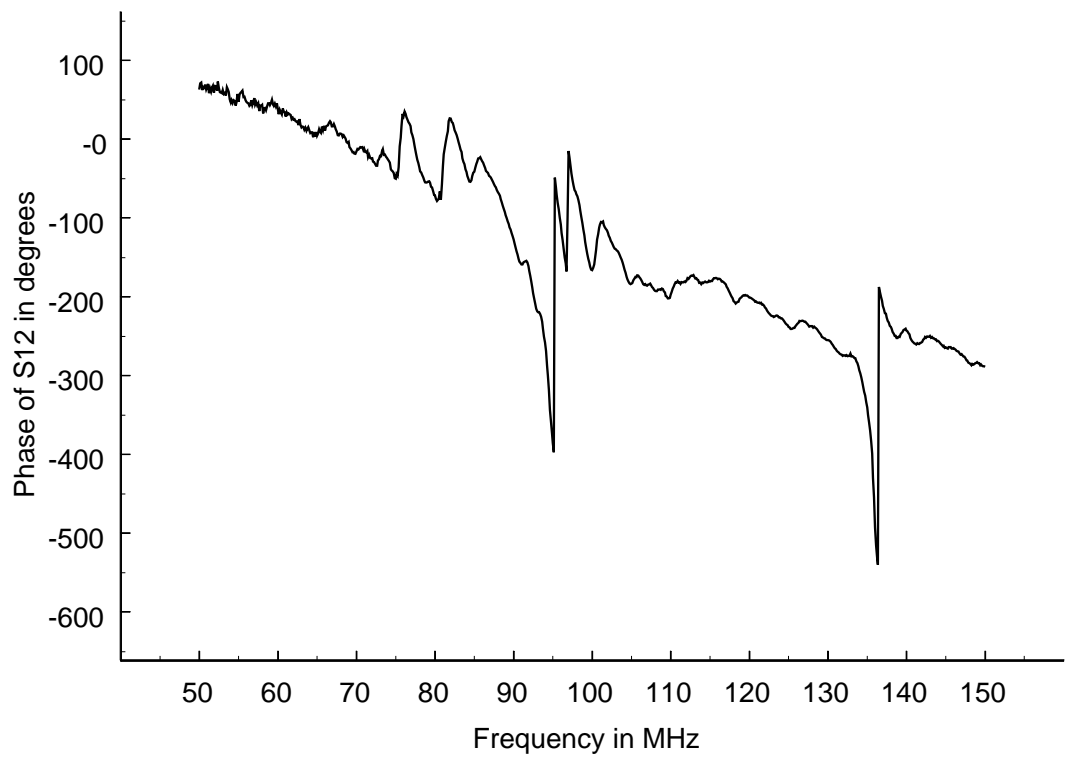


Figure 4.10. Measured phase of S_{12} ($d = 10$ cm).

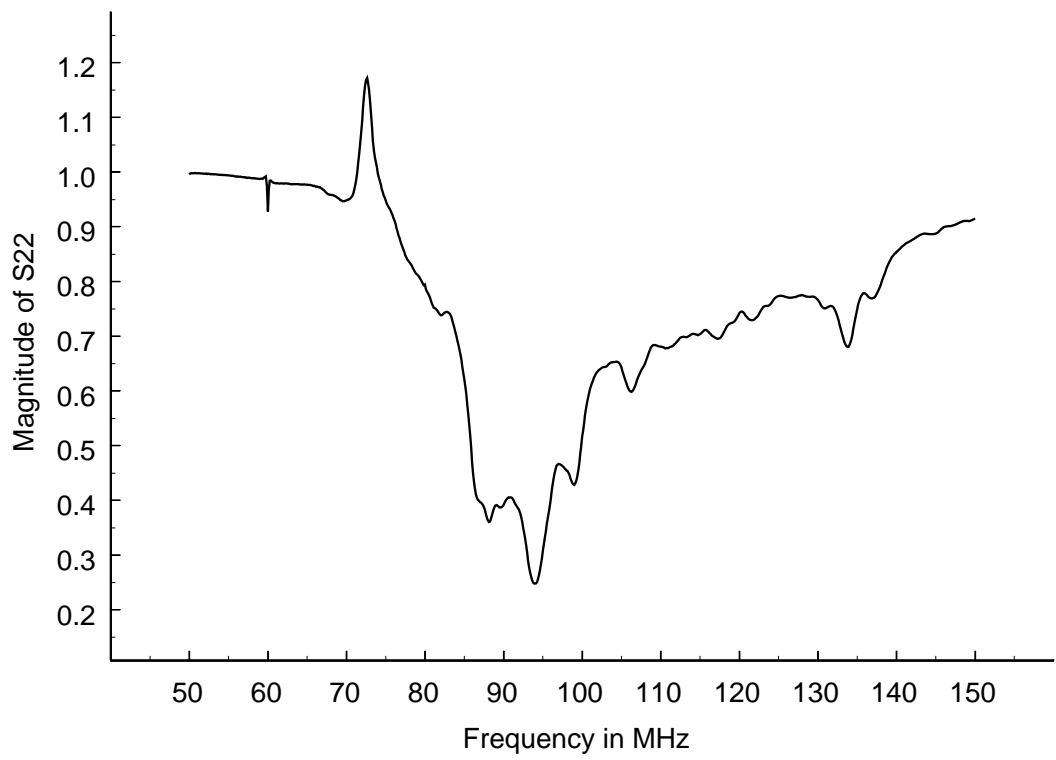


Figure 4.11. Measured magnitude of S_{22} ($d = 10$ cm).

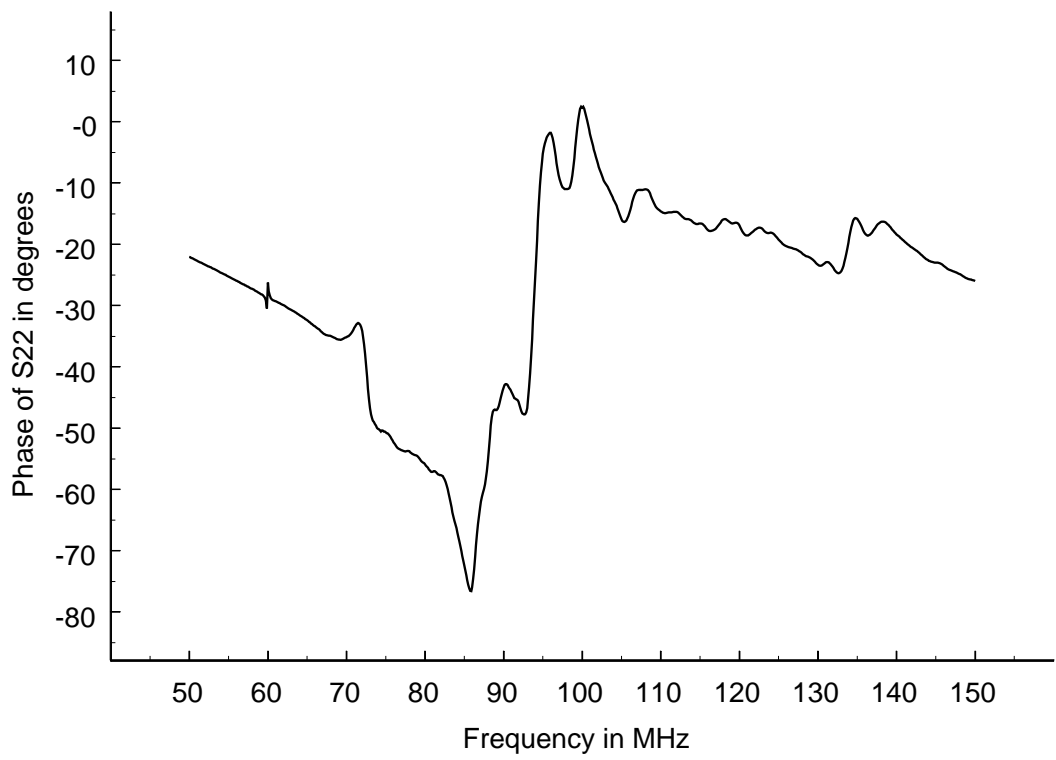


Figure 4.12. Measured phase of S_{22} ($d = 10$ cm).

CHAPTER 5

RESULTS AND ANALYSIS

5.1 Overview

Chapters 3 and 4 discussed the numerical and experimental models of the CISPR 25 testing setup. Numerical and measured S -parameters were obtained for four different positions of the wire harness on the table ($d = 5$ cm, 10 cm, 15 cm, and 20 cm). In addition, three different measurement techniques were tried in order to decide which method should be used.

This chapter will present the data collected from these experimental and numerical models. The three different measurement techniques at one wire harness location ($d = 10$ cm) will be compared in Section 5.2 to determine which measurement method is to be used for the rest of the harness locations. The methods will be evaluated by comparing each set of measured data to the numerical results obtained from the NEC model. The measured S -parameters and the S -parameters found from the NEC model for the remaining wire harness locations using the best measurement method will then be compared in Section 5.3.

5.2 Comparison of Measurement Methods

As discussed in Section 4.2 of Chapter 4, three different measurement methods were used with the wire harness located 10 cm from the table lip to determine the most accurate method. The measured S -parameters for all three methods are presented in this section and compared to the numerical results found by using NEC.

5.2.1 Method 1: Transformer Included in the S -Parameter Measurements

Figure 5.1 through Figure 5.8 display both the measured and numerical S -parameters for a wire harness distance of $d = 10$ cm. The measured results for these S -parameters were found by using measurement Method 1. As discussed in Section 4.2.1, measurement Method 1 used a transformer to balance the potentially unbalanced currents on the cable feeding the dipole antenna, but the method included the transformer as part of the measured network.

Figure 5.1 and Figure 5.2 are the magnitude and phase plots of S_{11} for both the numerical results found using NEC and the measured results found using measurement Method 1. The measured results seem to generally agree with the numerical results over the entire frequency band. Both results show that a large portion of incident energy is coupled into Port 1 only over a small frequency range where S_{11} dips from its larger value to a minimum valley. However, the numerical results predict the frequency of this minimum to occur at around 91 MHz, whereas the measured results show the minimum to occur around 95 MHz. The spectra of the numerical results appears to be shifted down in frequency by about 4 MHz compared to the measured results across the entire frequency band. This is also true for the phase of S_{11} shown in Figure 5.2. The phase of S_{11} indicates a resonance effect as it crosses zero degrees at 91 and 95 MHz for the numerical and measured results, respectively.

The magnitude and phase plots of S_{21} are shown in Figure 5.3 and Figure 5.4, respectively and the magnitude and phase plots of S_{12} are shown in Figure 5.3 and Figure 5.4, respectively for both the numerical results and the measured results found using measurement Method 1. Both the magnitude and the phase of S_{21} are nearly identical to those for S_{12} for both the numerical and the measured results over the entire frequency band. This is expected behavior for a reciprocal network or system. Notice that the measured magnitudes are quickly varying as a function of frequency

over the frequency band, whereas the numerical magnitudes are slowly varying. However, the envelope of the measured magnitudes are close to the envelope of the numerical magnitudes even though the measured results appear ragged. The measured phases also exhibit a ragged behavior over the frequency band in comparison to the numerical phases. Aside from a constant phase shift of about 150 degrees, the measured phases show roughly the same trend as the numerical phases. The constant phase shift could possibly be present due to effects from including the transformer in the measurements.

Figure 5.7 and Figure 5.8 show the magnitude and phase plots, respectively, of S_{22} for both the numerical and measured data. The measured results shown here using measurement Method 1 do not correspond well at all to the numerical results. The phase of S_{22} from the numerical results crosses zero degrees at around 95 MHz and the magnitude of the numerical results shows a minimum at the same frequency, indicating a resonance at 95 MHz. The measured results show no such phenomenon at this frequency. The general trend of the measured curves show no resemblance to those of the numerical curves.

Inadequacies in the correlation between the measured results using measurement Method 1 and the numerical results for S_{22} along with the general ragged behavior of the measured S_{21} and S_{12} results prompted the search for a new measurement method. Since the transformer balun was included in the measurements, perhaps calibrating the balun out of the measurements would improve the dipole antenna's input impedance and the ragged behavior shown in S_{21} and S_{12} would be deemphasized. This was the reason for developing measurement Method 2, described in Section 4.2.2. The measured results found using this method are described in the next subsection.

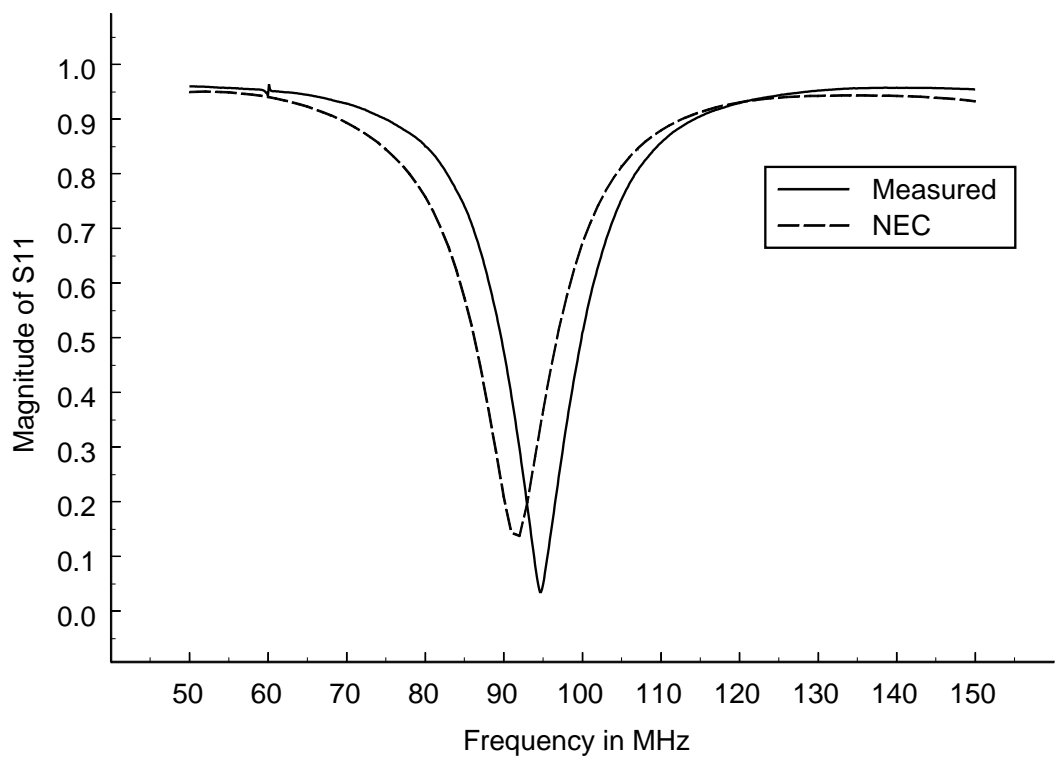


Figure 5.1. Magnitude of S_{11} ($d = 10$ cm) using method 1.

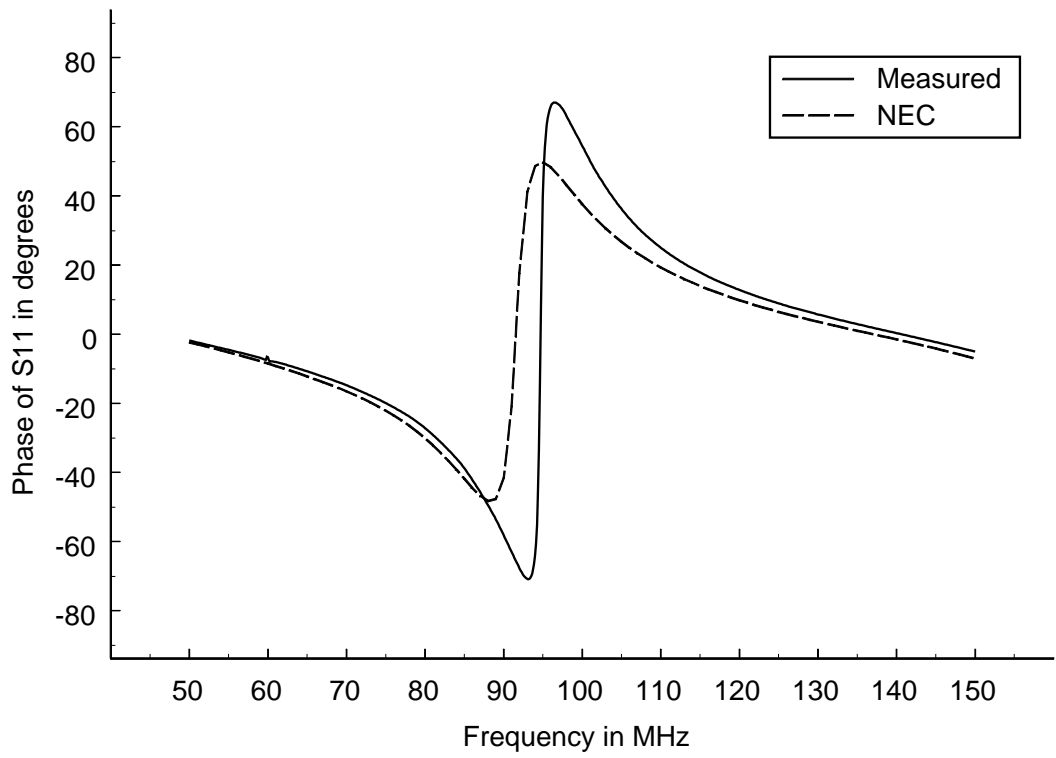


Figure 5.2. Phase of S_{11} ($d = 10$ cm) using method 1.

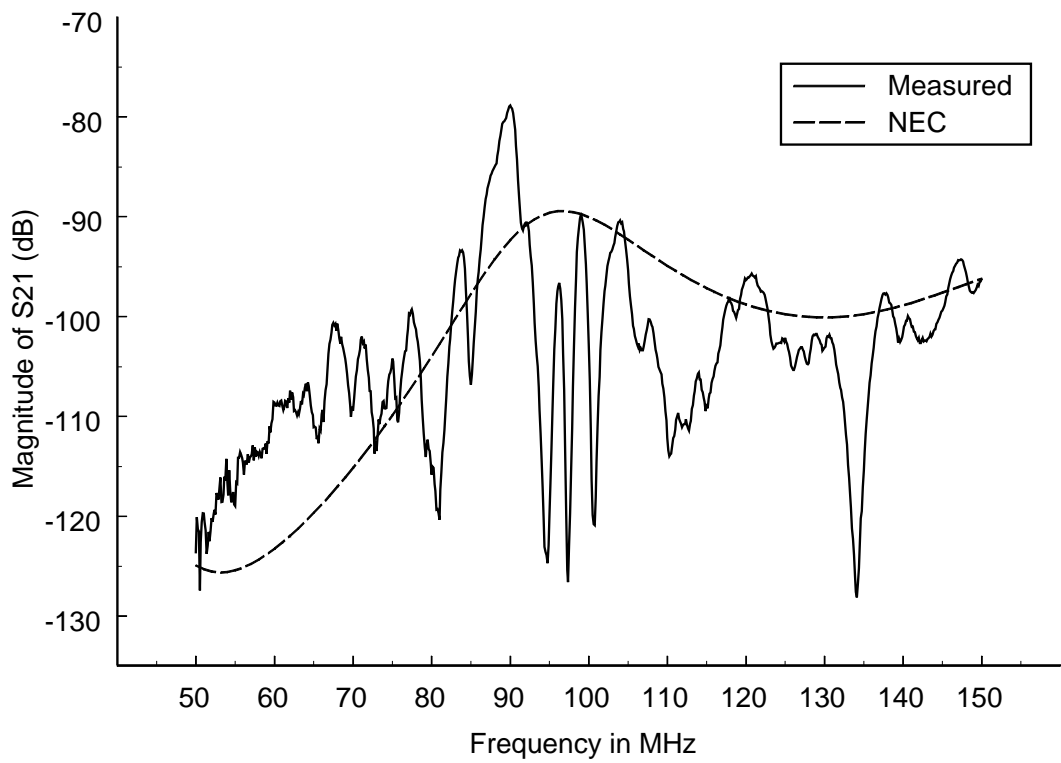


Figure 5.3. Magnitude of S_{21} (in dB) ($d = 10$ cm) using method 1.

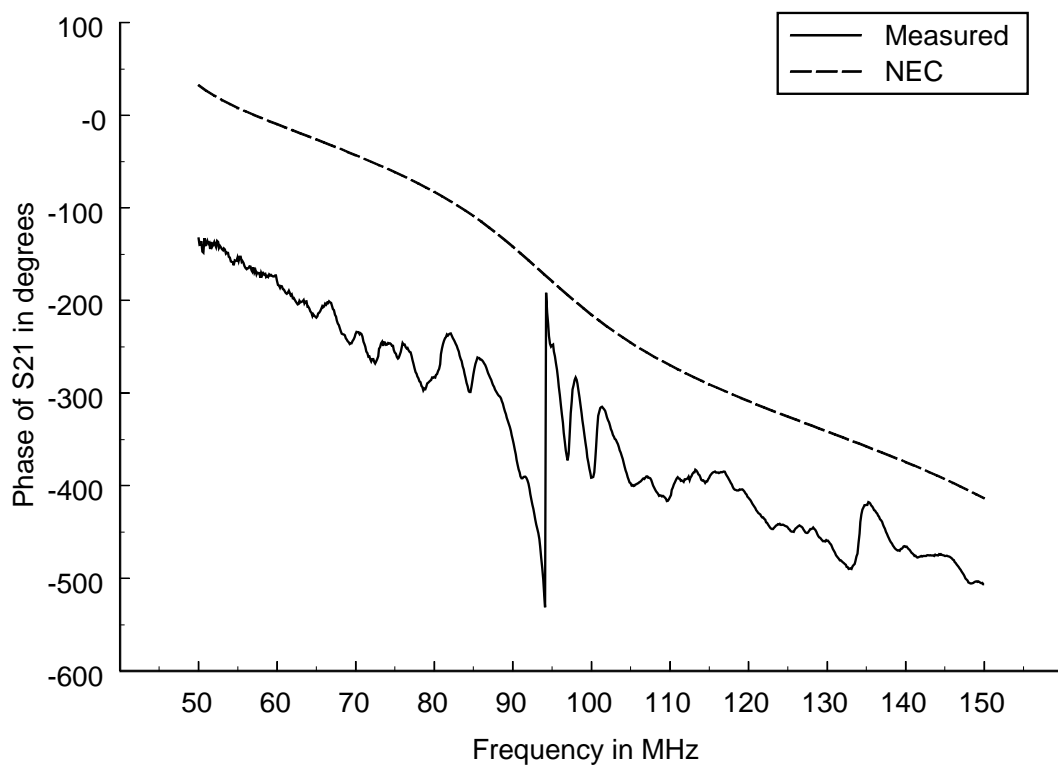


Figure 5.4. Phase of S_{21} ($d = 10$ cm) using method 1.

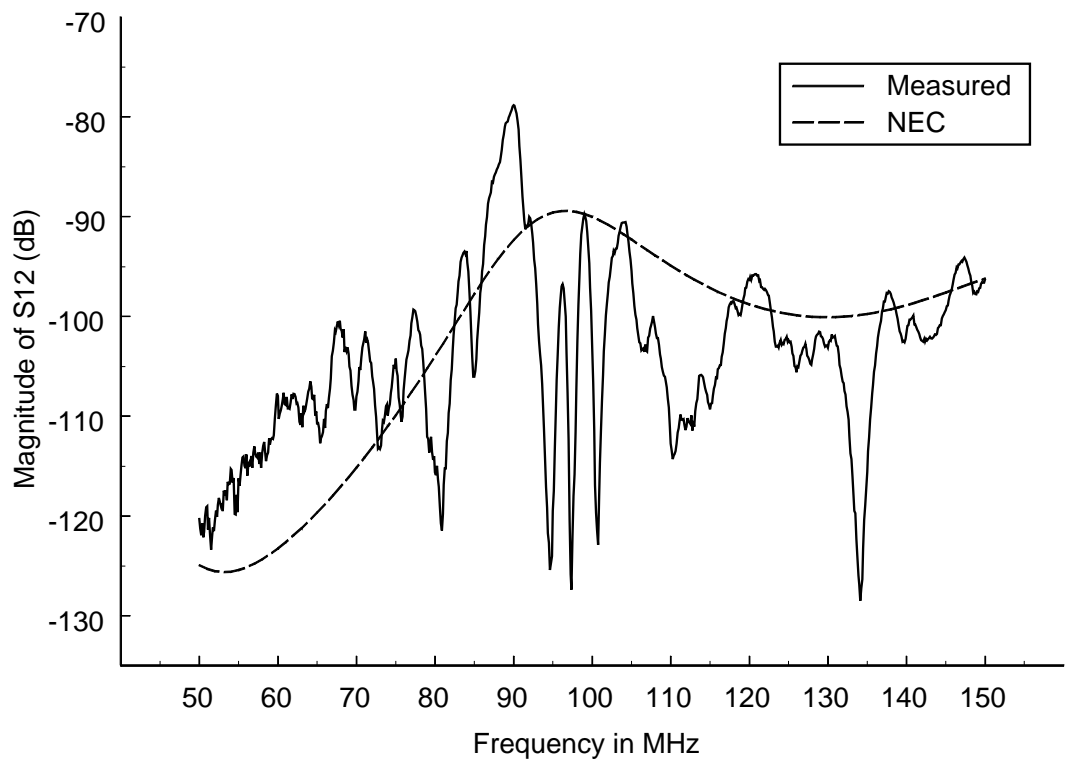


Figure 5.5. Magnitude of S_{12} (in dB) ($d = 10$ cm) using method 1.

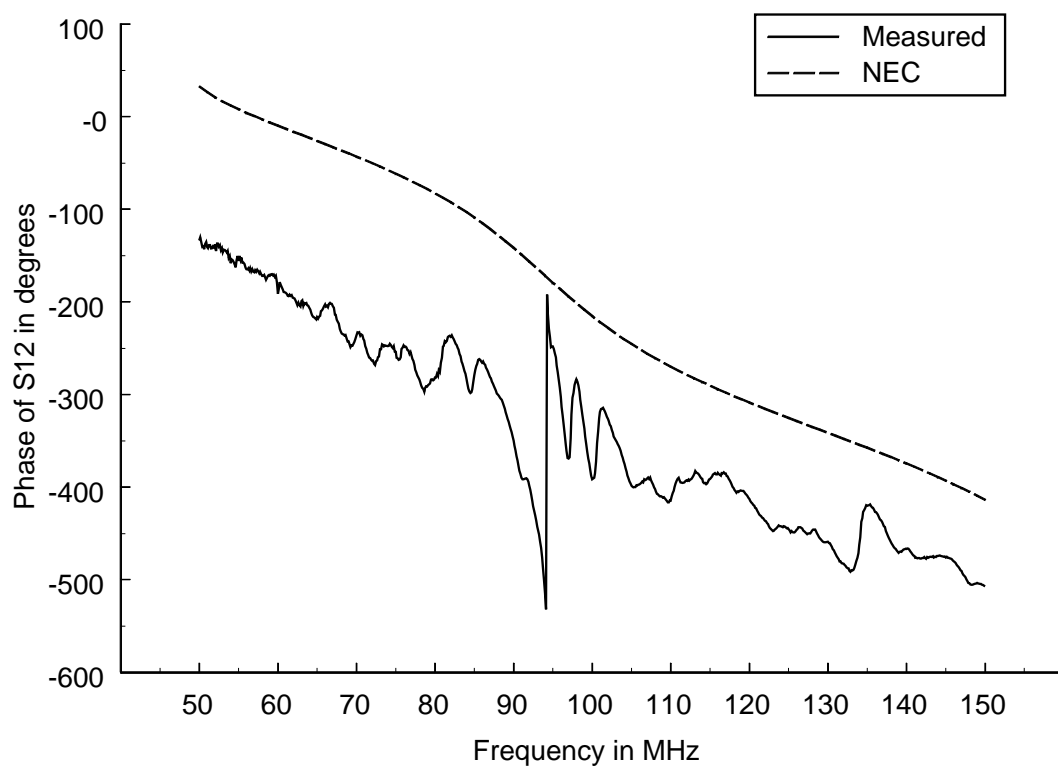


Figure 5.6. Phase of S_{12} ($d = 10$ cm) using method 1.

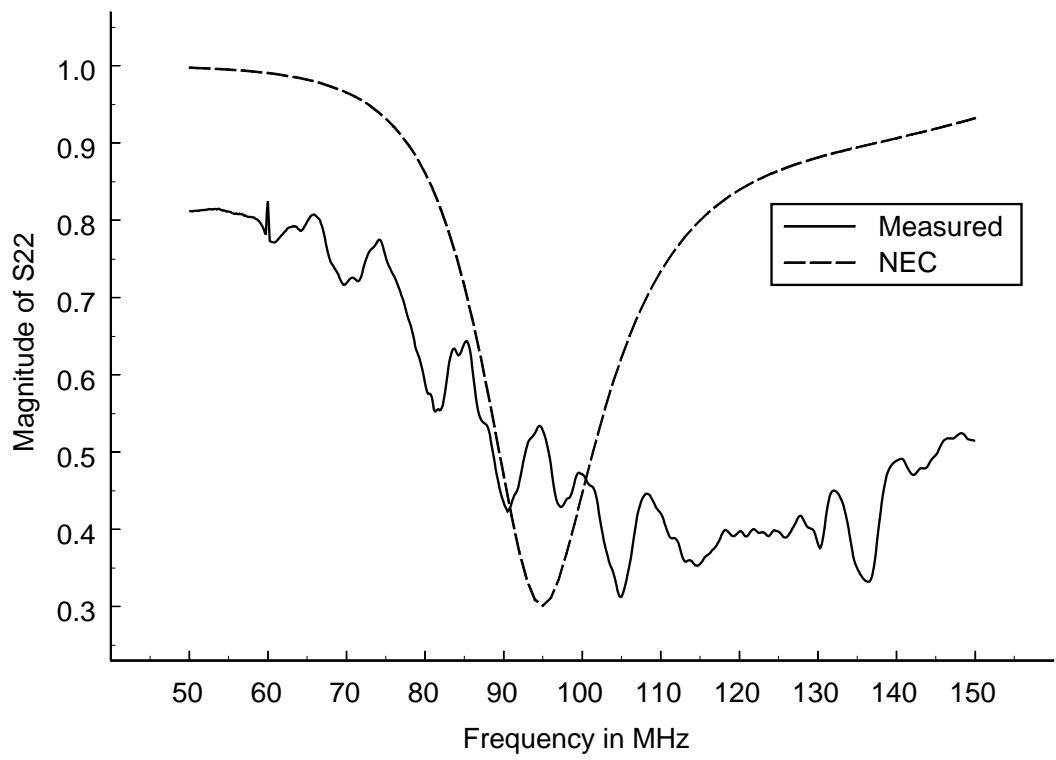


Figure 5.7. Magnitude of S_{22} ($d = 10$ cm) using method 1.

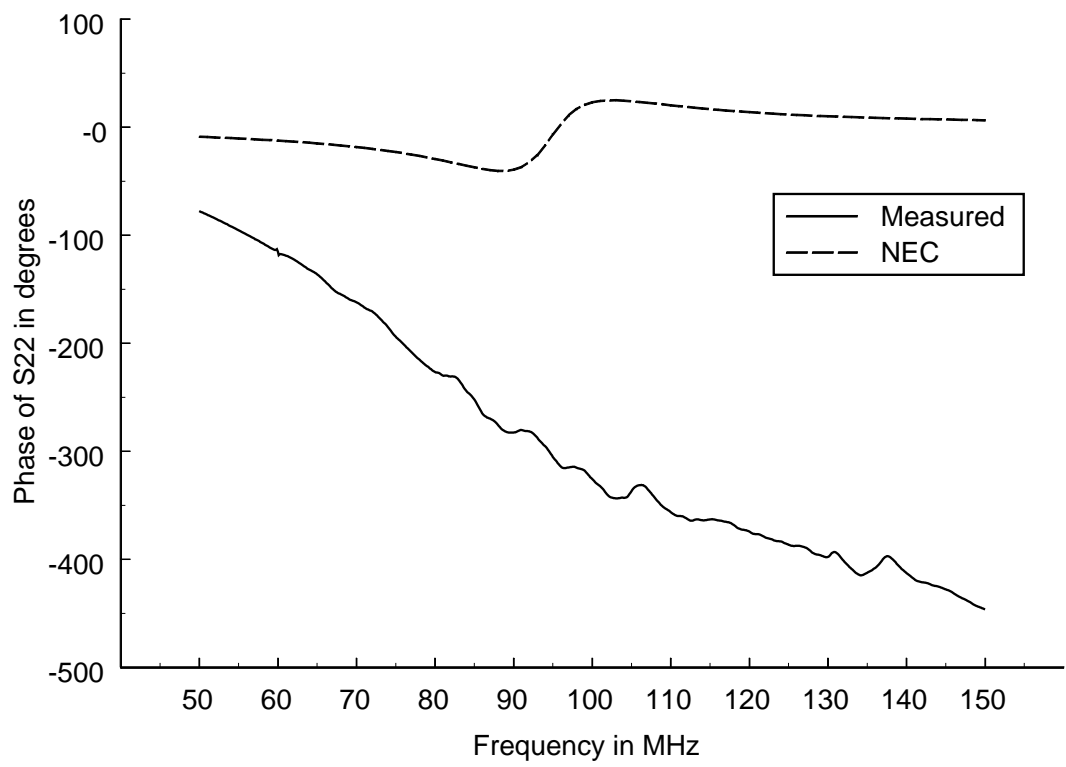


Figure 5.8. Phase of S_{22} ($d = 10$ cm) using method 1.

5.2.2 Method 2: Transformer Calibrated out of the Measurements

Figure 5.9 through Figure 5.16 show the S -parameters of the table-antenna system with a wire harness distance of $d = 10$ cm for both numerical results and measured results found using measurement Method 2. This measurement method was performed by moving the calibration plane for Port 2 as close to the dipole antenna's feed point as possible in such a way to remove the impedance and network characteristics of the transformer balun from the measurements while still utilizing the balancing characteristics of the transformer. This method is described in detail in Section 4.2.2.

Figure 5.9 and Figure 5.10 show the magnitude and phase plots of S_{11} for the numerical results and the measured results found using measurement Method 2. The measured results for both the magnitude and phase again follow the general trend of the numerical results but occurring about 4 MHz higher than the numerical results. The measured results using Method 2 are nearly identical to those found using Method 1. This is because the feed and the calibration plane to Port 1 was not changed from Method 1 to Method 2.

The magnitude and phase plots of S_{21} are shown in Figure 5.11 and Figure 5.12, respectively, and the magnitude and phase plots of S_{12} are shown in Figure 5.13 and Figure 5.14, respectively for both numerical and measured results. As in the results shown using Method 1, these results found using Method 2 indicate that $S_{21} = S_{12}$ over the entire frequency band, indicating a reciprocal system. The magnitudes found using Method 2, however, follow the numerical results much more closely than those found using Method 1. Although the results found using Method 2 are still quickly varying over the frequency band, much of the rapidly varying deviations has been reduced from the measured results found using Method 1. The measured phases found using Method 2 also provide a better match to the numerical results than those found using Method 1. A constant phase shift between the numerical and measured data still exists across the frequency band, but it is much smaller than the

one found using Method 1. This implies that the phase shift due to the transformer has been removed from the measured data.

Figure 5.15 and Figure 5.16 show the magnitude and phase curves of S_{22} for both numerical and measured data. Notice for Method 2 that the measured magnitude results are very close to those found numerically, unlike the results found using Method 1. Some quickly varying deviations still exist over the frequency band, but the general trends of the measured results and the numerical results are similar. This is also true for the phase curve, except that a constant phase shift does exist across the band.

The measured results found using Method 2 match the numerical results more closely than the measured results found using Method 1. A third measurement method was also performed using no balancing transformer. The results using this measurement method are discussed in the next subsection.

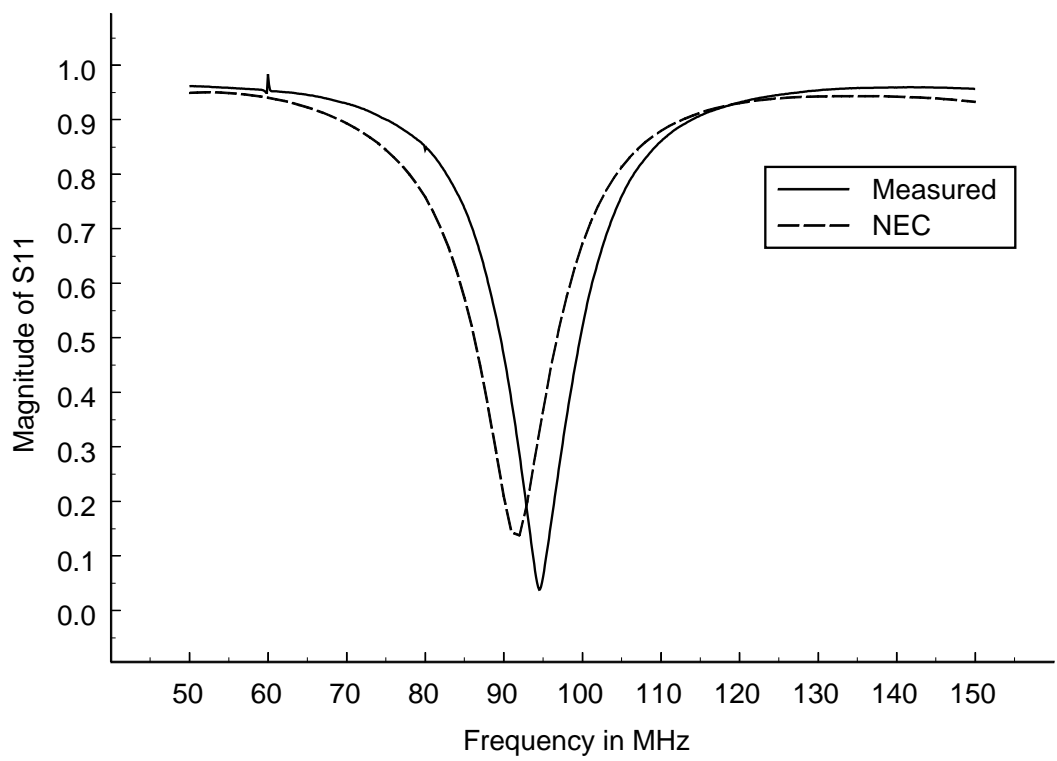


Figure 5.9. Magnitude of S_{11} ($d = 10$ cm) using method 2.

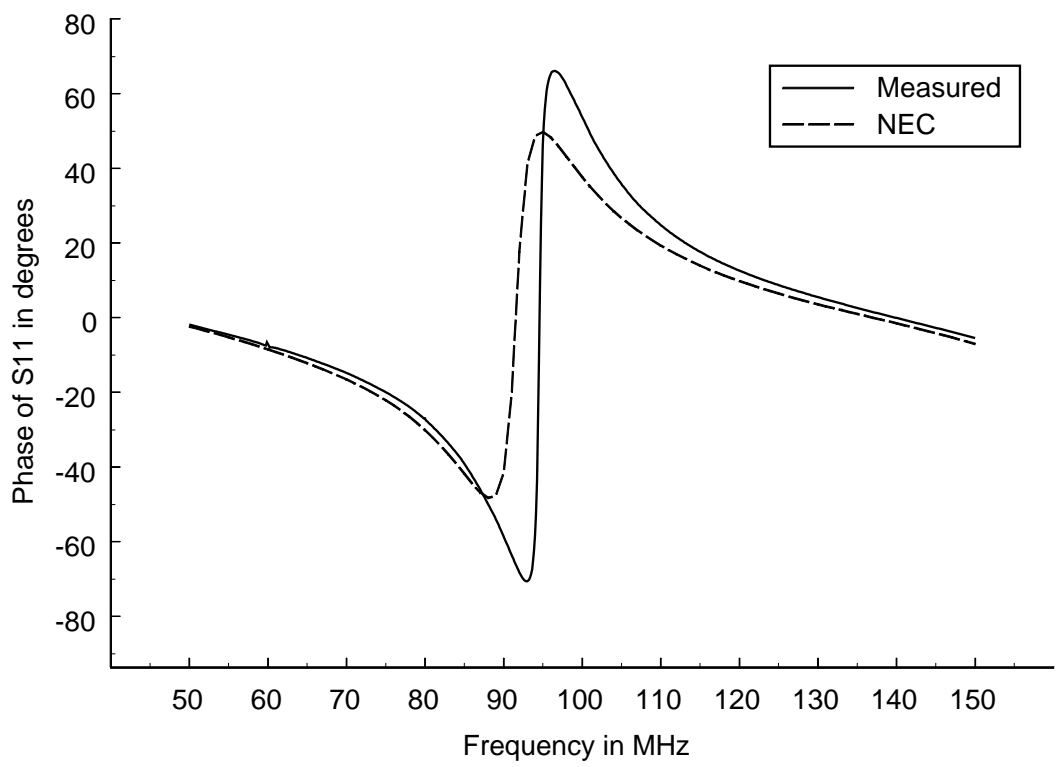


Figure 5.10. Phase of S_{11} ($d = 10$ cm) using method 2.

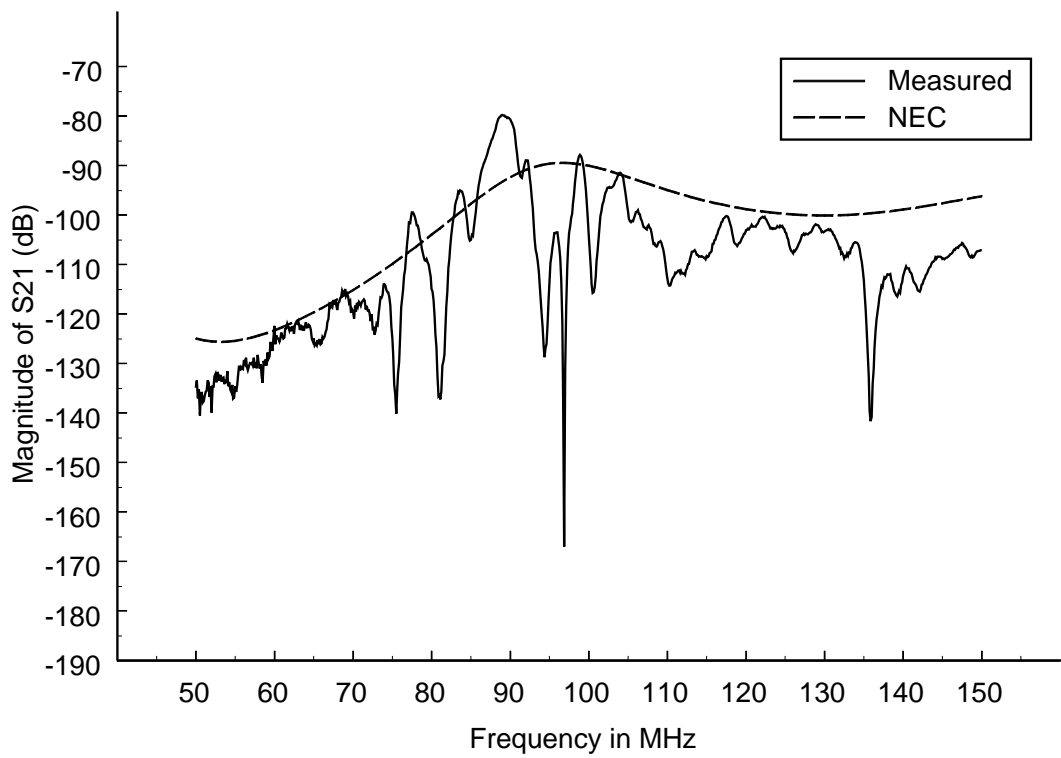


Figure 5.11. Magnitude of S_{21} (in dB) ($d = 10$ cm) using method 2.

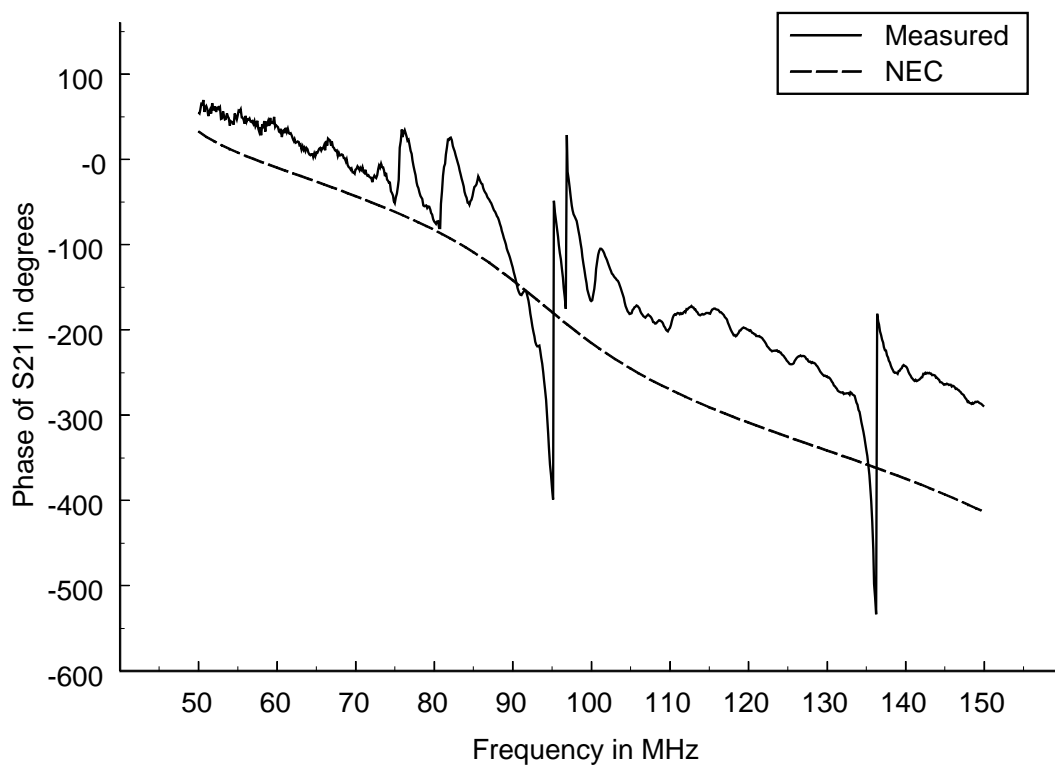


Figure 5.12. Phase of S_{21} ($d = 10$ cm) using method 2.

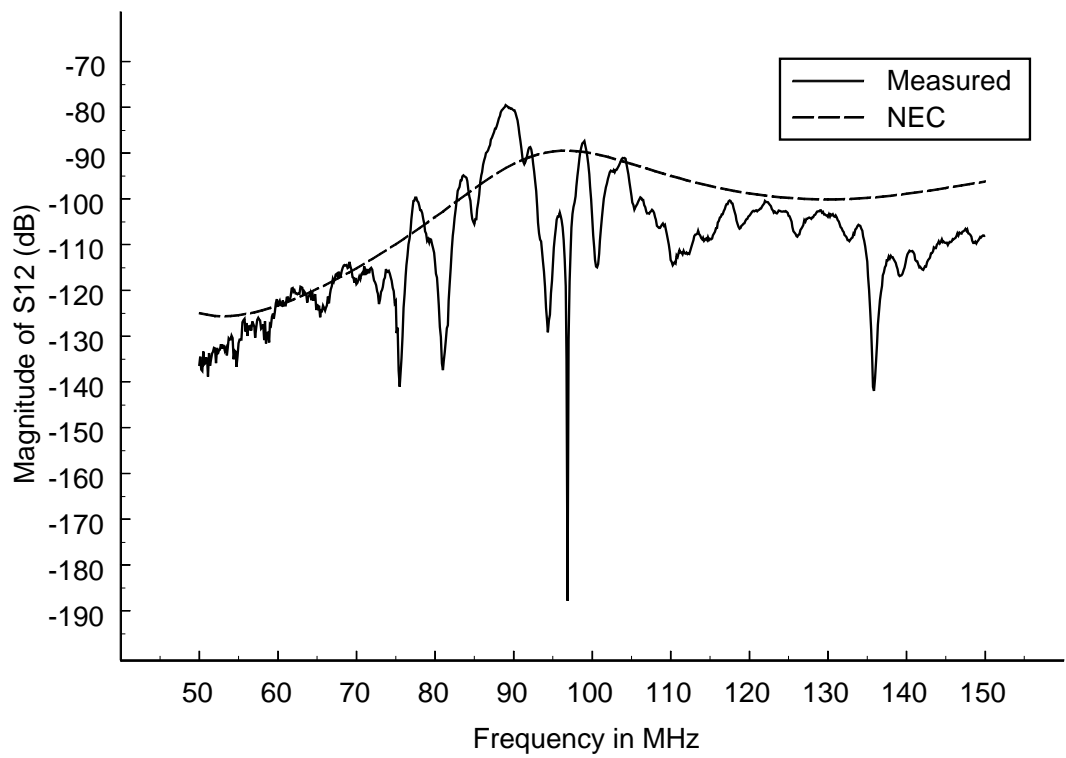


Figure 5.13. Magnitude of S_{12} (in dB) ($d = 10$ cm) using method 2.

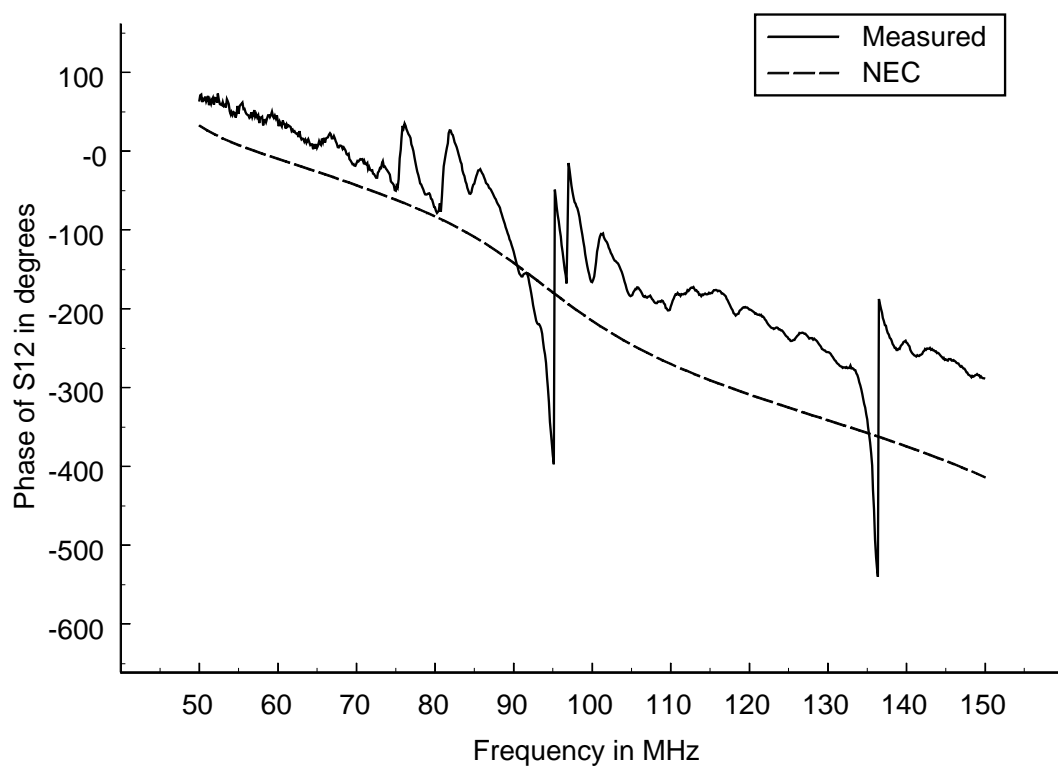


Figure 5.14. Phase of S_{12} ($d = 10$ cm) using method 2.

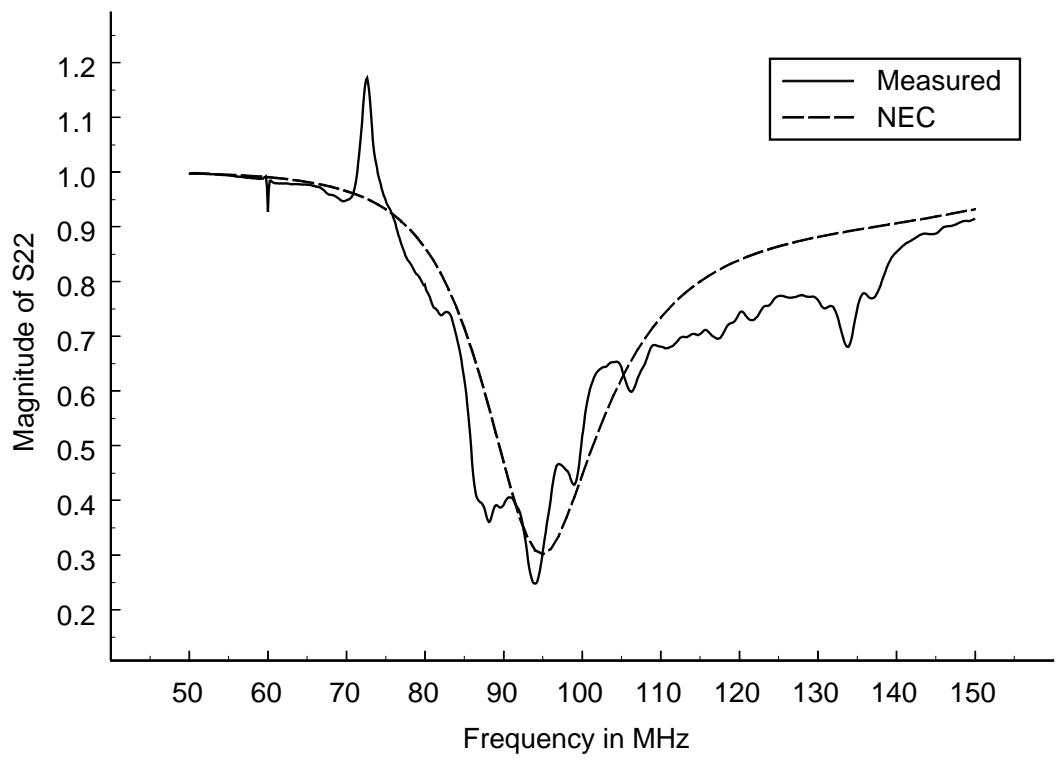


Figure 5.15. Magnitude of S_{22} ($d = 10$ cm) using method 2.

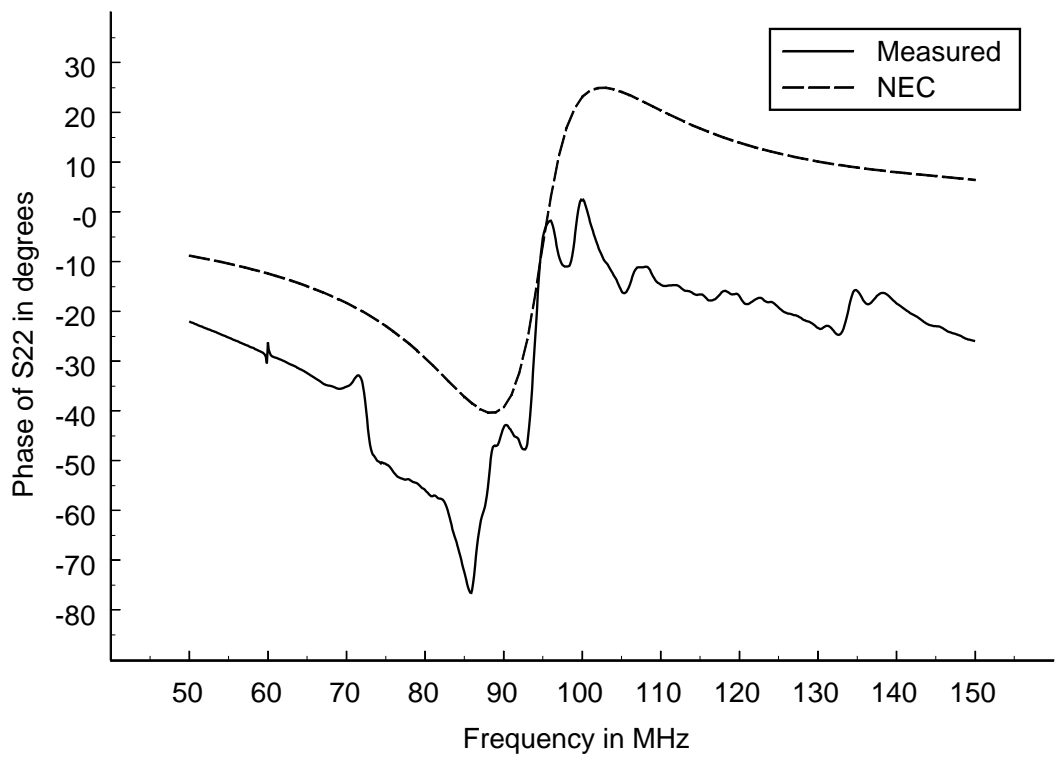


Figure 5.16. Phase of S_{22} ($d = 10$ cm) using method 2.

5.2.3 Method 3: Measurement with No Transformer Balun

A third measurement method, Method 3, was discussed in Section 4.2.3. This measurement method was performed by removing the transformer completely and performing the experiment with the dipole leads connected directly to the inner and outer conductors of the coaxial cable leading to the antenna. The S -parameters measured using Method 3 are plotted along with numerical results found using NEC for a wire harness distance of $d = 10$ cm in Figure 5.17 through Figure 5.24.

Figure 5.17 and Figure 5.18 show the magnitude and phase plots, respectively, of S_{11} for numerical results and results found using measurement Method 3. Notice that the measured magnitude and phase for Method 3 are very similar to those found using Methods 1 and 2. This is again because the measurement method did not affect the calibration plane or feeding arrangement for Port 1.

The magnitude and phase curves of S_{21} are shown in Figure 5.19 and Figure 5.20, respectively, and the the magnitude and phase curves of S_{12} are shown in Figure 5.21 and Figure 5.22, respectively, for numerical results and measured results using Method 3. The measured magnitudes found using Method 3 are much farther from the numerical results than the other two methods over the entire band. The phase also appears to have more rapidly varying deviations. The resulting effect of the current imbalance shows that Method 3 is inferior to the other methods for measuring S_{21} and S_{12} .

The magnitude and phase plots of S_{22} are shown in Figure 5.23 and Figure 5.24, respectively. Notice that the results found using Method 3 were better at following the numerical predictions for the magnitude than those found using Method 1, but not as close as those using Method 2. A large deviation between the numerical prediction and the measured magnitude using Method 3 can be seen at around 140 MHz when the measured magnitude dips considerably. This is probably due to imbalanced currents on the coaxial cable leading to the dipole antenna. The phase curve is also

an improvement over the measured found using Method 1.

After comparing all three measurement methods with the numerical results found from NEC, it is evident that Method 2 is the superior measurement method. The results found using this method follow the numerical results the closest for the magnitudes and phases of all of the S -parameters. Therefore, the measured results will be presented along with corresponding numerical results for the remaining wire harness distances studied only for measurement Method 2. These results are presented in the next section.

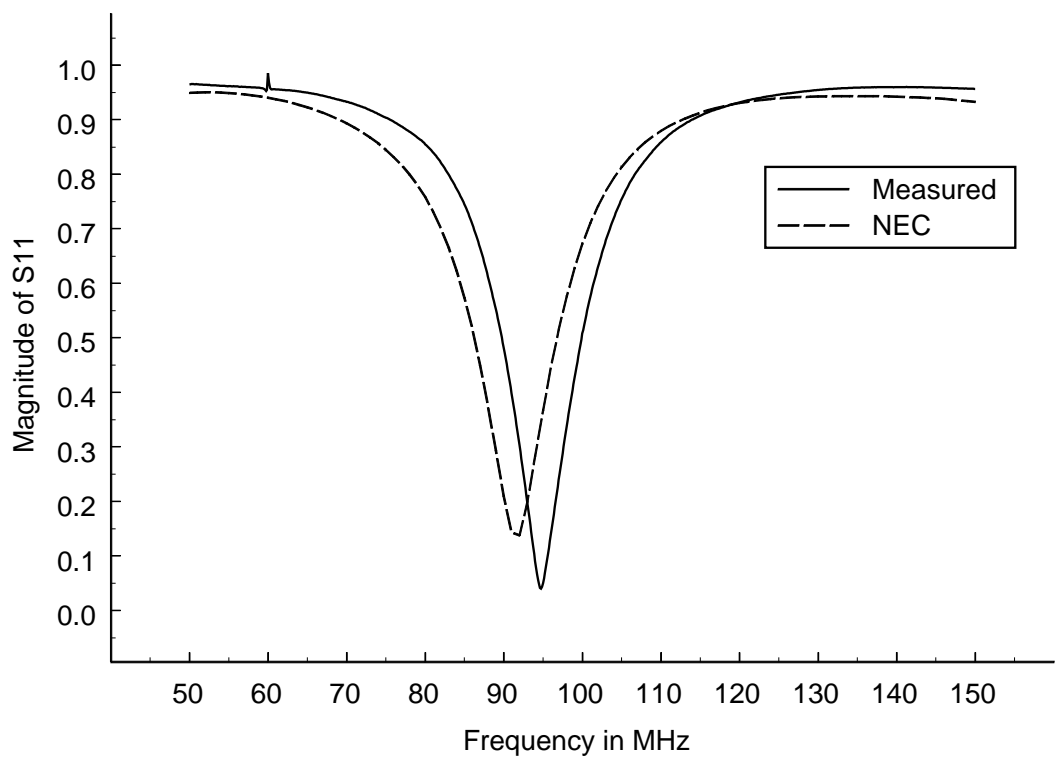


Figure 5.17. Magnitude of S_{11} ($d = 10$ cm) using method 3.

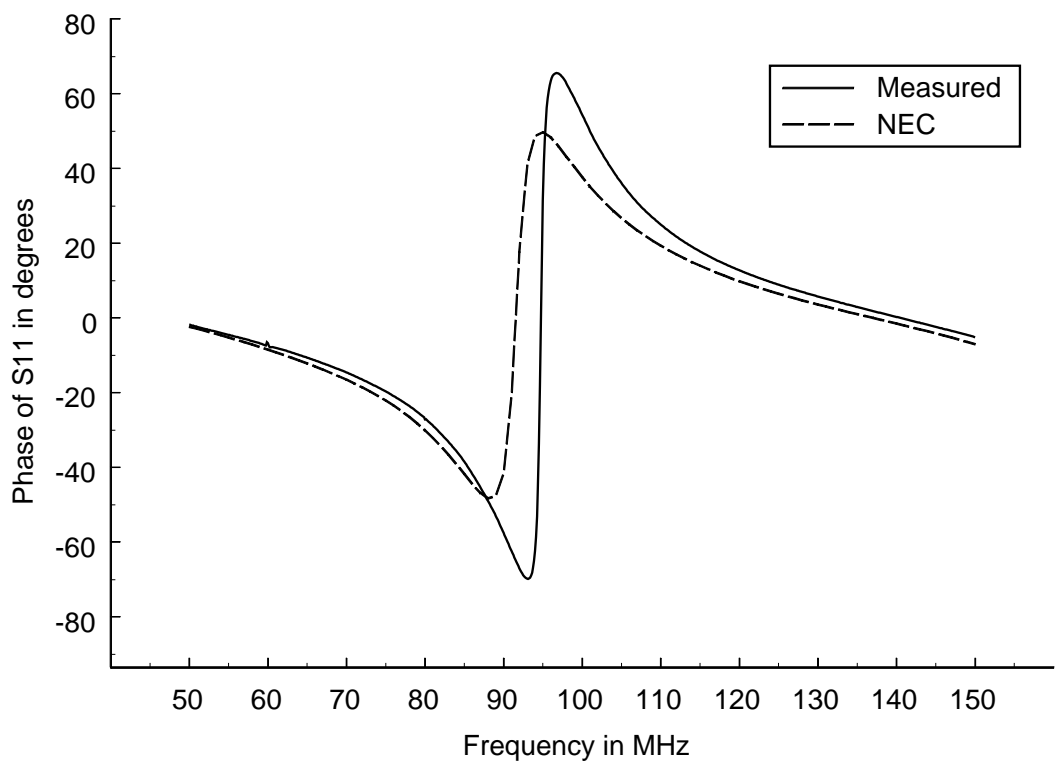


Figure 5.18. Phase of S_{11} ($d = 10$ cm) using method 3.

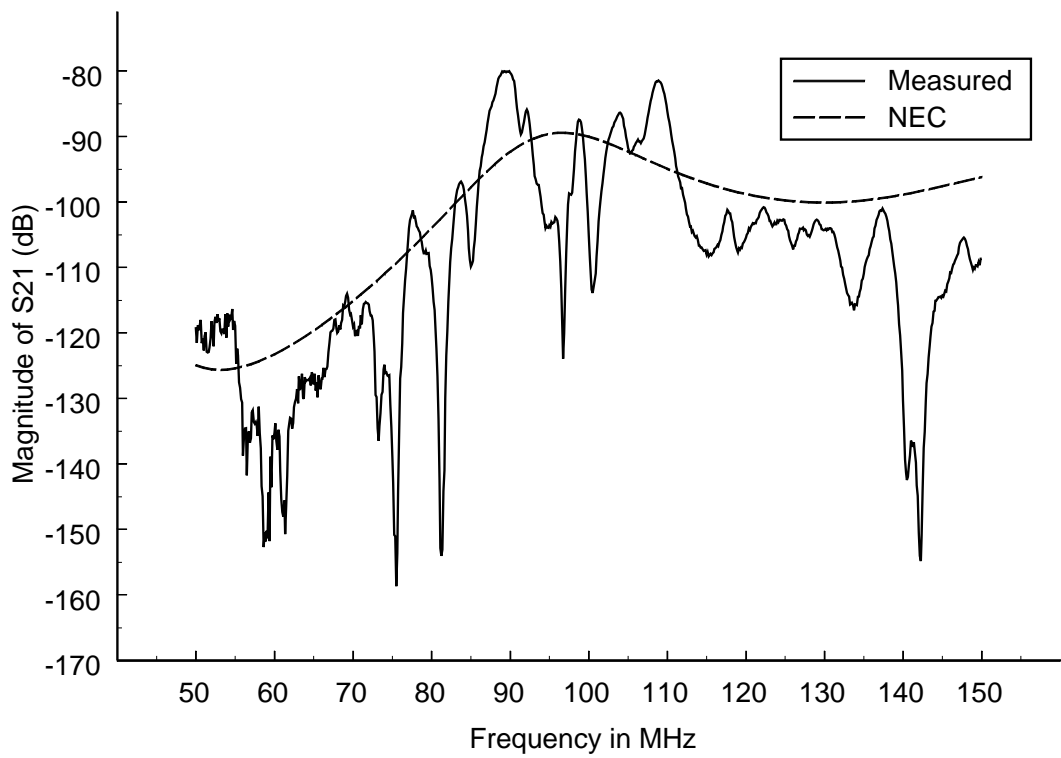


Figure 5.19. Magnitude of S_{21} (in dB) ($d = 10$ cm) using method 3.

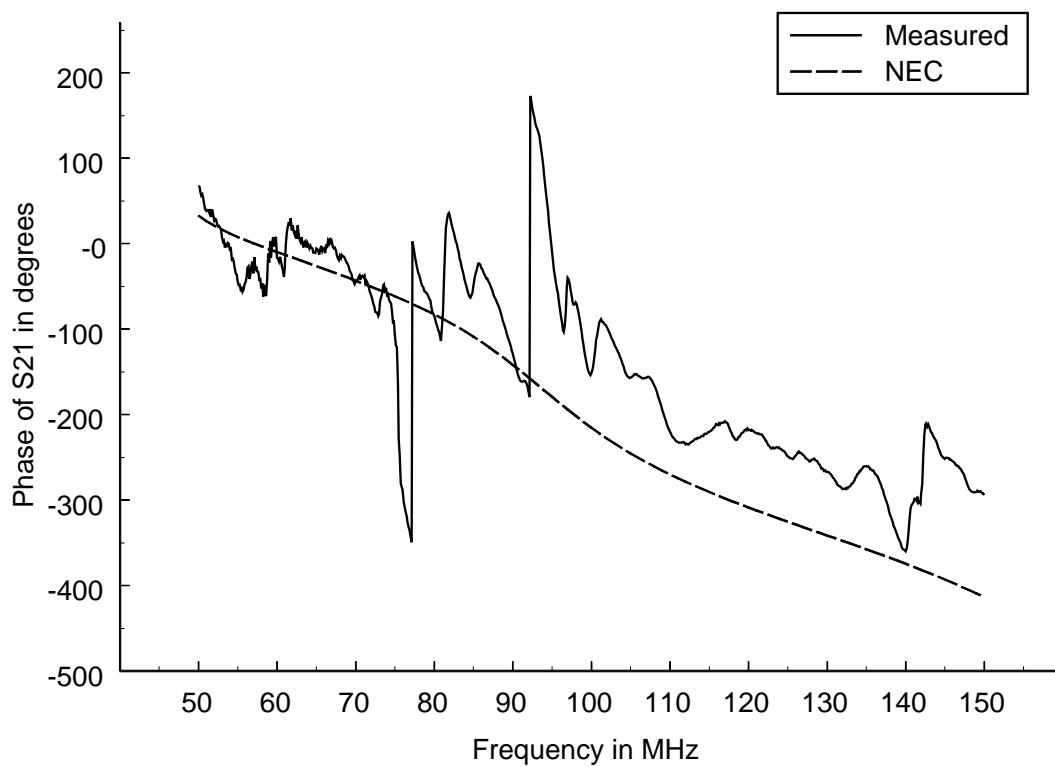


Figure 5.20. Phase of S_{21} ($d = 10$ cm) using method 3.

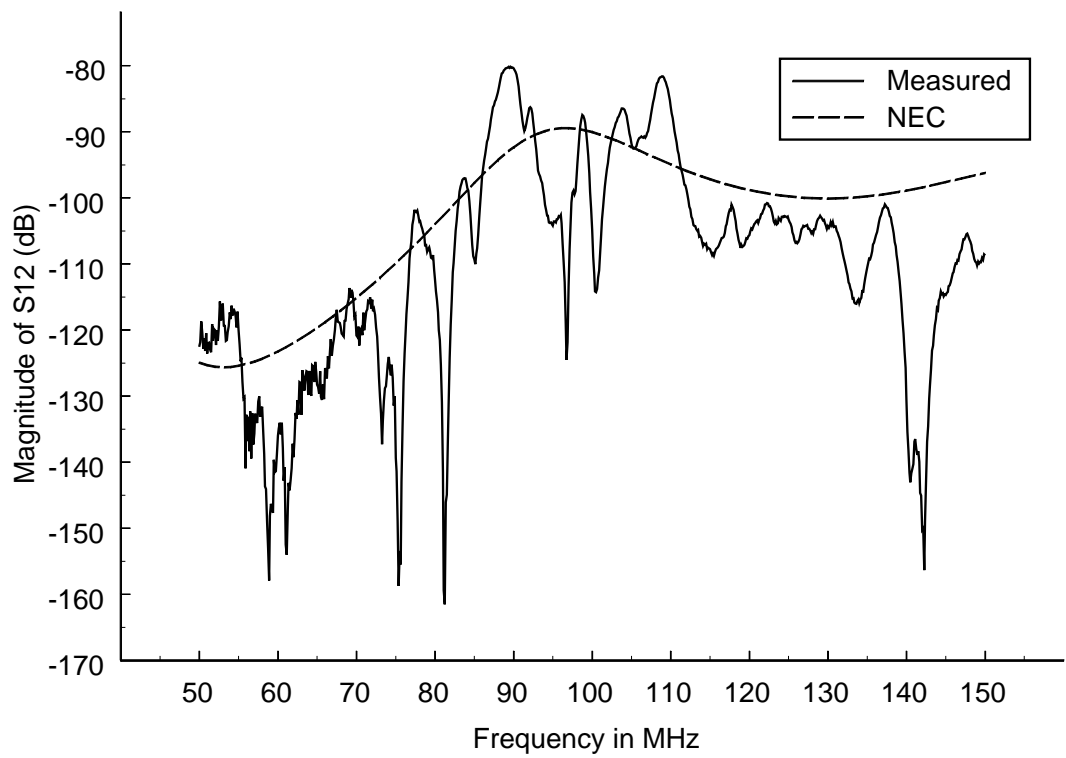


Figure 5.21. Magnitude of S_{12} (in dB) ($d = 10$ cm) using method 3.

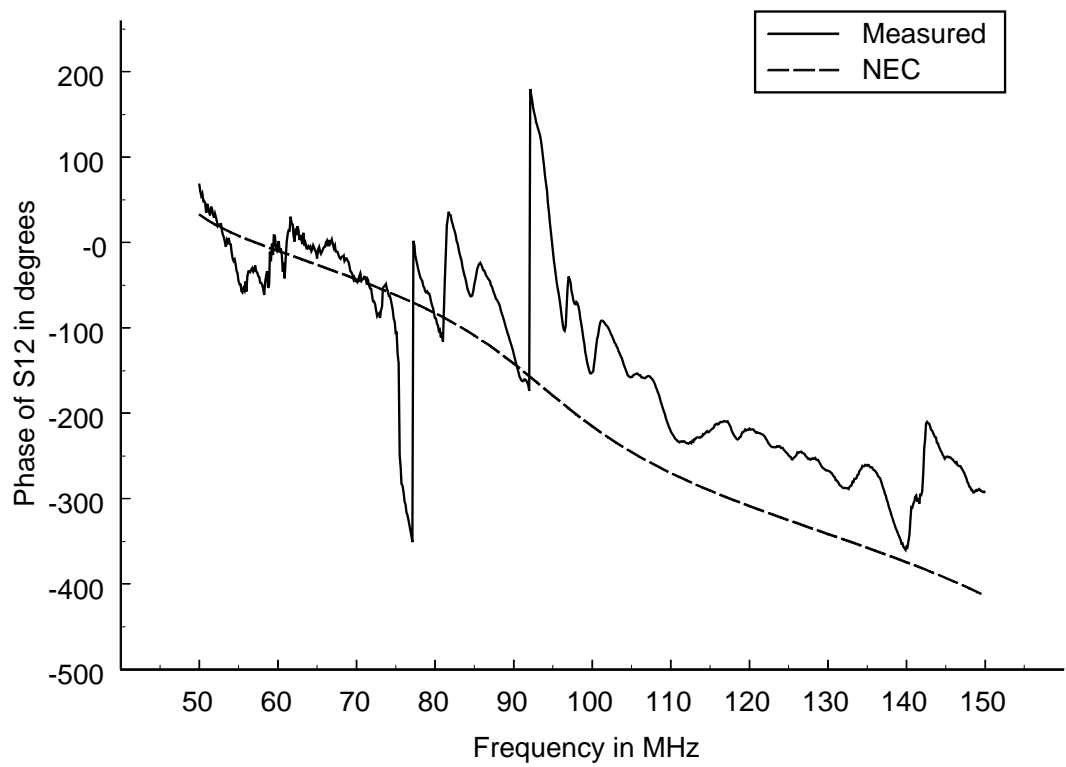


Figure 5.22. Phase of S_{12} ($d = 10$ cm) using method 3.

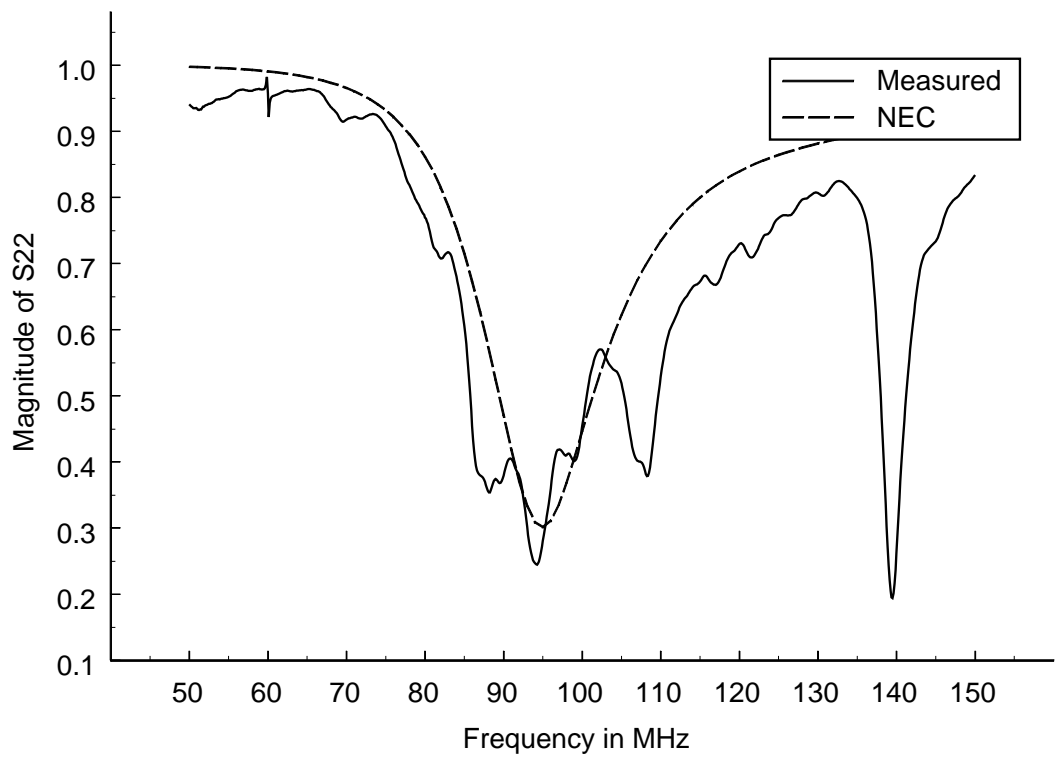


Figure 5.23. Magnitude of S_{22} ($d = 10$ cm) using method 3.

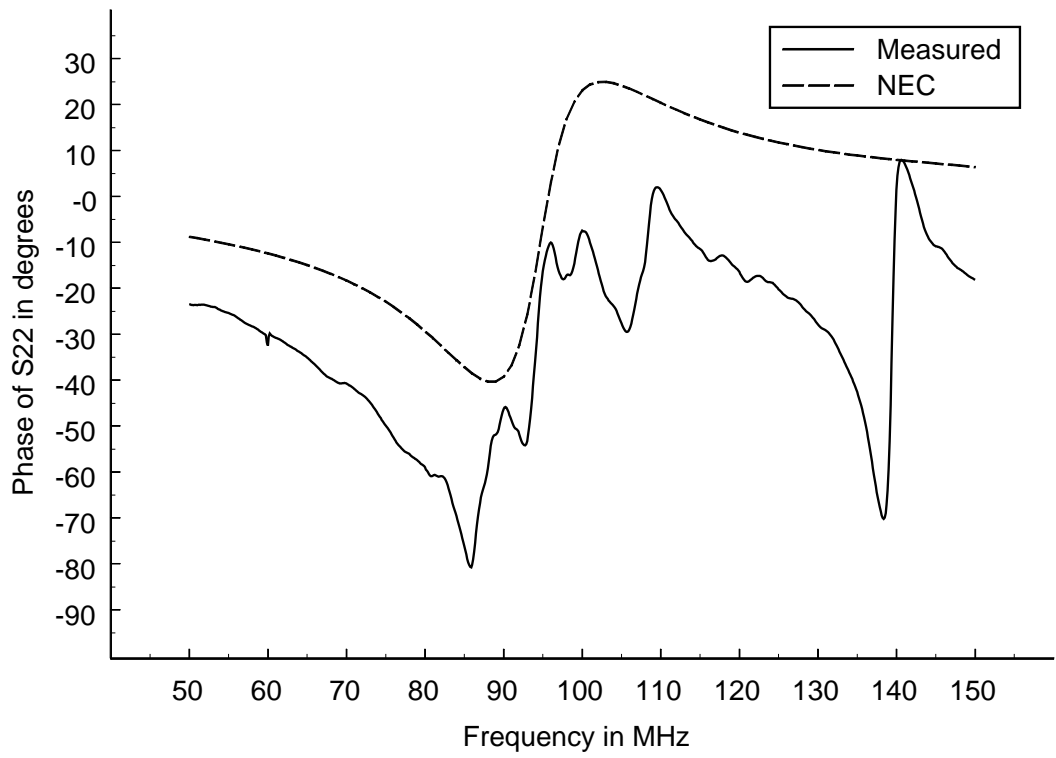


Figure 5.24. Phase of S_{22} ($d = 10$ cm) using method 3.

5.3 Comparison of Measured Results to Numerical Results

In the previous section, it was determined that Method 2 was the superior measurement method, and that this method would be used to obtain the measured data for the remaining wire harness locations studied. In this section, these measured results found using Method 2 are presented along with corresponding numerical results.

5.3.1 Results for a Wire Harness Location of $d = 5$ cm

The wire harness location d was changed to 5 cm on the experimental arrangement and the S -parameters of the system were measured using Method 2. New numerical results were also found using NEC after modifying the wire harness location in the numerical model. The magnitudes and phases of the measured and numerical S -parameters can be found in Figure 5.25 through Figure 5.32.

Figure 5.25 and Figure 5.26 show the magnitude and phase plots, respectively, of S_{11} for both the numerical and the measured data. Notice that the the measured resonant frequency remained around 95 MHz, although the resonant frequency found numerically shifted to around 93 MHz. The resonant frequency calculated numerically was previously 91 MHz for the $d = 10$ cm case. Other than this slight shift, the $d = 5$ cm results for S_{11} were very similar to those found for the $d = 10$ cm case.

The magnitude and phase curves of S_{21} are shown in Figure 5.27 and Figure 5.28, respectively, and the the magnitude and phase curves of S_{12} are shown in Figure 5.29 and Figure 5.30, respectively, for both the numerical and measured data taken for $d = 5$ cm. Notice that the magnitudes and phases of the measured data follow those of the numerical data similarly to the $d = 10$ cm case.

Figure 5.31 and Figure 5.32 show the numerical and measured data of the magnitude and phase of S_{22} , respectively. The measured results follow the numerical results similarly to the $d = 10$ cm case for both the magnitude and phase of S_{22} .

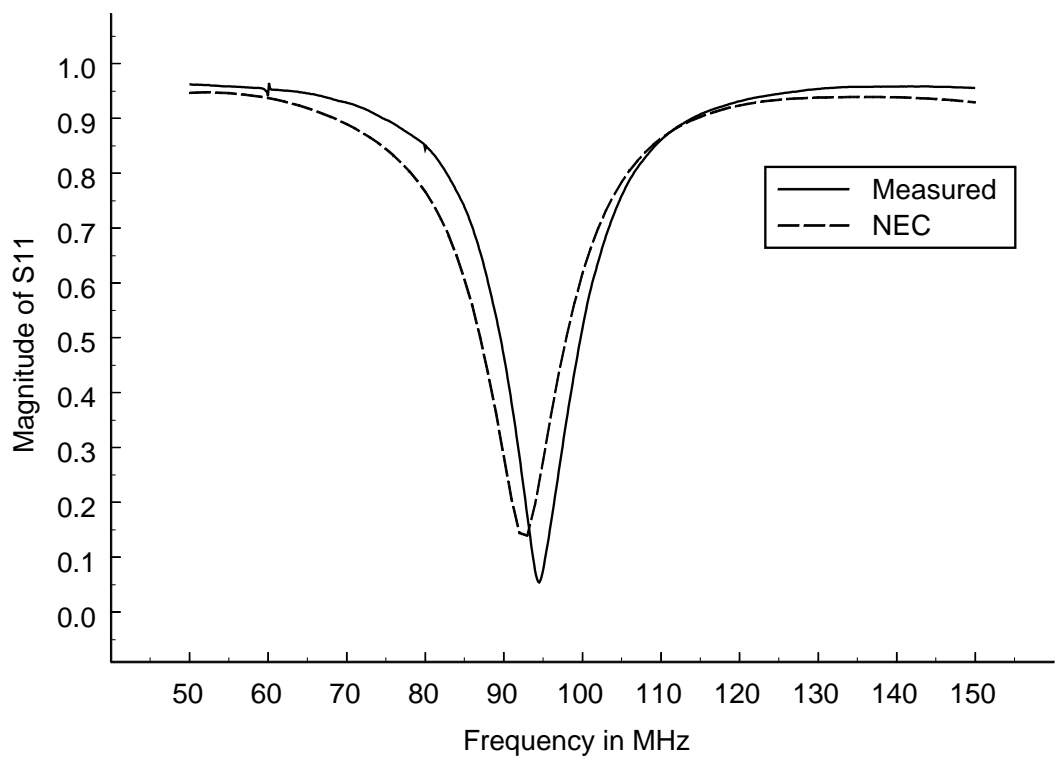


Figure 5.25. Magnitude of S_{11} ($d = 5$ cm) using method 2.

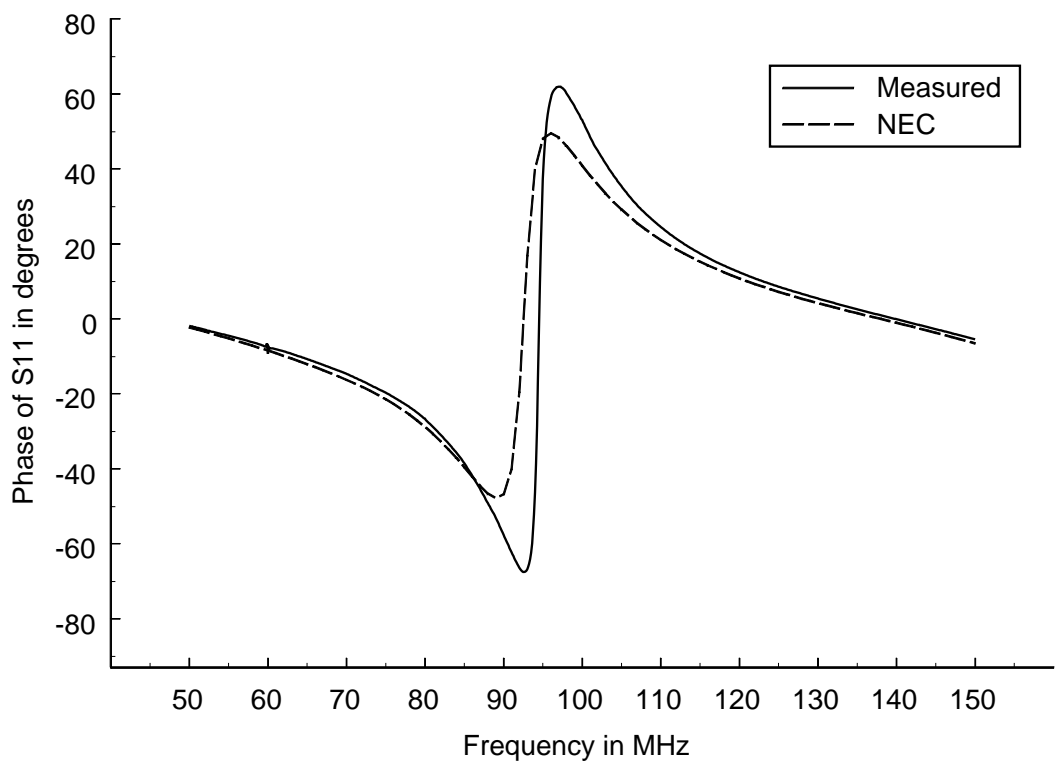


Figure 5.26. Phase of S_{11} ($d = 5$ cm) using method 2.

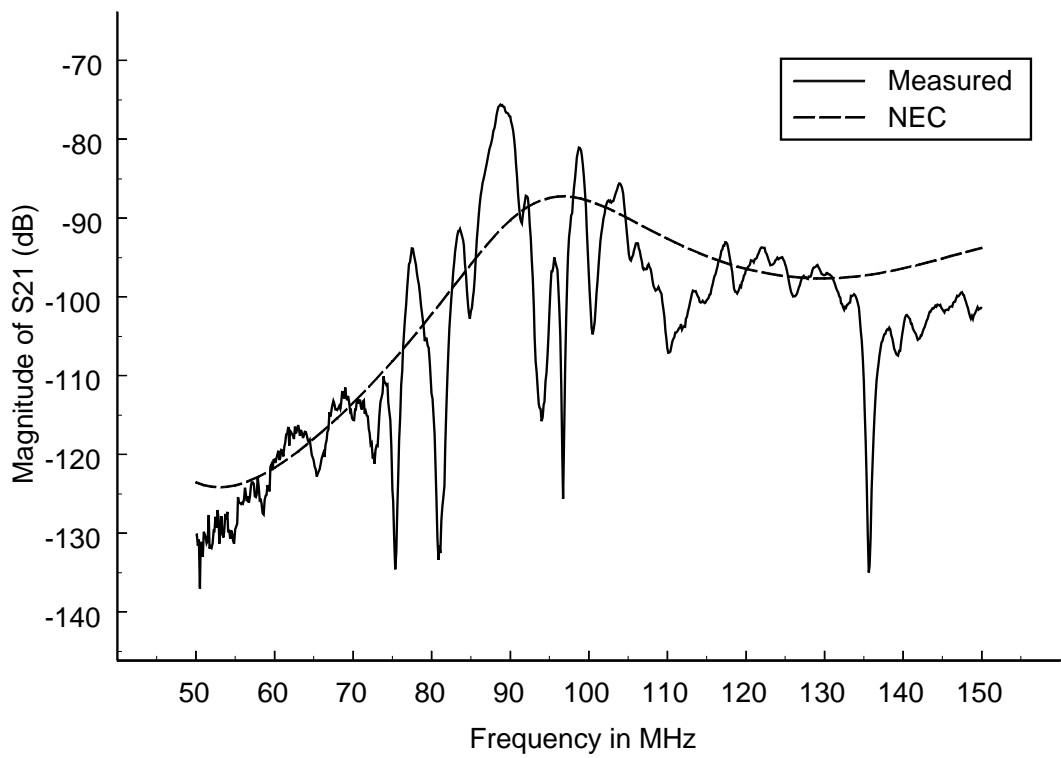


Figure 5.27. Magnitude of S_{21} (in dB) ($d = 5$ cm) using method 2.

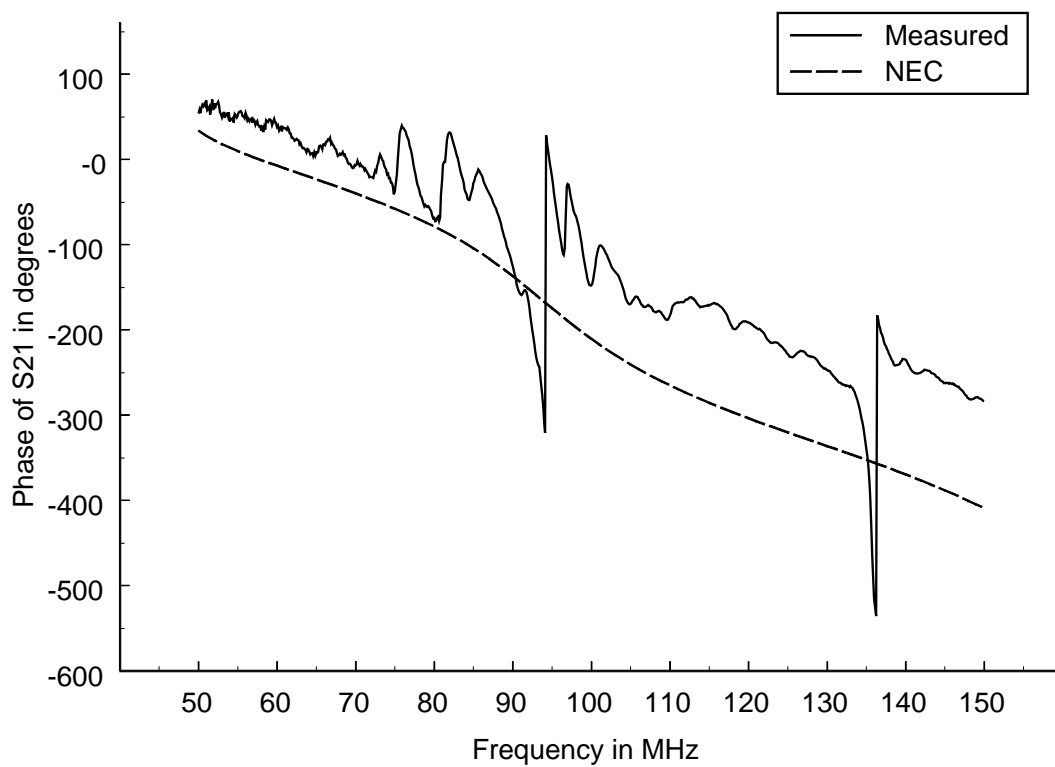


Figure 5.28. Phase of S_{21} ($d = 5$ cm) using method 2.

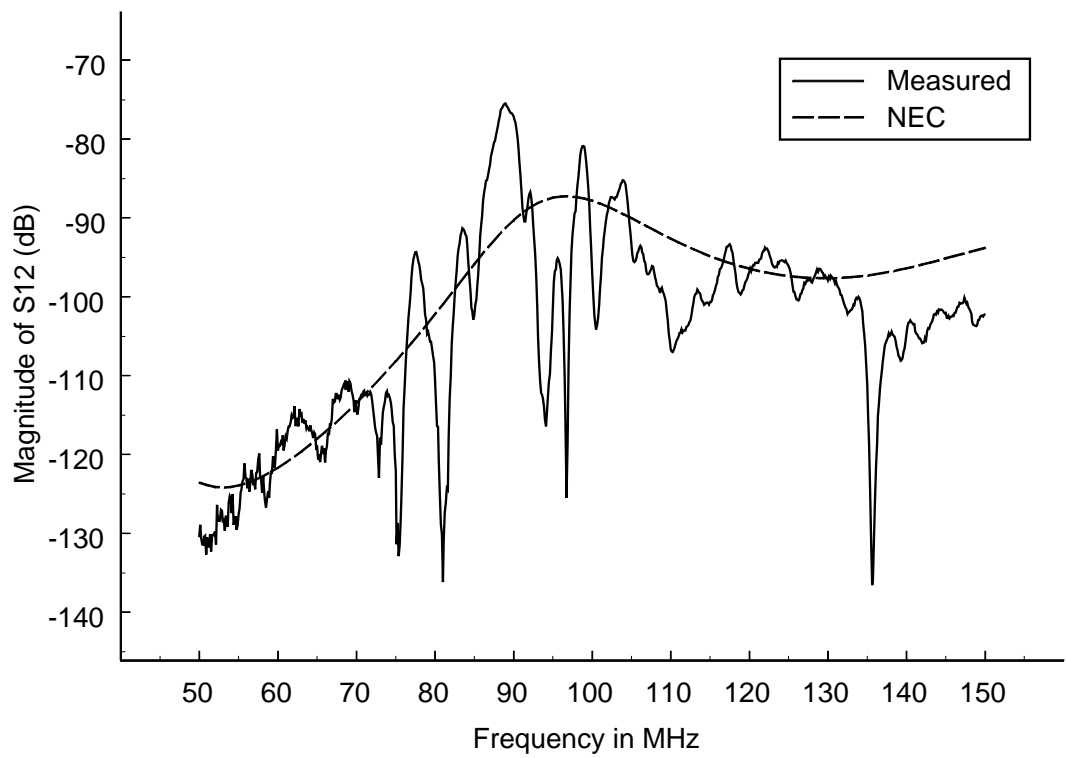


Figure 5.29. Magnitude of S_{12} (in dB) ($d = 5$ cm) using method 2.

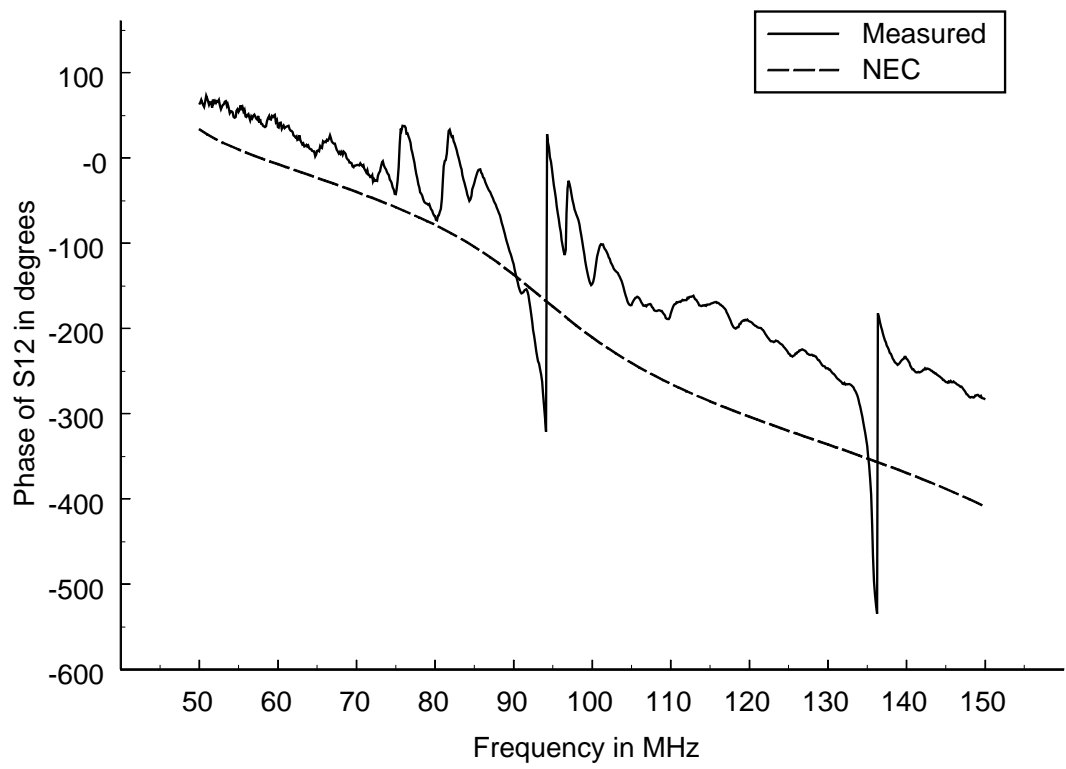


Figure 5.30. Phase of S_{12} ($d = 5$ cm) using method 2.

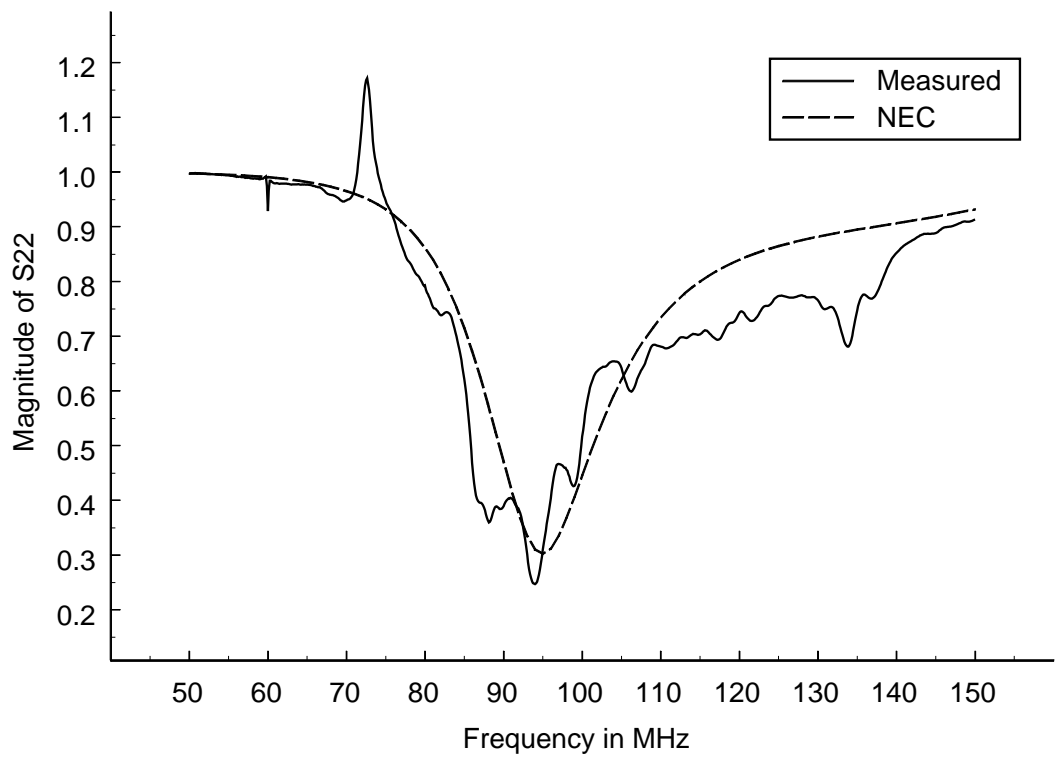


Figure 5.31. Magnitude of S_{22} ($d = 5$ cm) using method 2.

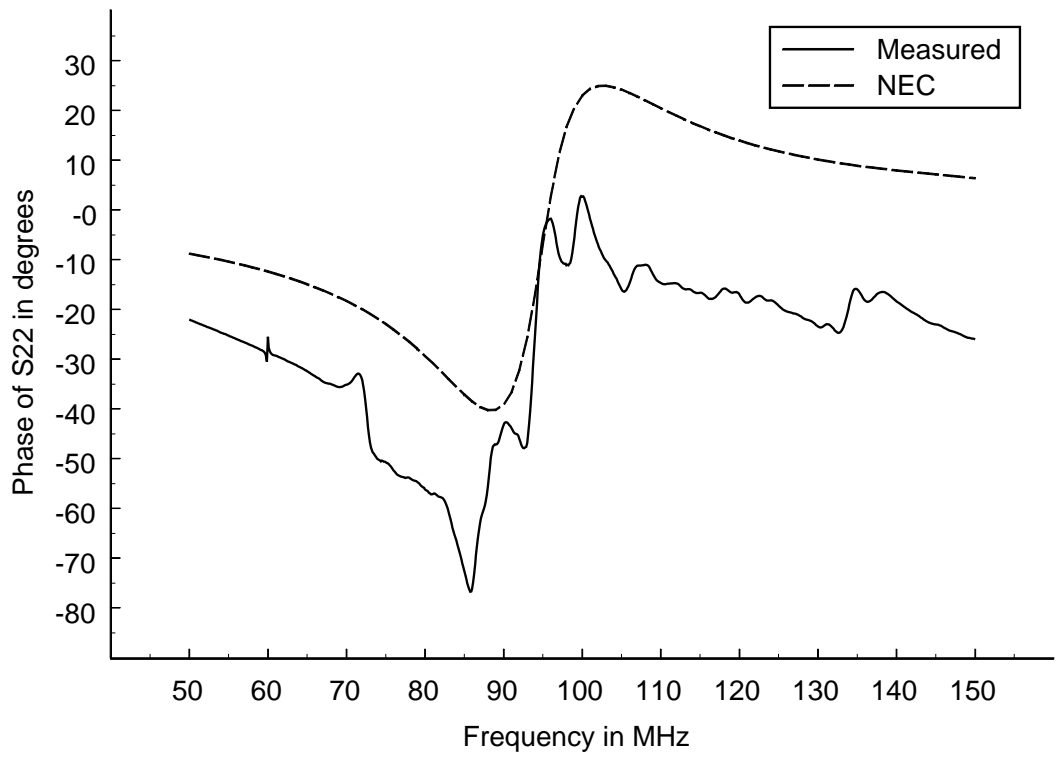


Figure 5.32. Phase of S_{22} ($d = 5$ cm) using method 2.

5.3.2 Results for a Wire Harness Location of $d = 15$ cm

The wire harness location d was changed to 15 cm on the experimental setup and the S -parameters of the system were again measured using Method 2. New numerical results were also found using NEC after modifying the wire harness location in the numerical model. The magnitudes and phases of the measured and numerical S -parameters can be found in Figure 5.33 through Figure 5.40.

Figure 5.33 and Figure 5.34 show the magnitude and phase plots, respectively, of S_{11} for both the numerical and the measured data. The resonant frequency of the table wire harness antenna was predicted to be back down around 90 to 91 MHz using the numerical results. The measured resonant frequency remained around 95 MHz. These magnitude and phase plots are also very similar to those found for the case where $d = 10$ cm.

The magnitude and phase curves of S_{21} are shown in Figure 5.35 and Figure 5.36, respectively, and the the magnitude and phase curves of S_{12} are shown in Figure 5.37 and Figure 5.38, respectively, for both the numerical and measured data taken for $d = 15$ cm. Notice that the magnitudes and phases of the measured data follow those of the numerical data similarly to the $d = 10$ cm case. The magnitudes are just slightly lower in amplitude because the transmitting and receiving antennae are further away from each other than in the case where $d = 10$ cm.

Figure 5.39 and Figure 5.40 show the numerical and measured data of the magnitude and phase of S_{22} , respectively. The measured results follow the numerical results similarly to the $d = 10$ cm case for both the magnitude and phase of S_{22} .

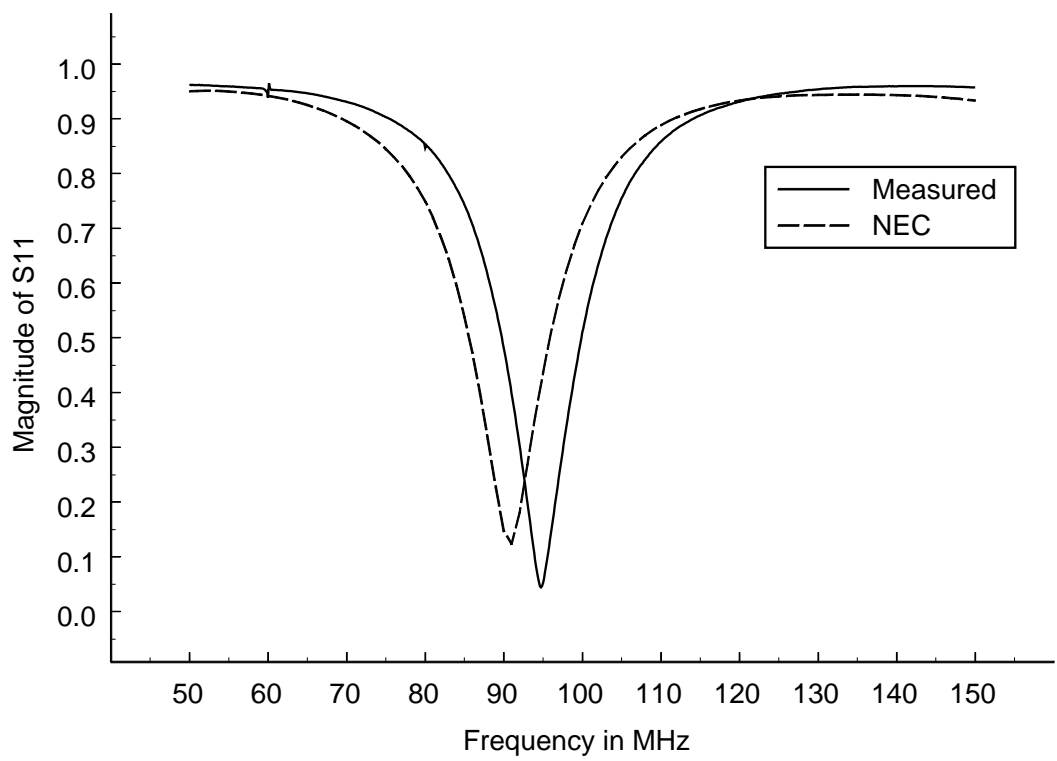


Figure 5.33. Magnitude of S_{11} ($d = 15$ cm) using method 2.

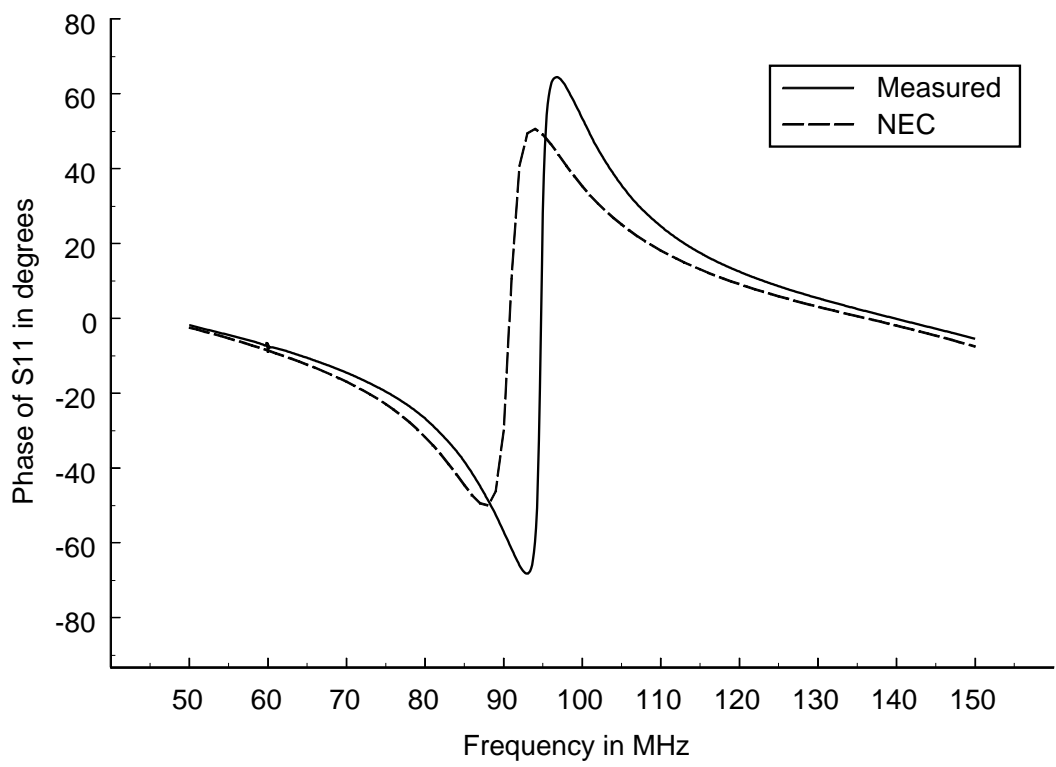


Figure 5.34. Phase of S_{11} ($d = 15$ cm) using method 2.

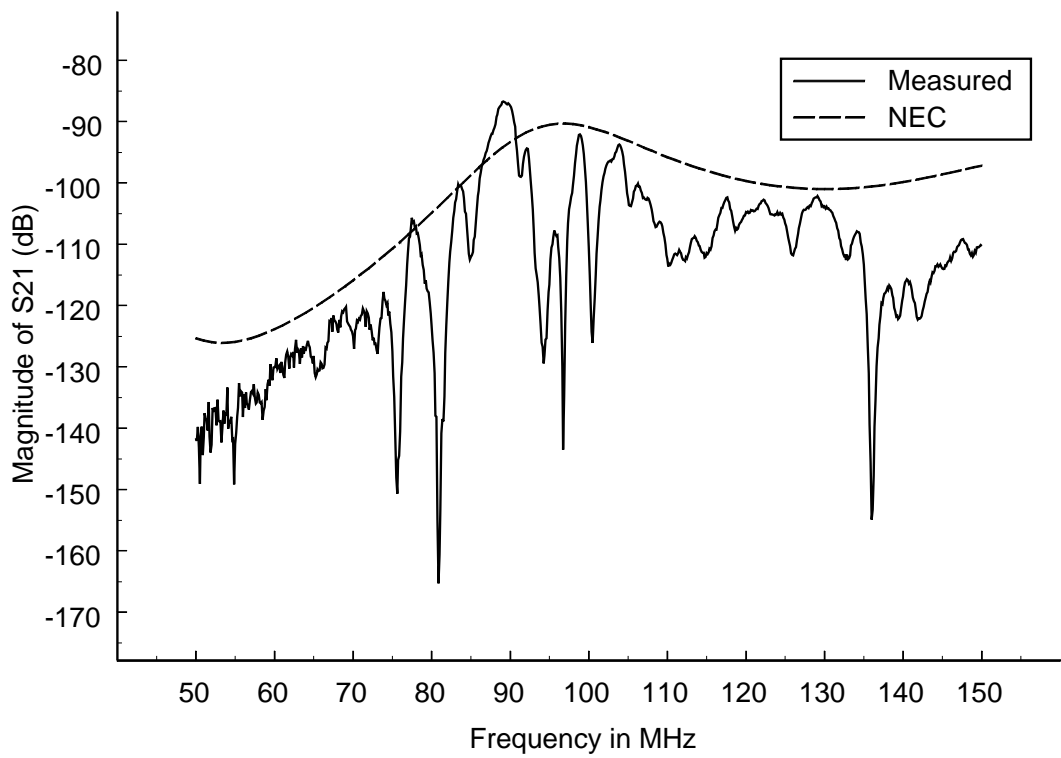


Figure 5.35. Magnitude of S_{21} (in dB) ($d = 15$ cm) using method 2.

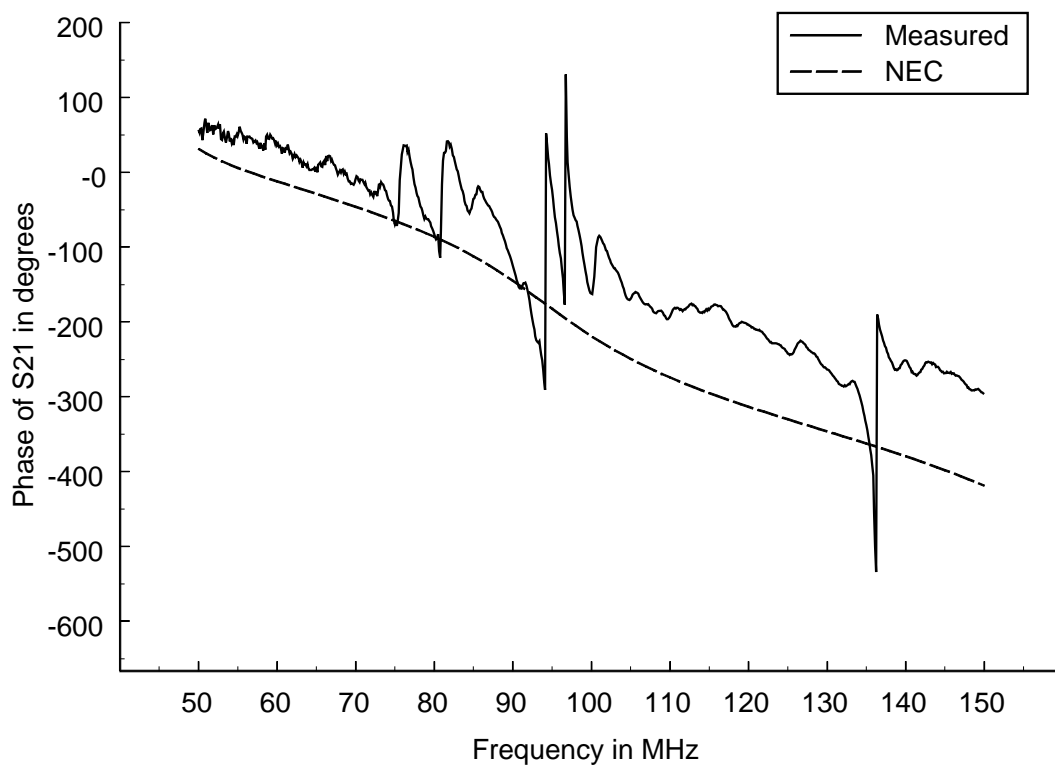


Figure 5.36. Phase of S_{21} ($d = 15$ cm) using method 2.

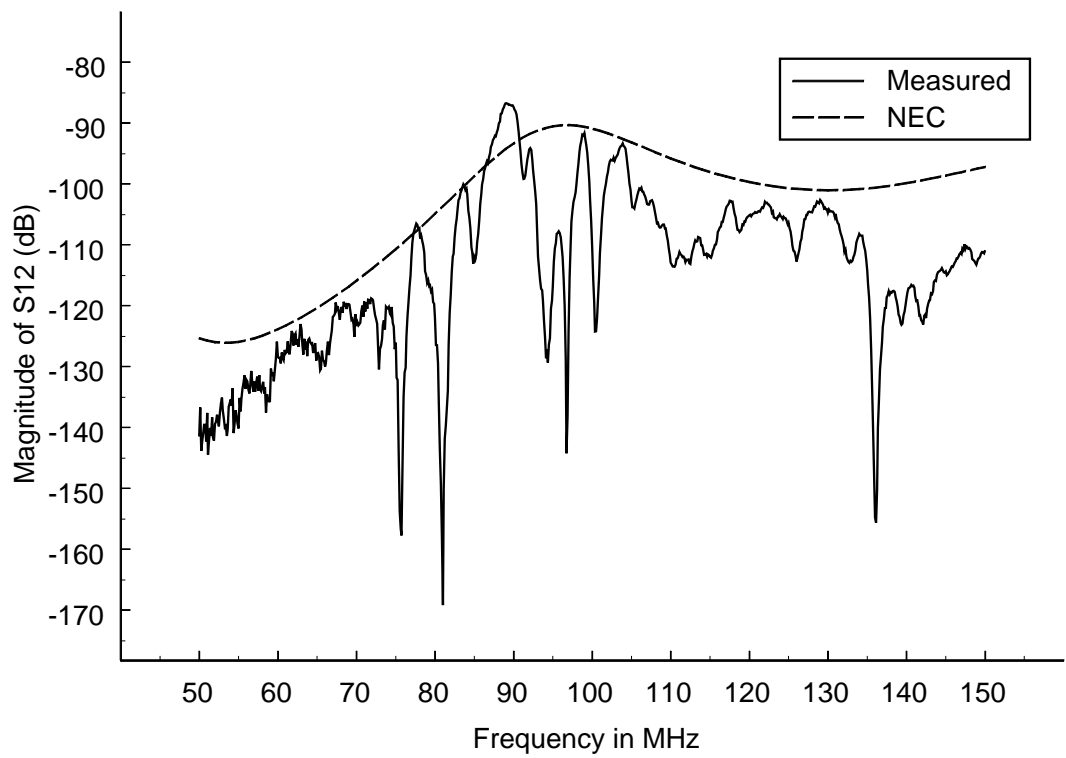


Figure 5.37. Magnitude of S_{12} (in dB) ($d = 15$ cm) using method 2.

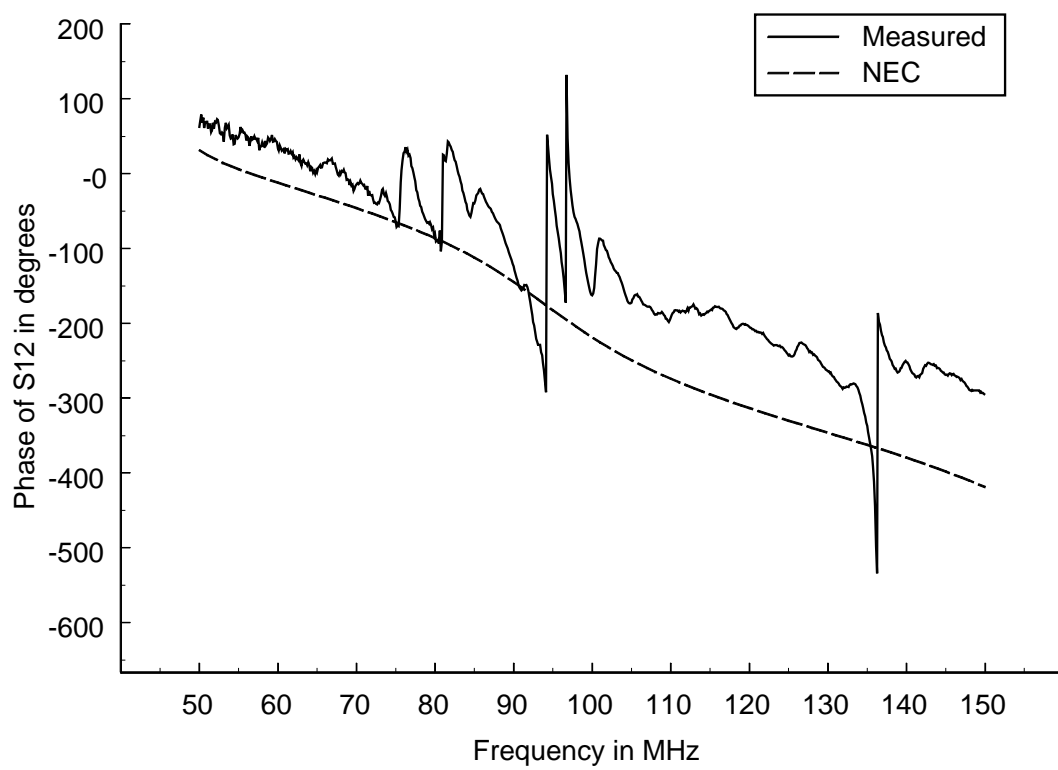


Figure 5.38. Phase of S_{12} ($d = 15$ cm) using method 2.

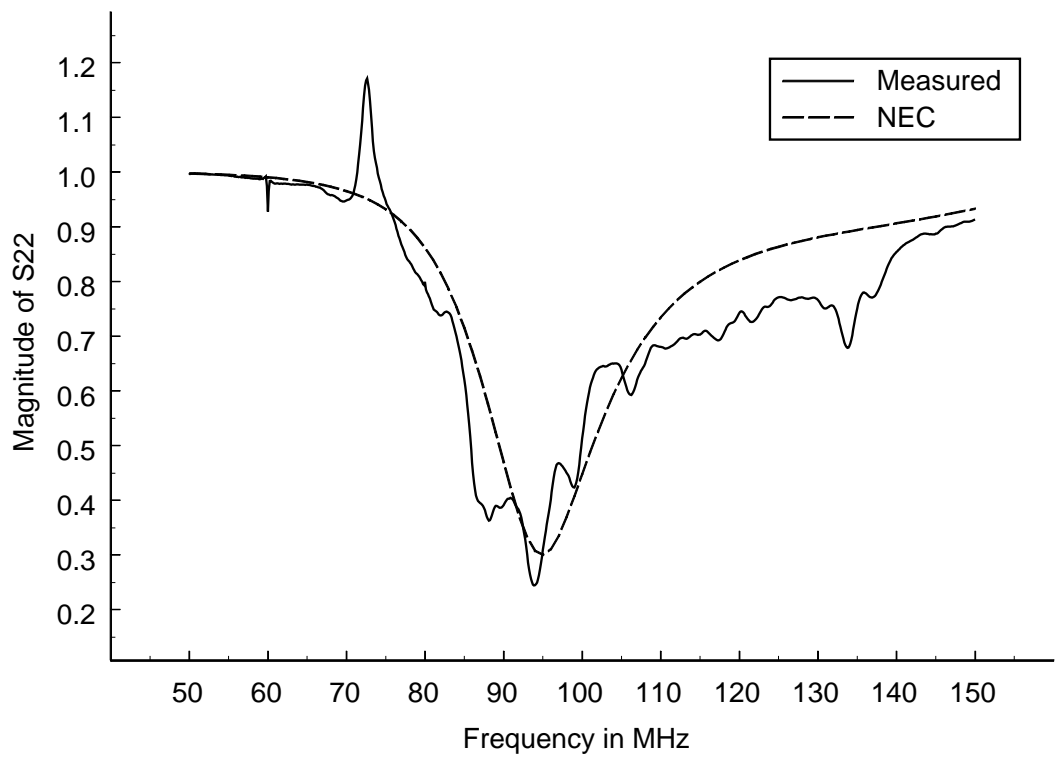


Figure 5.39. Magnitude of S_{22} ($d = 15$ cm) using method 2.

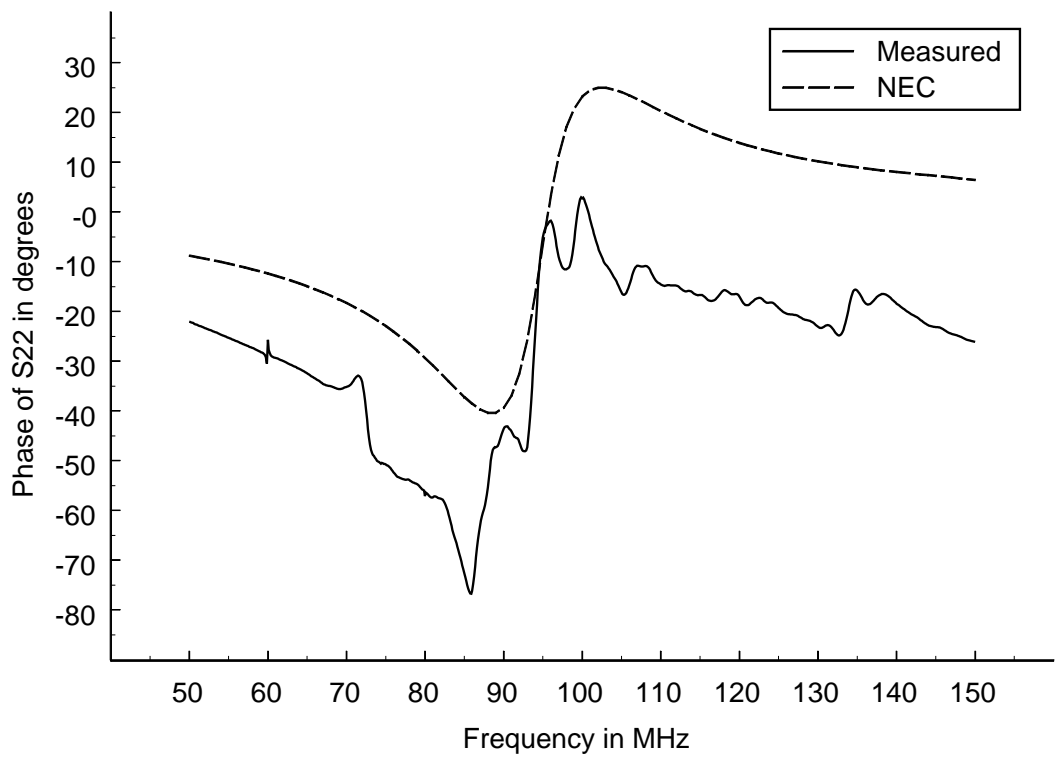


Figure 5.40. Phase of S_{22} ($d = 15$ cm) using method 2.

5.3.3 Results for a Wire Harness Location of $d = 20$ cm

The wire harness location d was changed to 20 cm on the experimental setup and the S -parameters of the system were again measured using Method 2. Numerical results were also found using NEC after modifying the wire harness location in the numerical model. The magnitudes and phases of the measured and numerical S -parameters can be found in Figure 5.41 through Figure 5.48.

Figure 5.41 and Figure 5.42 show the magnitude and phase plots, respectively, of S_{11} for both the numerical and the measured data. The resonant frequency of the table wire harness antenna was found to be around 90 to 91 MHz from the numerical results. The measured resonant frequency remained around 95 MHz. Again, these magnitude and phase plots are very similar to those found for the case where $d = 10$ cm.

The magnitude and phase curves of S_{21} are shown in Figure 5.43 and Figure 5.44, respectively, and the the magnitude and phase curves of S_{12} are shown in Figure 5.45 and Figure 5.46, respectively, for both the numerical and measured data taken for $d = 20$ cm. Notice that the magnitudes and phases of the measured data follow those of the numerical data similarly to the case where $d = 10$ cm, except that they are slightly lower in amplitude due to the increased distances between the ports.

Figure 5.47 and Figure 5.48 show the numerical and measured data of the magnitude and phase of S_{22} , respectively. The measured results follow the numerical results similarly to the $d = 10$ cm case for both the magnitude and phase of S_{22} .

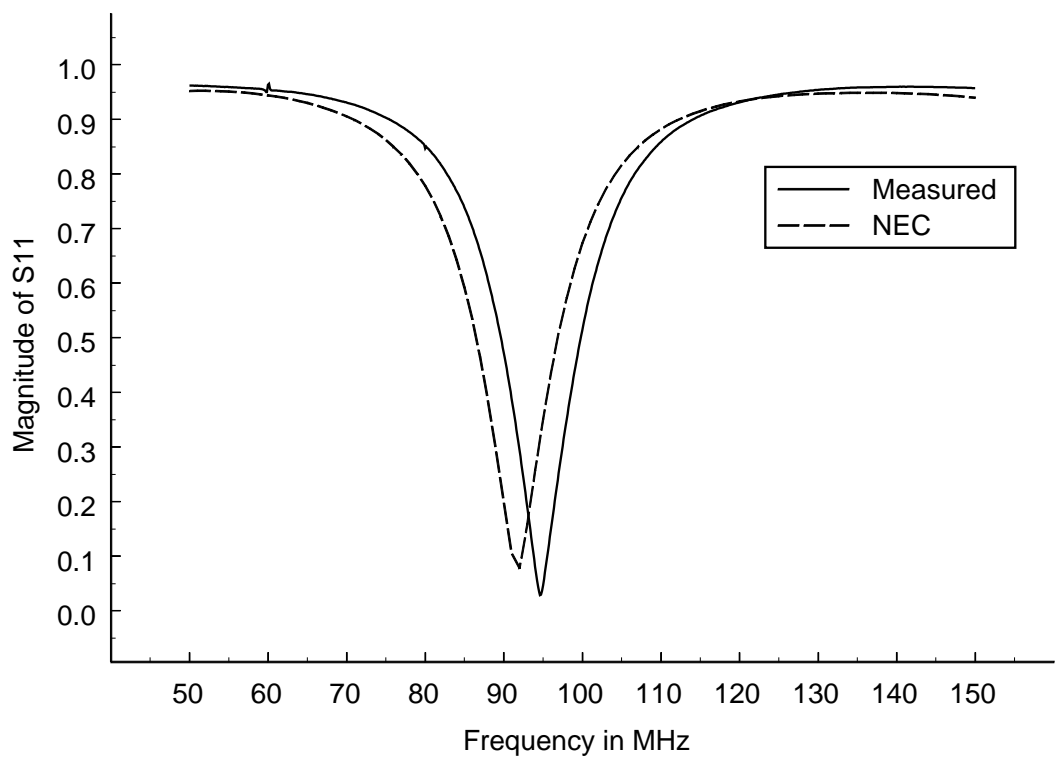


Figure 5.41. Magnitude of S_{11} ($d = 20$ cm) using method 2.

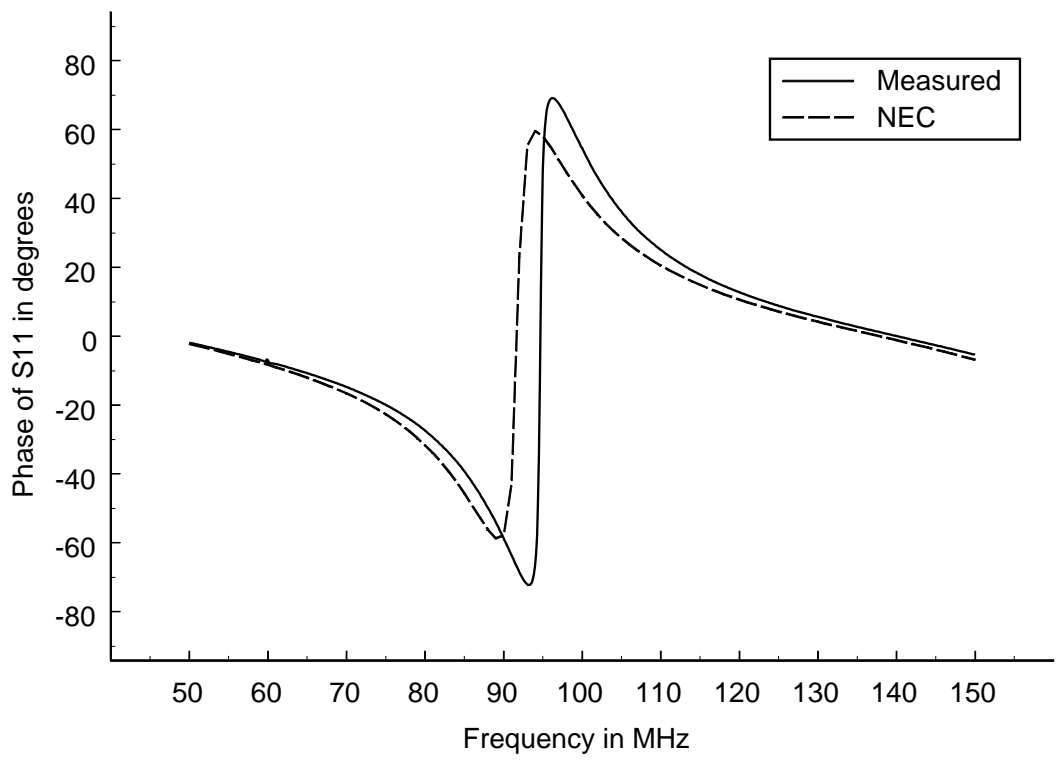


Figure 5.42. Phase of S_{11} ($d = 20$ cm) using method 2.

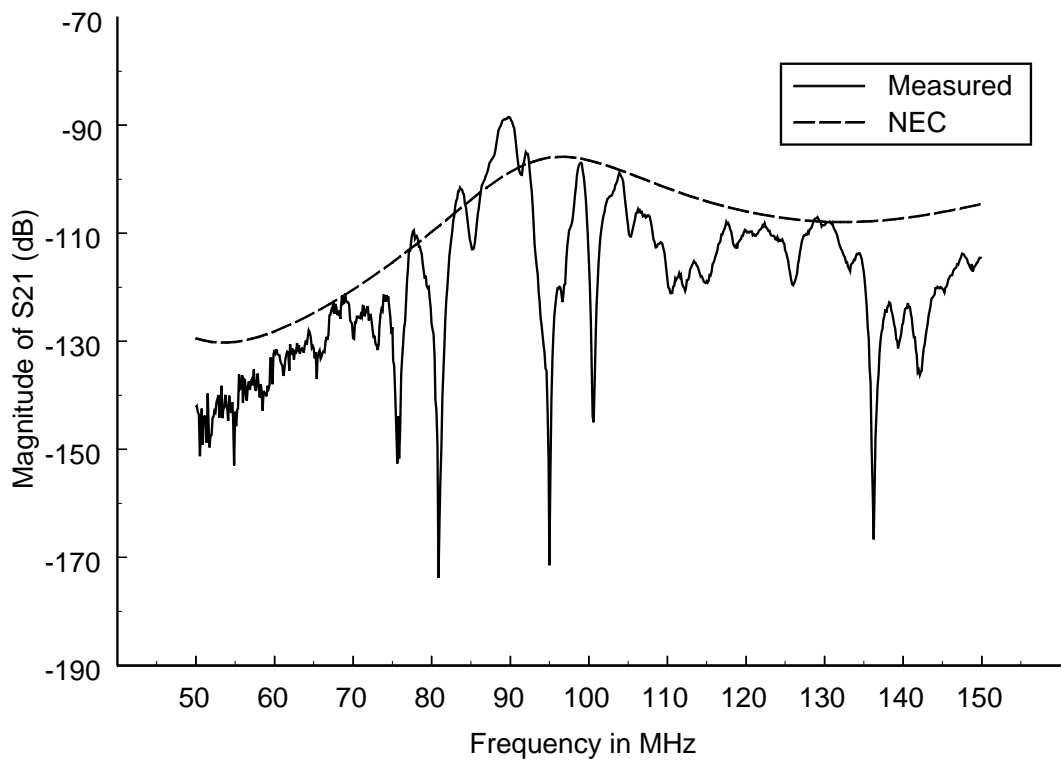


Figure 5.43. Magnitude of S_{21} (in dB) ($d = 20$ cm) using method 2.

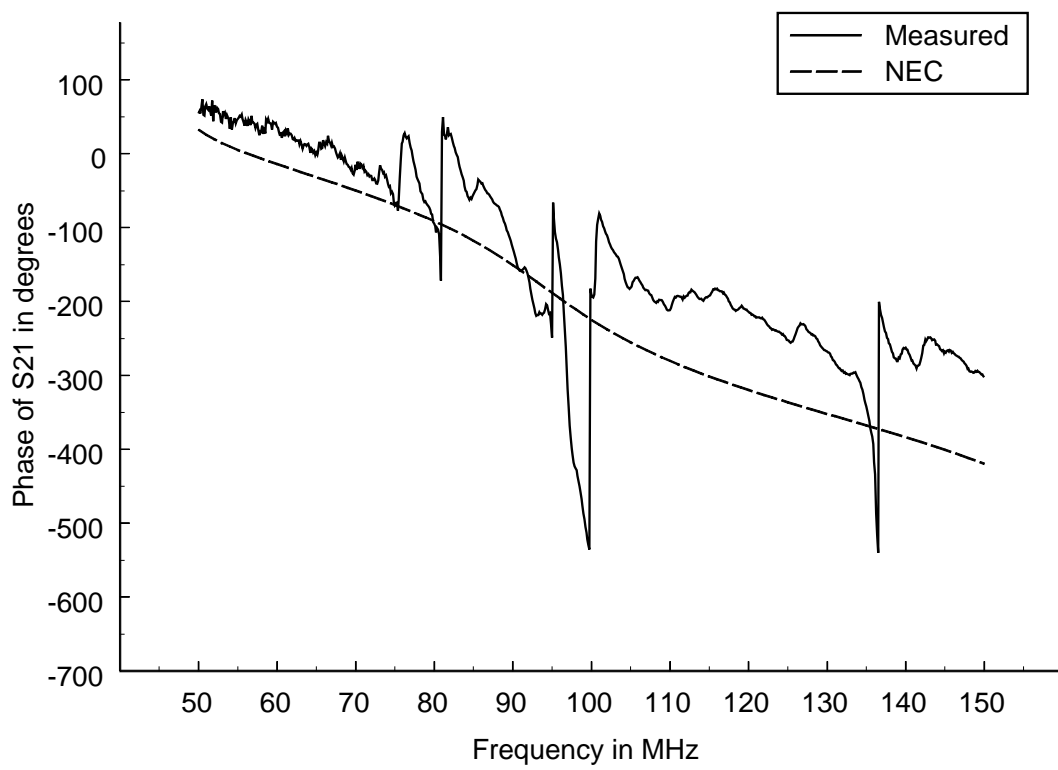


Figure 5.44. Phase of S_{21} ($d = 20$ cm) using method 2.

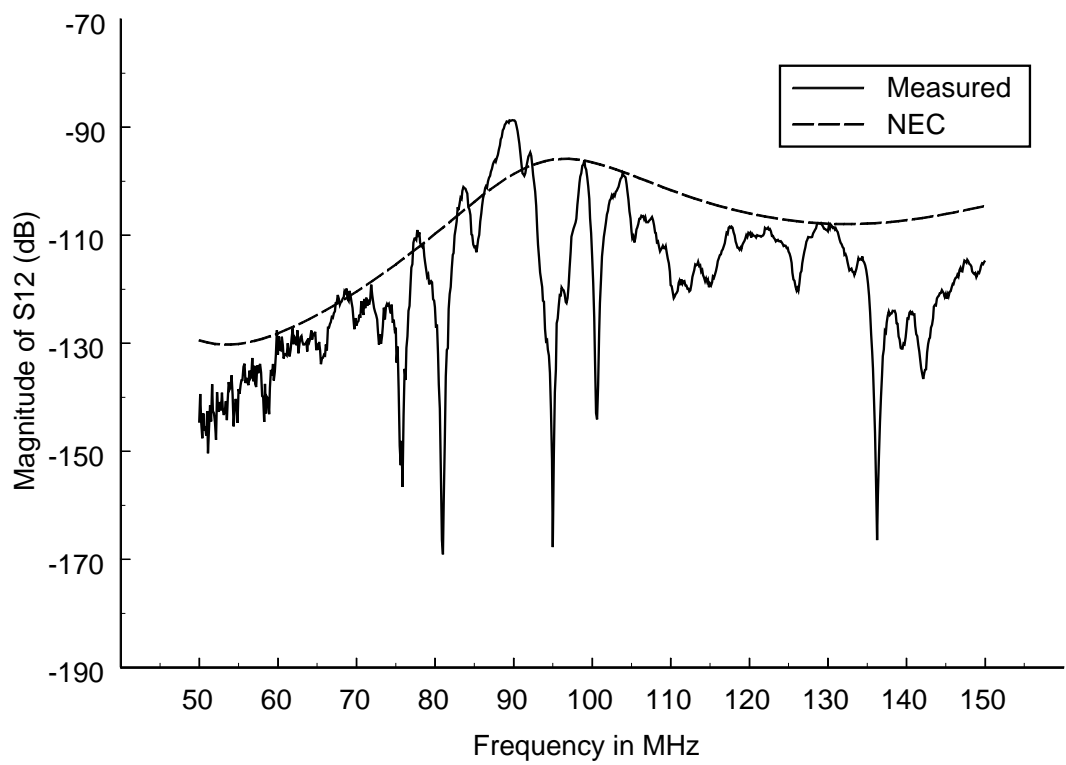


Figure 5.45. Magnitude of S_{12} (in dB) ($d = 20$ cm) using method 2.

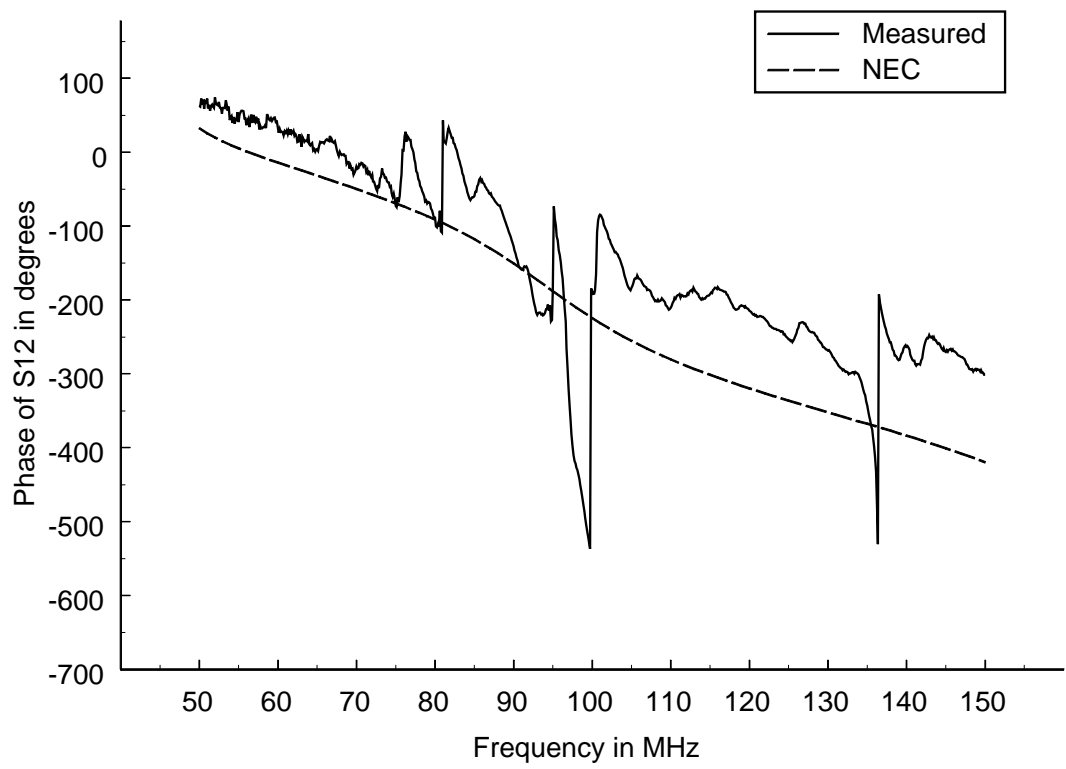


Figure 5.46. Phase of S_{12} ($d = 20$ cm) using method 2.

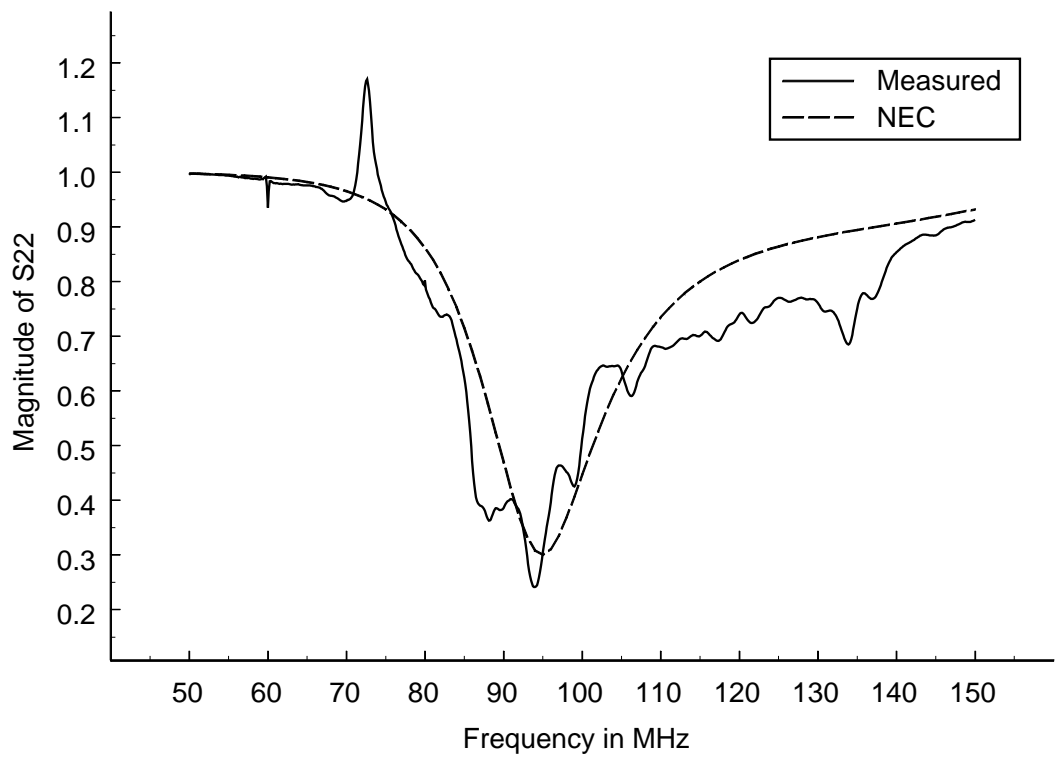


Figure 5.47. Magnitude of S_{22} ($d = 20$ cm) using method 2.

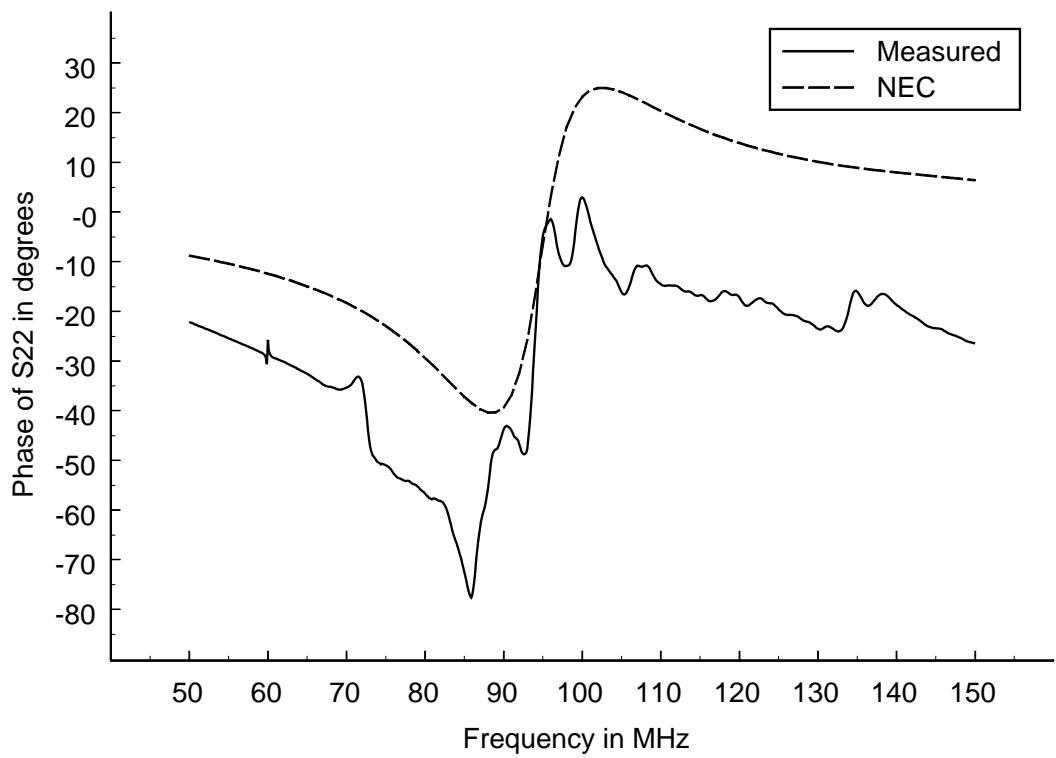


Figure 5.48. Phase of S_{22} ($d = 20$ cm) using method 2.

5.3.4 Numerical Results for All Wire Positions

Now that all of the numerical and measured results for all of the wire positions have been presented, the numerical results for the four different wire positions will be compared. Figure 5.49 and Figure 5.50 show the magnitudes and phases, respectively, of S_{11} for all four wire harness positions. Notice that the resonant frequency of the table-wire harness antenna decreases as the wire harness distance is increased. This is possibly due to the interaction of the wire harness with the edge of the table changing as the wire harness distance is varied.

Figure 5.51 and Figure 5.52 show the magnitudes and phases, respectively, of S_{21} for all four wire positions found using NEC. Notice that the magnitude of S_{21} decreases across the entire frequency band as the wire harness distance increases. This is because the distance between the dipole antenna and the wire harness increases as the wire harness distance d increases. However, the decrease in magnitude is not uniform as a function of wire harness position. The decrease in magnitude between the wire harness distances $d = 10$ cm and $d = 15$ cm is small in comparison to the decrease in magnitude between the wire harness distances $d = 15$ cm and $d = 20$ cm. Therefore the relationship between the distance between the terminal ports and the magnitudes of S_{21} are not simply related. The interaction of the wire harness with the edge complicates this relationship. The slopes of the phases of S_{21} increase slightly as the wire harness distance increases, indicating that the port separation is increasing.

The magnitudes and phases of S_{22} found using NEC for all the wire harness positions are shown in Figure 5.53 and Figure 5.54. It is evident that the wire harness position does not dramatically affect either the magnitude or the phase of S_{22} . Both the magnitude and phase curves for all the wire positions lie almost exactly on top of each other.

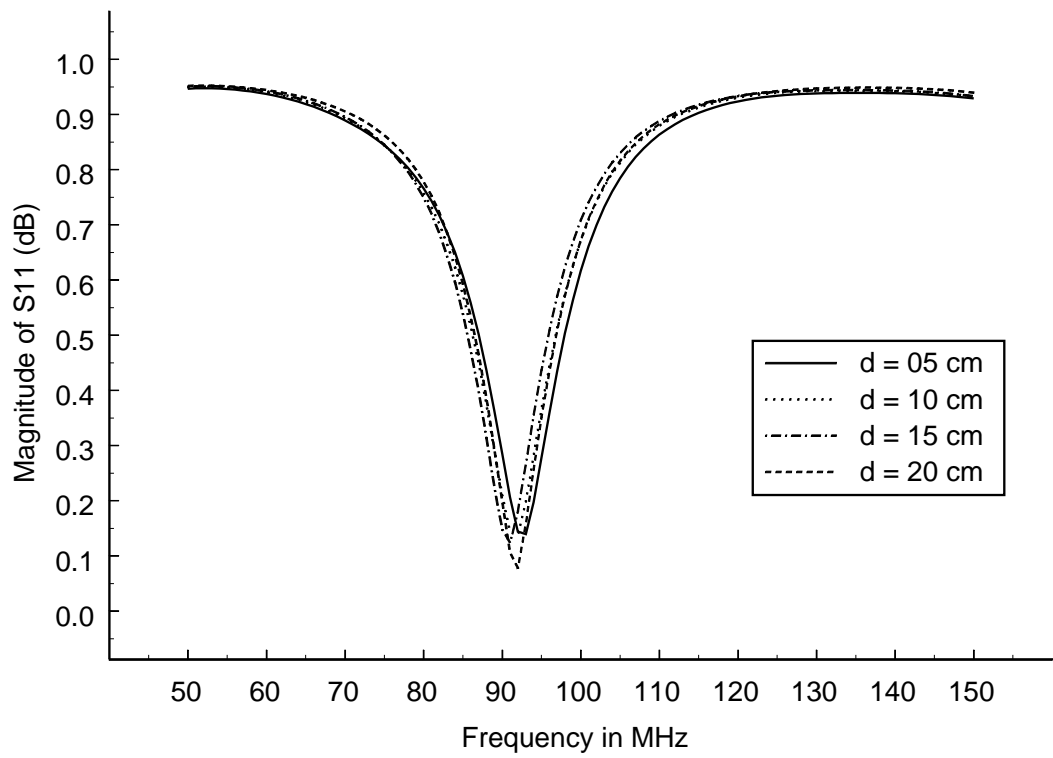


Figure 5.49. Numerical magnitudes of S_{11} for all wire harness positions.

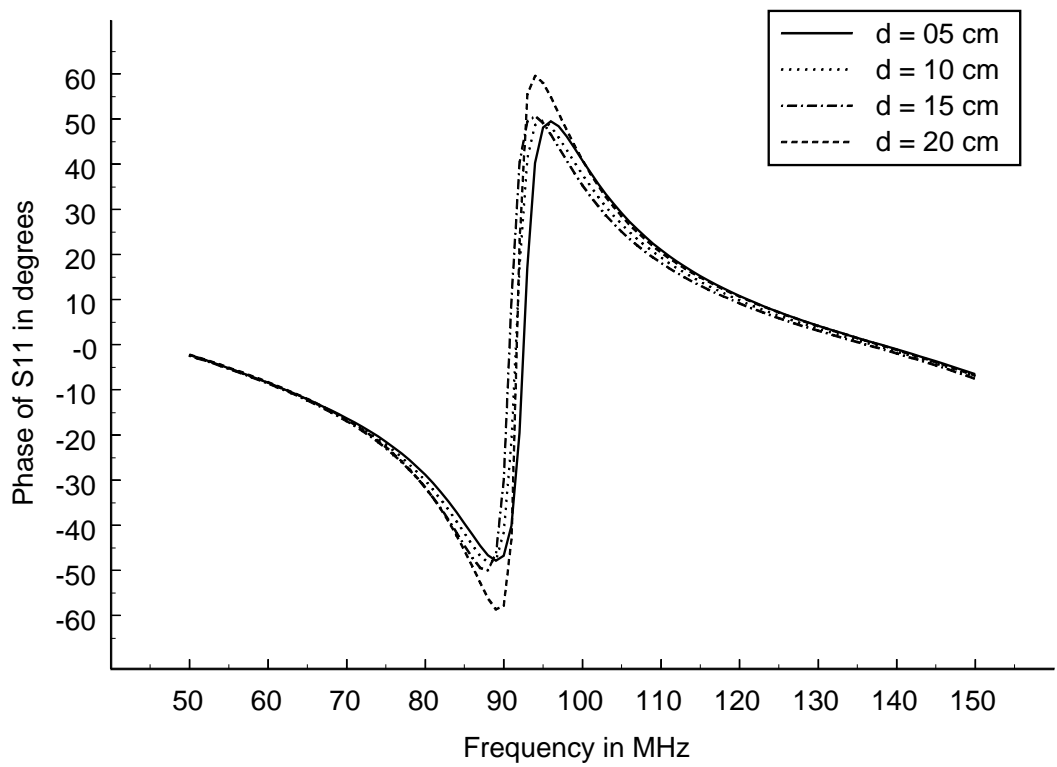


Figure 5.50. Numerical phases of S_{11} for all wire harness positions.

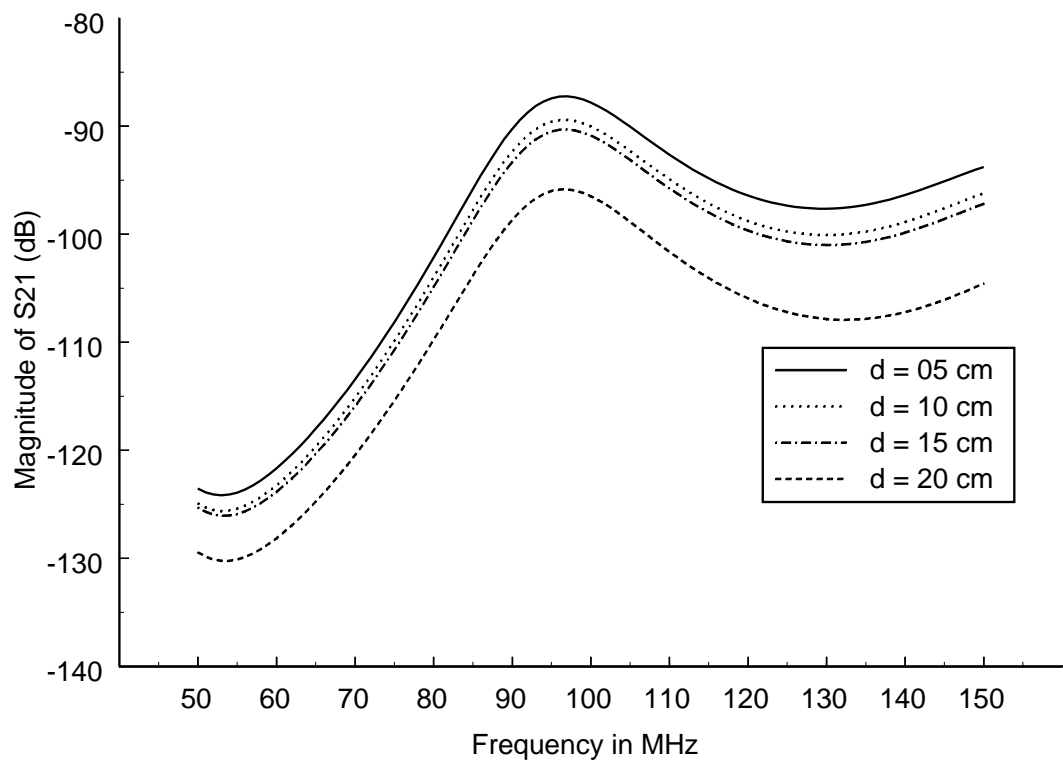


Figure 5.51. Numerical magnitudes of S_{21} for all wire harness positions.

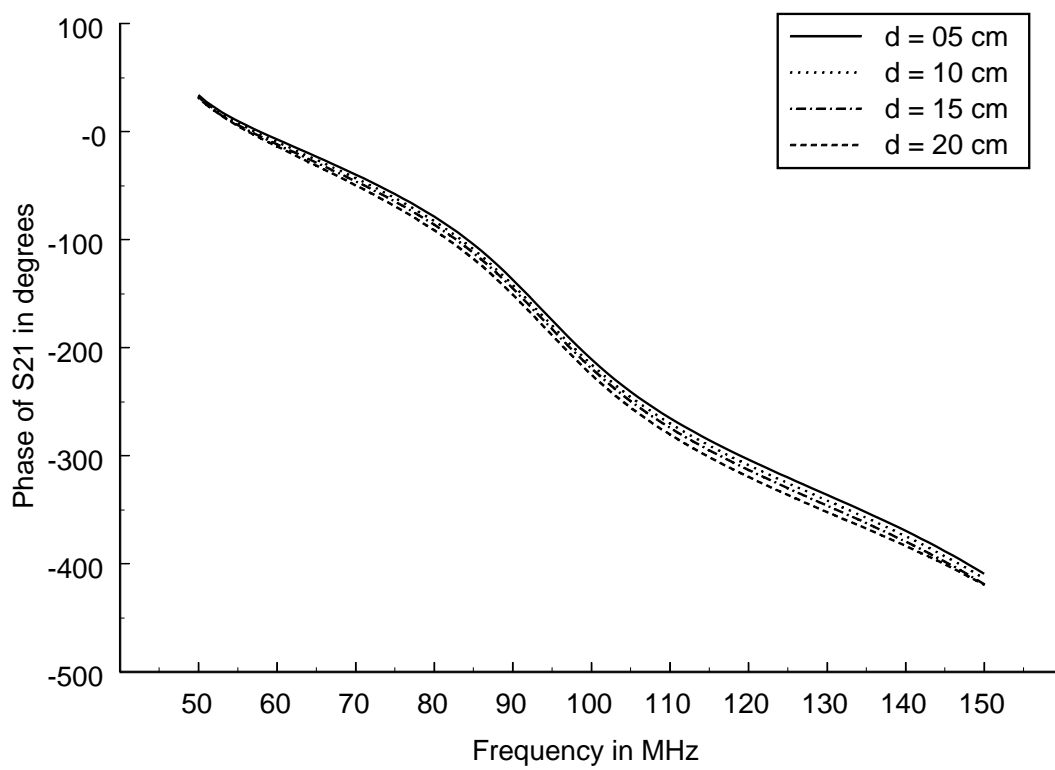


Figure 5.52. Numerical phases of S_{21} for all wire harness positions.

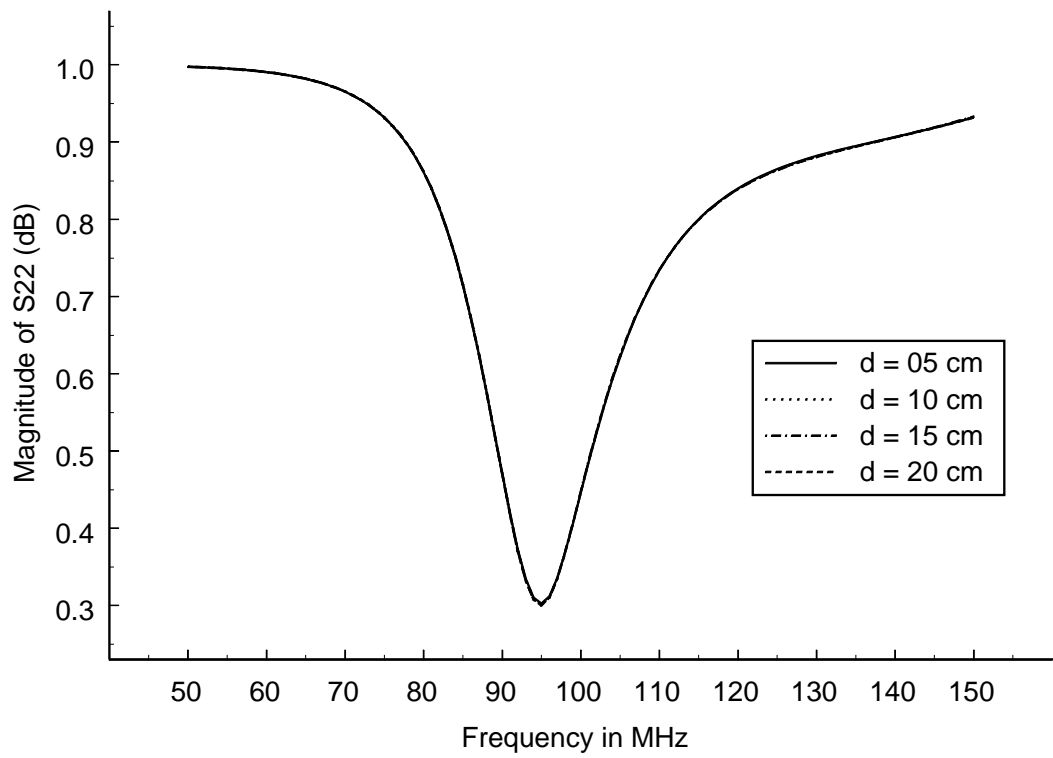


Figure 5.53. Numerical magnitudes of S_{22} for all wire harness positions.

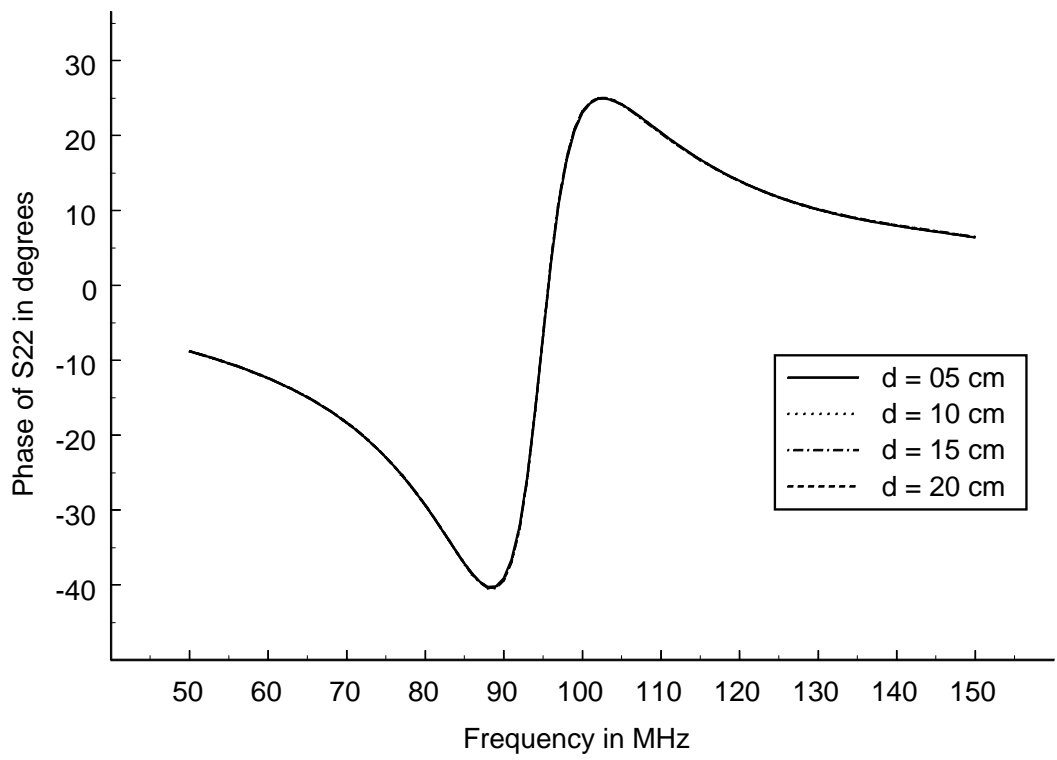


Figure 5.54. Numerical phases of S_{22} for all wire harness positions.

5.4 Conclusions

In this chapter, the results of the numerical model of the CISPR testing setup using NEC were compared with measured results. Three different methods were performed to determine the best method, and then this method was applied to all of the wire harness distances investigated. As shown in Section 5.2, it is evident that Method 2 is the best measurement method of the three investigated for this research. This measurement method was therefore performed to find the S -parameters of the table-antenna system for wire harness distances of $d = 5, 10, 15,$ and 20 cm.

The measured S -parameters in general matched those found numerically from NEC for all of the wire distances fairly well. For all of the wire harness distances, the shape of the measured magnitudes and phases of S_{11} were close to those found numerically, except that the numerically generated curves appeared slightly shifted in frequency below the measured curves.

The measured magnitudes and phases of S_{21} and S_{12} to an acceptable degree matched the numerical results found using NEC. The measured results had rapidly varying fluctuations as a function of frequency over the entire frequency band, but the general shape and amplitudes of the magnitudes were in fair agreement with the numerical results.

Both the magnitudes and phases of S_{22} found from measurement followed the general trend of the numerical results. Rapidly varying deviations in the magnitude and phase also appeared in the measured results. A constant phase shift between the measured and numerical curves also existed in the S_{22} phase plots.

Many factors could be the sources of the rapidly varying fluctuations found in the S_{21} , S_{12} , and S_{22} measurements. The calibration routine and the S -parameter network formulation in general rely on the assumption of linearity for validity. The transformer balun could be a non-linear device that possibly cannot be calibrated

out of the measurements. Another possibility is that the transformer only balances part of the common mode current on the cable leading to the dipole antenna, and the remaining unbalanced current is interfering with the measurements. This is plausible because the transformer-free measurements made using Method 3 exhibited more of the deviations observed from the measurements using Method 2.

The most probable source for the variations comes from the laboratory itself. The CISPR 25 specifications require the measurements to be performed in a shielded semianechoic chamber, but the measurements performed at MSU were over a ground plane open in a large laboratory. The laboratory contains several metallic cabinets, metallic support beams above the ground plane, a metallic roof, and various other conducting bodies. At the low frequency range investigated, 50 MHz to 150 MHz, the free space wavelengths range from 6 meters down to 2 meters. These conducting bodies are on the order of single wavelengths away from the table-antenna system. The presence of these bodies could introduce constructive or destructive interference depending on the frequency. Constructive and destructive interference could produce the rapidly varying fluctuations. The numerical model did not include any of these additional conducting structures, and this could be a prime source for the deviations between the numerical and measured results.

Another possible source of error from the laboratory is external electromagnetic interference from radio stations, computers, etc. that could be received by either antenna and be interpreted as signals originating from the network analyzer. This possibility of external electromagnetic interference was investigated by match terminating one port and measuring the received signal for a through measurement. Thus Port 1 was match terminated and S_{21} was measured, then Port 2 was match terminated and S_{12} was measured. For both measurements, any external electromagnetic interference present did not register above the noise floor of the HP 8510C network analyzer. Thus the possibility of external electromagnetic interference influencing the

measurements was neglected.

As discussed in Chapter 2, the goal of this thesis research was to develop a numerical model that could adequately predict the effects of currents existing on the wire harness above a table on measurements performed for a CISPR 25 radiated emissions test. The results discussed in this chapter show that the numerical model developed using NEC is able to predict the general trends of the S -parameters for a physical table / antenna system such as the CISPR 25 setup. As shown in Section 5.3.4, the numerical model predicts that the magnitude of S_{21} of the table-antenna system will decrease as the wire harness distance d increases. This agrees with physical intuition because the separation between the ports increases as the wire harness distance d increases. The slope of the phase of S_{21} increases as the wire harness distance increases, also indicating that the distance between the ports increases.

The measurements performed at MSU have many rapidly varying fluctuations compared to those predicted from the numerical model, but the general shapes of the S -parameters as a function of frequency are very similar. Variations in the wire harness location do not adversely affect the ability for the numerical model to predict the measured S -parameters of the system. Thus the numerical model serves as an adequate representation of the experimental setup at MSU and therefore should accurately predict the effects of different parameters on the CISPR 25 radiated emissions test.

CHAPTER 6

CONCLUSION

This thesis has presented a comparison between a numerical model and an experimental arrangement that both model the radiated emissions testing setup for modules as required by the CISPR 25 organization. The goals of this thesis, as discussed in Chapter 2, are to develop a numerical model of the CISPR 25 testing setup that predicts results obtained through experimental measurement of a similar setup, and to verify that the numerical model can accurately predict the effect of varying the wire harness distance on measurements. As discussed in Chapter 5, the numerical model developed does adequately predict the S -parameters of the experimental table-antenna arrangement constructed at MSU. Variations in the wire harness distance in the numerical model also lead to predictable results.

A description of the numerical model developed for this project using the Numerical Electromagnetics Code was given in Chapter 3. The numerical model was used to calculate the S -parameters of the table-antenna system. In Chapter 4, a description of the experimental setup constructed at MSU was discussed, and the methods and techniques used to measure the S -parameters of this system were explained.

Finally, Chapter 5 presented all of the numerical and measured results of the S -parameters of the table-antenna system. The numerical results were compared with the measured results for different measurement methods and various wire harness locations. Conclusions about the success of the numerical model and the experimental setup were drawn at the end of the chapter. As mentioned above, it was determined that the numerical model was successful in predicting the S -parameters of the system.

Although the goal of this research was achieved, further research could produce better results. NEC was used to numerically model the CISPR 25 testing setup for the research presented here. NEC is a good simulation tool that can be used for a

wide variety of electromagnetic structures, but it may not have been the best tool to use to model flat surfaces such as the metal table. A better numerical simulation could be developed with a method of moments solution dedicated to this structure instead of a multi-use program.

Another area of future research is further experimental verification of the numerical model. The use of a shielded anechoic chamber would be beneficial if the measurements were to be repeated. A better balun than the transformer used in the experimental setup used here could possibly also improve the measurements. It would still be helpful, however, to be able to de-embed the properties of the balun from the measurements.

Another note is that many of the problems encountered while performing this research seemed to stem from the frequency range investigated. The band of frequencies from 50 MHz to 150 MHz is nearing the upper limit of frequencies in which NEC can accurately model this system with the available computer power. However, the frequency band is much lower than the frequencies typically studied at MSU. This means that the measurement facilities at MSU are well equipped to investigate phenomenon at frequencies greater than 1 GHz, but frequencies far below this are not absorbed well by the microwave absorber available in MSU's laboratories.

The area of electromagnetic compatibility is a fast growing and interesting field in electrical engineering. As well as being an interest in academia, electromagnetic compatibility is becoming a primary concern in industry as testing standards and regulations become more prevalent. This thesis illustrates the need for more research into testing standards, numerical simulations, and measurement techniques to be used in this field.

APPENDICES

APPENDIX A

NEC GRID GENERATOR PROGRAM

A.1 Overview

A NEC input file can potentially contain many hundreds of lines of code. Each specification of a wire segment consists of a tag number and six wire coordinates (three starting point coordinates and three endpoint coordinates). This information not only has to be precisely calculated, it must be entered into the input file without typographical errors. Using a separate computer program to calculate the required position of each wire and then tabulate the results in the format that NEC recognizes is much more efficient and reliable than attempting to generate a NEC input file by hand. Thus, a NEC grid generating program was developed for this research project. The program was written in Fortran 90 and compiled with the same Digital Visual Fortran compiler that was used to compile the NEC-4 program used for numerical modeling.

A.2 Explanation of Program

The program `cmst1` is the grid computing code written to generate the NEC input file for this project. The program first calls the ‘beginning’ subroutine. This subroutine opens the output files that will be produced (`nec.in`, `nec.par`, and `zparinfo.par`), initializes variables, and determines which Z -parameter will be tested for each NEC run. The starting frequency, frequency range, and number of frequency points are also determined. This frequency information is written to the file `zparinfo.par`, which will be used by the program `zparmake` (explained Section B.2 of Appendix B) to aid in the computation of the Z -parameters of the table-antenna system.

Next, the subroutine ‘table’ is called. This subroutine calculates all of the coordinates of the wire segments and stores them in the 6×5000 matrix named ‘coordinates’.

The coordinates are calculated by first breaking the table up into six sections (as discussed in Section 3.3), then separating the wires into x -directed wires and y -directed wires, and finally calculating the maximum spacing between wires for each section. The subroutine then evaluates the positions of each wire. The coordinates of all the wires comprising the dipole antenna were then computed in the ‘table’ subroutine.

At the end of the subroutine, the ‘coordinates’ matrix is used to print out all of the wire coordinates to the `nec.in` file to be used by NEC. These coordinates are given to NEC in the format

```
GW  ITG  NS  XW1  YW1  ZW1  XW2  YW2  ZW2  RAD
```

where `GW` is NEC’s straight wire specification command, `ITG` is the tag number for all the segments of the wire, `NS` is the number of segments on the wire, `XW1`, `YW1`, and `ZW1` are the x , y , and z coordinates of the first end of the wire, `XW2`, `YW2`, and `ZW2` are the x , y , and z coordinates of the second end of the wire, and `RAD` is the wire’s radius [4]. All coordinates and radii are assumed to be in meters.

Before the ‘table’ subroutine is ended, the `nec.par` file is created. This file contains the information about which wires were x -directed, y -directed, and other possible directions, as well as the wire tag numbers of the port 1 and port 2 that are used for the network formulation of the table-antenna system discussed in Chapter 3. The modified NEC-4 program will use these pieces of information to determine which currents to write to different output files.

The next subroutine called is named ‘exite’. The purpose of this subroutine is to end the wire geometry section, write the excitation and load commands, and add a ground plane under the table to the `nec.in` file. A voltage source was chosen in the `EX` NEC structure excitation command. The voltage source was placed at either the dipole’s feed point or the table’s driving point depending on which Z -parameter calculation was chosen when the program was run. The NEC impedance loading

command `LD` was used to load the antenna at various positions, depending on which Z -parameter was being calculated. The load was written to the `nec.in` file in a resistance and reactance format. This corresponds to a load type '4' in NEC [4].

Finally, the subroutine 'finish' is called to end the program `cmst1`. The NEC command `EN` is written to the `nec.in` file, which identifies the end of the input for the NEC program. The files are then closed, and the program is terminated. The source code for the program `cmst1` is included in the next section.

A.3 Source Code for cmst1

The following is the Fortran source code for the program cmst1.

```
      program cmst1

c*****
c      This program will generate a NEC4 input file for Chris Coleman's
c      MS thesis project
c
c      The NEC input file generated is called 'nec.in'
c
c      latest revision: 5/20/99
c
c*****

      call beginning
      call table
      call exite
      call finish
      end

      subroutine beginning
c*****
c      Subroutine 'beginning' initializes the program. It
c      specifies the frequencies, how the antenna terminals
c      should be loaded, and what input and output files should
c      be generated.
c*****

      common/bbeginning1/minfreq,maxfreq,maxseg
      common/bbeginning2/spacing,wrad
      common/btag/tag
      common/gnd/gndflag
      common/xqf/xqflag
      common/frqstuff/freqflag,freqstep,freqnum
      common/zpar_vars/zpar_flag

      real*8 minfreq,maxfreq,freqstep,spacing,wrad
      integer*4 tag,gndflag,xqflag,freqflag,freqnum,maxseg,
+      zpar_flag
```

```

c      'zpar_flag' will determine which voltages will be
c      applied and which segments will be shorted or opened.
c      'zpar_flag=1' will be used to measure z21 and z12
c      'zpar_flag=2' will be used to measure z11
c      'zpar_flag=3' will be used to measure z22

      write(*,*) 'zpar_flag=0 is a normal NEC run (300 Ohm load
+ at antenna terminals)'
      write(*,*) 'zpar_flag=1 Applies V1, shorts port 2,
+ measures z21 and z12'
      write(*,*) 'zpar_flag=2 Applies V1, opens port 2, and
+ measures z11'
      write(*,*) 'zpar_flag=3 Applies V2, opens port 1, and
+ measures z22'

      write(*,*) ' '
      write(*,*) 'Enter zpar_flag NOW!'
      read(*,*) zpar_flag

c      'zpar_flag' is displayed on the screen so that the user
c      can check that the program does have the correct value.
c      Then an explanation of what type of operation will be made
c      for the particular choice of zpar_flag.
      write(*,*) 'zpar_flag=',zpar_flag
      if(zpar_flag.eq.0) then
        write(*,*) 'normal NEC run (300 Ohm load
+ at antenna terminals)'
      else if(zpar_flag.eq.1) then
        write(*,*) ' Applies V1, measures z21 and z12'
      else if(zpar_flag.eq.2) then
        write(*,*) ' Applies V1, opens port 2, and
+measures z11'
      else if(zpar_flag.eq.3) then
        write(*,*) ' Applies V2, opens port 1, and
+measures z22'
      end if

c      Now the program will set values for geometries, frequencies,
c      and excitations

c      'gndflag=1' puts a ground plane under the table.
c      This flag will be used by another subroutine
      gndflag=1

c      The flag xqflag=1 will exite the table with a plane wave

```

```

c      xqflag=2 will exite the table with current from
c      the wire harness
      xqflag=2

c      these next two variables specify the minimum and
c      maximum frequencies (in Hz)
      minfreq=50000000.
      maxfreq=150000000.

c      'freqflag=1' will choose frequency stepping, and
c      'freqflag.ne.1' will not use frequency stepping
      freqflag=1

c      The freqstep variable specifies the frequency stepping
c      increment (in MHz), and freqnum specifies the number
c      of points
      freqnum=101
      freqstep=(maxfreq-minfreq)/(freqnum-1)

c      'maxseg' is the maximum number of segments
      maxseg=3000

c      This 'spacing' variable specifies the maximum allowable
c      grid spacing (lambda over 10). All grid spacing will be
c      equal or smaller than this
      spacing=.1*(3.E+8 / maxfreq)

c      'wrad' is the wire radius
      wrad=.001

c      'tag' is an important variable
c      used to keep track of the segment numbers
      tag=1

c      Now 'nec.in' will be opened. This is the input file
c      to NEC.
      open(10,file='nec.in',status='unknown')
c      The following are just comments written for the NEC
c      input code
      write(10,100)
      write(10,110)
100    format("cm      NEC input file for CISPR table")
110    format('ce      Written by Chris Coleman')

c      'nec.par' will be used to tell NEC4 information about

```

```

c      the wire tag numbers used for x and y directed segments
      open(20,file='nec.par',status='unknown')

c      'zparinfo.par' will be used by a z-parameter computation
c      program
      open(30,file='zparinfo.par',status='unknown')
      write(30,120) minfreq, maxfreq, freqnum
      write(30,*) 'minfreq, maxfreq, freqnum'
120    format(f13.0,f13.0,i5)

      return
      end

c*****
c*****
      subroutine table
c*****
c      subroutine table is the new table drawing routine
c*****
      real*8 l(50),
      + tabheight,wireh,
      + l_ant_ov2,h_r_ant,
      + minfreq,maxfreq,
      + spacing,wrad,
      + coordinates(6,5000),spac(50)
      integer*4 tag,maxseg,nseg,ilist(50),wiretag(10),
      + xtmin,xtmax,ytmin,ytmax,ztmin,ztmax,otmin,otmax,
      + terminal_tag(50)
      common/bbeginning1/minfreq,maxfreq,maxseg
      common/bbeginning2/spacing,wrad
      common/btag/tag
      common/harness/wiretag

c      'nseg' is the number of segments per wire
      nseg=1

c      'wireh' is the height of the wire above the table
      wireh=.05
      tabheight=.9

c      'l_ant_ov2' is the length of the receiving antenna over 2,
c      and 'h_r_ant' is the height of the receiving antenna
      l_ant_ov2=.75
      h_r_ant=1

```

```

c      These are the physical dimensions of the table in meters
      l(1)=2.44
      l(2)=1.22
      l(7)=1.5
      l(3)=(l(1)-l(7))/2
      l(4)=l(1)-(l(3)+l(7))
c      l(5) is the distance the wire radiator lies back from the
c      table lip
      l(5)=.05
      l(6)=l(2)-l(5)
      l(8)=l(1)/2
      l(9)=l(2)+1
      l(10)=h_r_ant
      l(11)=l_ant_ov2

```

```

c*****
c*****This is the beginning of the x-directed wire section
      xtmin=tag

```

```

c      This section draws the
c      x-directed back section 1 of the table

```

```

c      ilist(1) is the number of points in the y-direction
      ilist(1)=int(l(6)/spacing)+1
c      ilist(2) is the number of points in the x-direction
      ilist(2)=int(l(3)/spacing)+1
      spac(1)=l(6)/ilist(1)
      spac(2)=l(3)/ilist(2)
      do j=1,ilist(1)
        do i=1,ilist(2)
          coordinates(1,tag)=spac(2)*(i-1)
          coordinates(4,tag)=spac(2)*i
          coordinates(2,tag)=spac(1)*(j-1)
          coordinates(5,tag)=coordinates(2,tag)
          coordinates(3,tag)=tabheight
          coordinates(6,tag)=tabheight
          tag=tag+1
        end do
      end do

```

```

c      This section draws the
c      x-directed back section 2 of the table

```

```

c      ilist(1) is the number of points in the y-direction
c      ilist(3) is the number of points in the x-direction
      ilist(3)=int(l(7)/spacing)+1
      spac(3)=l(7)/ilist(3)
      do j=1,ilist(1)
        do i=1,ilist(3)
          coordinates(1,tag)=l(3)+spac(3)*(i-1)
          coordinates(4,tag)=l(3)+spac(3)*i
          coordinates(2,tag)=spac(1)*(j-1)
          coordinates(5,tag)=coordinates(2,tag)
          coordinates(3,tag)=tabheight
          coordinates(6,tag)=tabheight
          tag=tag+1
        end do
      end do

```

```

c      This section draws the
c      x-directed back section 3 of the table

```

```

c      ilist(1) is the number of points in the y-direction
c      ilist(4) is the number of points in the x-direction
      ilist(4)=int(l(4)/spacing)+1
      spac(4)=l(4)/ilist(4)
      do j=1,ilist(1)
        do i=1,ilist(4)
          coordinates(1,tag)=l(1)-l(4)+spac(4)*(i-1)
          coordinates(4,tag)=l(1)-l(4)+spac(4)*i
          coordinates(2,tag)=spac(1)*(j-1)
          coordinates(5,tag)=coordinates(2,tag)
          coordinates(3,tag)=tabheight
          coordinates(6,tag)=tabheight
          tag=tag+1
        end do
      end do

```

```

c      This section draws the
c      x-directed back section 4 of the table

```

```

c      ilist(5) is the number of points in the y-direction
      ilist(5)=int(l(5)/spacing)+1
c      ilist(2) is the number of points in the x-direction
      spac(5)=l(5)/ilist(5)

```

```

do j=1,ilist(5)+1
  do i=1,ilist(2)
    coordinates(1,tag)=spac(2)*(i-1)
    coordinates(4,tag)=spac(2)*i
    coordinates(2,tag)=l(6)+spac(5)*(j-1)
    coordinates(5,tag)=coordinates(2,tag)
    coordinates(3,tag)=tabheight
    coordinates(6,tag)=tabheight
    tag=tag+1
  end do
end do

```

```

c      This section draws the
c      x-directed back section 5 of the table

```

```

c      ilist(5) is the number of points in the y-direction
c      ilist(3) is the number of points in the x-direction
do j=1,ilist(5)+1
  do i=1,ilist(3)
    coordinates(1,tag)=l(3)+spac(3)*(i-1)
    coordinates(4,tag)=l(3)+spac(3)*i
    coordinates(2,tag)=l(6)+spac(5)*(j-1)
    coordinates(5,tag)=coordinates(2,tag)
    coordinates(3,tag)=tabheight
    coordinates(6,tag)=tabheight
    tag=tag+1
  end do
end do

```

```

c      This section draws the
c      x-directed back section 4 of the table

```

```

c      ilist(5) is the number of points in the y-direction
c      ilist(4) is the number of points in the x-direction
do j=1,ilist(5)+1
  do i=1,ilist(4)
    coordinates(1,tag)=l(1)-l(4)+spac(4)*(i-1)
    coordinates(4,tag)=l(1)-l(4)+spac(4)*i
    coordinates(2,tag)=l(6)+spac(5)*(j-1)
    coordinates(5,tag)=coordinates(2,tag)
    coordinates(3,tag)=tabheight
    coordinates(6,tag)=tabheight
    tag=tag+1
  end do
end do

```

```

        end do
    end do

c      This is the end of the x-directed section
    xtmax=tag

c*****
c*****This is the beginning of the y-directed wire section
    ytmin=tag

c      This section draws the
c      y-directed back section 1 of the table

c      ilist(1)=int(l(6)/spacing)+1 from the x-directed section 1
c      spac(1)=l(6)/ilist(1) from the x-directed section 1
c      ilist(2)=int(l(3)/spacing)+1 from the x-directed section 1
c      spac(2)=l(3)/ilist(2) from the x-directed section 1
    do i=1,ilist(2)
        do j=1,ilist(1)
            coordinates(1,tag)=spac(2)*(i-1)
            coordinates(4,tag)=coordinates(1,tag)
            coordinates(2,tag)=spac(1)*(j-1)
            coordinates(5,tag)=spac(1)*j
            coordinates(3,tag)=tabheight
            coordinates(6,tag)=tabheight
            tag=tag+1
        end do
    end do

c      This section draws the
c      y-directed back section 2 of the table

c      ilist(1)=int(l(6)/spacing)+1 from the x-directed section 1
c      spac(1)=l(6)/ilist(1) from the x-directed section 1
c      ilist(3)=int(l(7)/spacing)+1 from the x-directed section 2
c      spac(3)=l(7)/ilist(3) from the x-directed section 2
    do i=1,ilist(3)
        do j=1,ilist(1)
            coordinates(1,tag)=l(3)+spac(3)*(i-1)
            coordinates(4,tag)=coordinates(1,tag)
            coordinates(2,tag)=spac(1)*(j-1)
            coordinates(5,tag)=spac(1)*j
        end do
    end do

```

```

        coordinates(3,tag)=tabheight
        coordinates(6,tag)=tabheight
        tag=tag+1
    end do
end do

c      This section draws the
c      y-directed back section 3 of the table

c      ilist(1)=int(l(6)/spacing)+1 from the x-directed section 1
c      spac(1)=l(6)/ilist(1) from the x-directed section 1
c      ilist(4)=int(l(4)/spacing)+1 from the x-directed section 3
c      spac(4)=l(4)/ilist(4) from the x-directed section 3
do i=1,ilist(4)+1
    do j=1,ilist(1)
        coordinates(1,tag)=l(1)-l(4)+spac(4)*(i-1)
        coordinates(4,tag)=coordinates(1,tag)
        coordinates(2,tag)=spac(1)*(j-1)
        coordinates(5,tag)=spac(1)*j
        coordinates(3,tag)=tabheight
        coordinates(6,tag)=tabheight
        tag=tag+1
    end do
end do

c      This section draws the
c      y-directed front section 4 of the table

c      ilist(5)=int(l(5)/spacing)+1 from the x-directed section 4
c      spac(5)=l(5)/ilist(5) from the x-directed section 4
c      ilist(2)=int(l(2)/spacing)+1 from the x-directed section 1
c      spac(2)=l(4)/ilist(2) from the x-directed section 1
do i=1,ilist(2)
    do j=1,ilist(5)
        coordinates(1,tag)=spac(2)*(i-1)
        coordinates(4,tag)=coordinates(1,tag)
        coordinates(2,tag)=l(6)+spac(5)*(j-1)
        coordinates(5,tag)=l(6)+spac(5)*j
        coordinates(3,tag)=tabheight
        coordinates(6,tag)=tabheight
        tag=tag+1
    end do
end do

```

```

c      This section draws the
c      y-directed front section 5 of the table

c      ilist(5)=int(l(5)/spacing)+1 from the x-directed section 4
c      spac(5)=l(5)/ilist(5) from the x-directed section 4
c      ilist(3)=int(l(3)/spacing)+1 from the x-directed section 3
c      spac(3)=l(3)/ilist(3) from the x-directed section 3
do i=1,ilist(3)
  do j=1,ilist(5)
    coordinates(1,tag)=l(3)+spac(3)*(i-1)
    coordinates(4,tag)=coordinates(1,tag)
    coordinates(2,tag)=l(6)+spac(5)*(j-1)
    coordinates(5,tag)=l(6)+spac(5)*j
    coordinates(3,tag)=tabheight
    coordinates(6,tag)=tabheight
    tag=tag+1
  end do
end do

c      This section draws the
c      y-directed front section 6 of the table

c      ilist(5)=int(l(5)/spacing)+1 from the x-directed section 4
c      spac(5)=l(5)/ilist(5) from the x-directed section 4
c      ilist(4)=int(l(4)/spacing)+1 from the x-directed section 3
c      spac(4)=l(4)/ilist(4) from the x-directed section 3
do i=1,ilist(4)+1
  do j=1,ilist(5)
    coordinates(1,tag)=l(1)-l(4)+spac(4)*(i-1)
    coordinates(4,tag)=coordinates(1,tag)
    coordinates(2,tag)=l(6)+spac(5)*(j-1)
    coordinates(5,tag)=l(6)+spac(5)*j
    coordinates(3,tag)=tabheight
    coordinates(6,tag)=tabheight
    tag=tag+1
  end do
end do

c      This is the end of the y-directed section
      ytmx=tag

```

```

c*****
c*****This is the beginning of the z-directed wire section
      ztmin=tag

c      This is the end of the z-directed section
      ztmax=tag

c*****
c*****This is the beginning of the other-directed wire section
      otmin=tag

c      This section draws the x-directed wire radiator
c      This line sets the end wire of the harness to be exited
do i=1,ilist(3)*10
      coordinates(1,tag)=l(3)+spac(3)*(i-1)/10
      coordinates(4,tag)=l(3)+spac(3)*i/10
      coordinates(2,tag)=l(6)
      coordinates(5,tag)=coordinates(2,tag)
      coordinates(3,tag)=tabheight+wireh
      coordinates(6,tag)=coordinates(3,tag)
      tag=tag+1
end do

c      This section draws the z-directed wire radiator
      ilist(6)=int(10*wireh/spacing)+1
      spac(6)=wireh/ilist(6)
      wiretag(1)=tag+ilist(6)/2
do i=1,ilist(6)
      coordinates(1,tag)=l(3)
      coordinates(4,tag)=coordinates(1,tag)
      coordinates(2,tag)=l(6)
      coordinates(5,tag)=coordinates(2,tag)
      coordinates(3,tag)=tabheight+spac(6)*(i-1)
      coordinates(6,tag)=tabheight+spac(6)*i
      tag=tag+1
end do

c      This section draws the z-directed wire radiator
      wiretag(2)=tag+ilist(6)/2
do i=1,ilist(6)
      coordinates(1,tag)=l(1)-l(4)
      coordinates(4,tag)=coordinates(1,tag)
      coordinates(2,tag)=l(6)

```

```

        coordinates(5,tag)=coordinates(2,tag)
        coordinates(3,tag)=tabheight+spac(6)*(i-1)
        coordinates(6,tag)=tabheight+spac(6)*i
        tag=tag+1
    end do

c*****This section draws the dipole antenna
    ilist(7)=20
    l(12)=l(11)/(2*ilist(7)+1)
    spac(7)=(l(11)-l(12))/ilist(7)
c    This next point defines the feed point
    coordinates(1,tag)=l(8)-l(12)
    coordinates(4,tag)=l(8)+l(12)
    coordinates(2,tag)=l(9)
    coordinates(5,tag)=coordinates(2,tag)
    coordinates(3,tag)=l(10)
    coordinates(6,tag)=l(10)
    wiretag(3)=tag
    tag=tag+1

c    Now some of the important tag locations will be written
c    to the screen
    write(*,*) 'Port 1 (wiretag(1))=', wiretag(1)
    write(*,*) 'Location of 50 Ohm load (wiretag(2))=', wiretag(2)
    write(*,*) 'Port 2 (wiretag(3))=', wiretag(3)

    do i=1,ilist(7)
        coordinates(1,tag)=l(8)-l(12)-(i-1)*spac(7)
        coordinates(4,tag)=l(8)-l(12)-i*spac(7)
        coordinates(2,tag)=l(9)
        coordinates(5,tag)=coordinates(2,tag)
        coordinates(3,tag)=l(10)
        coordinates(6,tag)=coordinates(3,tag)
        tag=tag+1
    end do

    do i=1,ilist(7)
        coordinates(1,tag)=l(8)+l(12)+(i-1)*spac(7)
        coordinates(4,tag)=l(8)+l(12)+i*spac(7)
        coordinates(2,tag)=l(9)
        coordinates(5,tag)=coordinates(2,tag)
        coordinates(3,tag)=l(10)
    end do

```

```

        coordinates(6,tag)=coordinates(3,tag)
        tag=tag+1
    end do

c      this is the end of the other-directed section
      otmax=tag

c*****
c*****This part writes out the wires from the coordinate matrix
c      to the nec input file

      do i=1,tag-1
          write(10,100) 'gw',i,nseg,coordinates(1,i),
+          coordinates(2,i),coordinates(3,i),coordinates(4,i),
+          coordinates(5,i),coordinates(6,i),wrad
      end do

c*****
c*****This is the 'nec.par' writing section

c write to the nec.par file
      write(20,*) xtmin
      write(20,*) xtmax
      write(20,*) ytmin
      write(20,*) ytmax
      write(20,*) ztmin
      write(20,*) ztmax
      write(20,*) otmin
      write(20,*) otmax
      write(20,*) tag-1
      write(20,*) wiretag(1)
      write(20,*) wiretag(3)

100    format(a2,i6,i3,f10.4,F10.4,F10.4,F10.4,F10.4,F10.4,F10.4)
      return
      end

c*****

```

```

C*****
      subroutine exite

C*****
C      subroutine exite is a function used
C      to write the exitation card
C*****
      integer*4 gndflag,xqflag,freqflag,freqnum,maxseg,
+      wiretag(10),zpar_flag
      real*8 minfreq,maxfreq,freqstep,maxf100,minf100,
+      xcurp,cmom,
+      tabheight
      common/bbeginning1/minfreq,maxfreq,maxseg
      common/gnd/gndflag
      common/xqf/xqflag
      common/frqstuff/freqflag,freqstep,freqnum
      common/harness/wiretag
      common/zpar_vars/zpar_flag

C      These nex frequencies are made so that they are in MHz.
      maxf100=maxfreq/1000000.
      minf100=minfreq/1000000.

C      tabheight is the table height
      tabheight=.9

C      The geometry ends with the 'ge' command
      if(gndflag.eq.1) then
        write(10,200) 'ge    -1'
      else
        write(10,100) 'ge'
      end if

      if(xqflag.ne.0) then
        if(freqflag.eq.1) then
          write(10,105) 'fr','0',freqnum,'0','0',minf100,
+          freqstep/1000000.
        else
          write(10,110) 'fr','0','1','0','0',maxf100
        end if
      end if

C      This section loads the
C      wire radiator at the end of the wire
      write(10,140) 'ld','4',wiretag(2),'1','1','50.','0'

```

```

c      These next lines load the
c      dipole receiving antenna at the center
c      The loading is dependent on
c      which z-parameter is being calculated
if(zpar_flag.eq.0) then
  write(10,140) 'ld','4',wiretag(3),'1','1','300.','0'
end if
if(zpar_flag.eq.2) then
  write(10,140) 'ld','4',wiretag(3),'1','1','9999999999.','0'
end if
if(zpar_flag.eq.3) then
  write(10,140) 'ld','4',wiretag(1),'1','1','9999999999.','0'
end if

if(xqflag.eq.1) then
  write(10,120) 'ex','1','1','1','0','0.','0.','0.'
end if

c*****
c      This section will generate the voltage excitation on the
c      wire harness (if xqflag=2)
if(xqflag.eq.2) then
  if(zpar_flag.eq.0) then
    write(10,121) 'ex','0',wiretag(1),'1','0','1.'
  end if
  if(zpar_flag.eq.1) then
    write(10,121) 'ex','0',wiretag(1),'1','0','1.'
  end if
  if(zpar_flag.eq.2) then
    write(10,121) 'ex','0',wiretag(1),'1','0','1.'
  end if
  if(zpar_flag.eq.3) then
    write(10,121) 'ex','0',wiretag(3),'1','0','1.'
  end if
end if

if(gndflag.eq.1) then
c      This statement creates the ground plane under the table.
  write(10,210) 'gn','1'
end if

```

```

        if(xqflag.ne.0) then
c      NEC uses this statement as a signal to calculate the currents.
        write(10,130) 'xq'
        end if

100     format(a2)
105     format(a2,a6,i8,a8,a8,f8.2,f8.2)
110     format(a2,a6,a8,a8,a8,f8.2)
120     format(a2,a6,a8,a8,a8,a8,a8,a8)
121     format(a2,a6,i8,a8,a8,a8)
125     format(a2,a6,a6,a6,a6,f9.4,f9.4,f9.4,a6,a6,f9.4)
130     format(a2)
140     format(a2,a6,i8,a8,a8,a13,a8)
200     format(a8)
210     format(a2,a6)

        return
        end

c*****
c*****
        subroutine finish

c*****
c      subroutine finish completes the program
c*****
        write(10,100) 'en'
        close(10)
        close(20)
        close(30)
100     format(a2)
        return
        end

```

APPENDIX B

ADDITIONAL FORTRAN PROGRAMS

B.1 Overview

As well as the grid-generating program `cmst1` discussed in Appendix A, additional Fortran programs were written for use in this project. Three important programs, `zparmake`, `sparconv` and `sphase` will be discussed in this appendix. The Fortran source code for the three programs will also be included.

B.2 Z-Parameter Calculation Program

The program `zparmake` was written to take the input files `cur_p1z1.txt`, `cur_p2z1.txt`, `cur_p1z2.txt`, and `cur_p2z3.txt` created from NEC during various NEC runs, and use the data to compute the Z -parameters of the table-antenna system. The equations governing the relations between the measured currents and the Z -parameters were discussed in Chapter 3.

The subroutine ‘`readfiles`’ is called for the first step performed by `zparmake`. In this subroutine all of the input and output files are opened and variables are initialized. The input files are read and the currents are stored in complex arrays. These arrays are passed to the next subroutine.

Next, the subroutine ‘`zmake`’ processes the raw currents stored in the arrays found by the subroutine ‘`readfiles`’. The Z -parameters are computed in this subroutine using the relations discussed in Section 3.4. These Z -parameters are then written to the files `z11_num.txt`, `z21_num.txt` and `z22_num.txt`. Finally, the subroutine ‘`finish`’ closes all the files and finishes the program. The source code for the program `zparmake` is included in the next section.

B.3 Source Code for zparamake

The following is the source code for the program zparamake.

```

      program zparamake
c*****
c      This program will make z-parameters from measured currents
c      taken from NEC output
c
c      It is assumed that the applied voltage for either
c      port 1 or port 2 is 1 Volt
c
c      This program was last modified on 5/21/99
c*****

      call readfiles
      call zmake
      call finish
      end

      subroutine readfiles
c*****
c      This subroutine reads in the output files generated
c      from the modified NEC program. The subroutine then
c      puts them into matrices so that they can be manipulated
c      into Z-parameters
c*****

      common /matrix/ num_mat
      common /freqs/ minfreq,maxfreq,nof
      common /currents/ ncur_p1z1,ncur_p1z2,ncur_p2z1,
+   ncur_p2z3

      complex*16 num_mat(2,2,201),ncur_p1z1(201),
+   ncur_p1z2(201),
+   ncur_p1z3(201),
+   ncur_p2z1(201),
+   ncur_p2z3(201)
      real*8 minfreq,maxfreq,treal,timag
      integer nof

c      Files 10,20,40,60 are the modified-NEC output files that
c      contain information about the Z-parameters. File 70
```

```

c      ('zparinfor.par') contains frequency and number of data
c      point taken information.
      open(10,file='cur_p1z1.txt',status='unknown')
      open(20,file='cur_p1z2.txt',status='unknown')
      open(40,file='cur_p2z1.txt',status='unknown')
      open(60,file='cur_p2z3.txt',status='unknown')
      open(70,file='zparinfo.par',status='unknown')

c      Files 80-82 are the Z-parameter output files.
c      It is assumed that z21=z12.
      open(80,file='z11_num.txt',status='unknown')
      open(81,file='z21_num.txt',status='unknown')
      open(82,file='z22_num.txt',status='unknown')

c      Now the minimum and maximum frequencies, as well as the
c      number of frequency points will be read in from
c      'zparinfo.par'.
      read(70,*) minfreq,maxfreq,nof
      write(*,*) minfreq,maxfreq,nof

c      Now the NEC output files will be read
      do i=1,nof
        read(10,*) treal,timag
        ncur_p1z1(i)=dcmplx(treal,timag)
      end do

      do i=1,nof
        read(20,*) treal,timag
        ncur_p1z2(i)=dcmplx(treal,timag)
      end do

      do i=1,nof
        read(40,*) treal,timag
        ncur_p2z1(i)=dcmplx(treal,timag)
      end do

      do i=1,nof
        read(60,*) treal,timag
        ncur_p2z3(i)=dcmplx(treal,timag)
      end do

      return

```

```

end

      subroutine zmake
c*****
c      This subroutine takes the raw current from the
c      NEC output and calculates the Z-parameters of the
c      two port network.
c*****

      common /matrix/ num_mat
      common /freqs/ minfreq,maxfreq,nof
      common /currents/ ncur_p1z1,ncur_p1z2,ncur_p2z1,
+   ncur_p2z3

      complex*16 num_mat(2,2,201),ncur_p1z1(201),
+   ncur_p1z2(201),ncur_p2z1(201),
+   ncur_p2z3(201),z11(201),z21(201),
+   z22(201)
      real*8 minfreq,maxfreq,Vapp,treal,timag
      integer nof

c      Vapp is the applied test voltage to the ports
      Vapp=1

c      Now the Z-parameters will be calculated.
      do i=1,nof
         z11(i)=Vapp/ncur_p1z2(i)
         treal=dreal(z11(i))
         timag=dimag(z11(i))
         write(80,100) treal,timag
      end do

      do i=1,nof
         z22(i)=Vapp/ncur_p2z3(i)
         treal=dreal(z22(i))
         timag=dimag(z22(i))
         write(82,120) treal,timag
      end do

      do i=1,nof
         z21(i)=-z22(i)*ncur_p2z1(i)/ncur_p1z1(i)
         treal=dreal(z21(i))
         timag=dimag(z21(i))
         write(81,110) treal,timag

```

```

end do

100   format(f9.4,'      ',f9.4)
110   format(f10.5,'      ',f10.5)
120   format(f10.4,'      ',f10.4)
      return
      end

      subroutine finish
c*****
c      This subroutine will close all the files.
c*****

      close(10)
      close(20)
      close(40)
      close(60)
      close(70)
      close(80)
      close(81)
      close(82)

      return
      end

```

B.4 Z-Parameter to S-Parameter Conversion and Data Processing Program

The program `sparconv` is another program used extensively for this project. After measurements from the HP 8510C Network Analyzer were stored to disk and the theoretical Z -parameters were calculated, the program `sparconv` was used to format all of the measured and numerical data so that it could be displayed using the commercial plotting program Axum.

The program `sparconv` begins by calling the ‘readfiles’ subroutine. This subroutine opens all of the input and output files that will be used by the program. The input files that are opened are the Z -parameter output files created by the `zparmake` program and an S -parameter measurement file created by the HP 8510C. The measured file created by the HP 8510C contains information about the measurement performed (date, time, number of points, starting and stopping frequencies, format of stored data, etc.) followed by the four S -parameters separated by text in real and imaginary format. The subroutine then reads in the S -parameters and stores them in a matrix.

Next, the subroutine ‘stoz’ is called. This subroutine calculates the Z -parameters from the measured S -parameters and writes them to the file `measzpar.txt`. Since S -parameters were chosen as a format to compare measured and theoretical data, the measured Z -parameters are not included in this thesis.

The subroutine ‘ztos’ is called next. This subroutine reads in all of the theoretical Z -parameters stored in the output files created by the program `zparmake` and converts them to S -parameters. The theoretical S -parameters are then stored in a matrix to be used in another subroutine.

The subroutine ‘data_output’ is then called to write the measured and theoretical S -parameters to eight separate output files (four for the measured parameters and

four for the theoretical parameters) in magnitude and phase format. Before the parameters are written to the output files, the phase is unwrapped so that it appears more continuous. In fact, another short Fortran program was written to further unwrap the phase of the S -parameters. This program, `sphase`, is discussed in the Section B.6. After the 'data_output' subroutine has written the output files, all of the input and output files are closed and the `sparconv` program ends. The source code for this program is included in the next section.

B.5 Source Code for sparconv

The following is the source code for the program sparconv.

```

      program sparconv
c*****
c      this program will read in S-parameter measurements
c      and Z-parameter numerical calculations, convert the numerical
c      Z-parameters to S-parameters, and output the results into
c      several files so that they can be easily plotted using Axum.
c      This program was last modified on 5/19/99
c*****

      call readfiles
      call stoz
      call ztos
      call data_output
      end

      subroutine readfiles
c*****
c      This subroutine will read in the measured S-parameters
c      and put them into a 2 by 2 by nop matrix where nop is the
c      number of points
c*****

      common /matrix/ meas_matrix,nop
      common /freqs/f_min,f_max
      common /meas_s/ms

      real*8 s_real,s_imag,f_min,f_max
      integer readflag,nop,endflag
      complex*16 meas_matrix(2,2,5000),ms(2,2,5000)
      character btemp*80, filename*80

      write(*,*) 'Enter measured S-parameter filename'
      read(*,*) filename

c      Now all of the files that are needed will be opened.
c      File 10 is the measured S-parameter file taken from
c      the HP 8510c Network analyzer.
      open(10,file=filename,status='unknown')

c      Files 11-13 are the NEC-calculated Z-parameters (Z21=Z12)
      open(11,file='z11_num.txt',status='unknown')
```

```

open(12,file='z21_num.txt',status='unknown')
open(13,file='z22_num.txt',status='unknown')

c   Files 20 and 30 are measured S and Z parameters put in
c   files so that they could be easily displayed in Matlab.
open(20,file='measspar.txt',status='unknown')
open(30,file='measzpar.txt',status='unknown')

c   Files 31-34 are the measured S-parameters in a format where
c   they can be plotted using Axum. The first column in each file
c   is the frequency (in MHz), the second column is the magnitude
c   of the S-parameter (S21 and S12 are in dB), and the third
c   column is the phase.
open(31,file='s11.txt',status='unknown')
open(32,file='s21.txt',status='unknown')
open(33,file='s12.txt',status='unknown')
open(34,file='s22.txt',status='unknown')

c   Files 35-38 are the NEC-calculated S-parameters in a format
c   where they can be plotted using Axum. The first column in each
c   file is the frequency (in MHz), the second column is the
c   magnitude of the S-parameter (S21 and S12 are in dB), and the
c   third column is the phase.
open(35,file='ns11.txt',status='unknown')
open(36,file='ns21.txt',status='unknown')
open(37,file='ns12.txt',status='unknown')
open(38,file='ns22.txt',status='unknown')

readflag=0
c   This do loop looks in the measurement file for the letters
c   'SEG_LIST_BEGIN' because frequency information will follow.
do while (readflag.eq.0)
  read(10,*) btemp
  if(btemp.eq.'SEG_LIST_BEGIN') then
    write(*,*) btemp
    readflag=1
  end if
end do

c   Now the minimum frequency, the maximum frequency, and the
c   number of points is read in. 'btemp' is just a dummy
c   variable used to read in (but not use) a character string.
read(10,*) btemp,f_min,f_max,nop

c   This next loop looks for the letters 'BEGIN' so that it knows

```

```

c      when the S-parameter measurements start.
      readflag=0
      do while (readflag.eq.0)
        read(10,*) btemp
        if(btemp.eq.'BEGIN') then
          write(*,*) btemp
          readflag=1
        end if
      end do

      endflag=0
      do j=1,2
        do k=1,2
          do i=1,nop
            read(10,*) s_real,s_imag
c      meas_matrix(k,j,i) is the measured S_parameter matrix that
c      will be converted to a measured Z-parameter matrix for
c      use by other programs
            meas_matrix(k,j,i)=dcmplx(s_real,s_imag)
c      'ms' is the measured S-parameter matrix (S_kj matrix).
            ms(k,j,i)=meas_matrix(k,j,i)
            write(20,100) s_real,s_imag
          end do
c      This extra read in of 'btemp' is because there is character
c      information separating the S-parameter lists
            read(10,*) btemp
            if(btemp.ne.'END') then
              write(*,*) 'END not correctly reached'
            end if
            endflag=endflag+1
            if(endflag.ne.4) then
              read(10,*) btemp
            end if
          end do
        end do
      end do

100   format(f14.10,'      ',f14.10)
      close(10)
      close(20)
      return
      end

```

```

subroutine stoz

```

```

C*****
c      this subroutine (pilfered from Rothwell's 2port.for)
c      converts s-parameters to z-parameters
C*****

      common /matrix/ m,nop

      complex*16 m(2,2,5000),dummy(2,2,5000)
      complex*16 den
      integer nop
      real*8 z0

c      z0 is the characteristic impedance of the two port network.
c      It is assumed to be 50 Ohms for convenience.
      z0=50.

      do i=1,4*nop
          den=((1.-m(1,1,i))*(1.-m(2,2,i))-m(1,2,i)*m(2,1,i))/z0
          dummy(1,1,i)=(1.+m(1,1,i))*(1.-m(2,2,i))+
+           m(1,2,i)*m(2,1,i)
          dummy(1,2,i)=2.*m(1,2,i)
          dummy(2,1,i)=2.*m(2,1,i)
          dummy(2,2,i)=(1.-m(1,1,i))*(1.+m(2,2,i))+
+           m(1,2,i)*m(2,1,i)

c      This next line checks the value of the denominator
c      and then sets it to a small value if it is zero so that
c      no divide by zero is performed.
          if(cdabs(den).eq.0.) den=(1.e-20,0)

          m(1,1,i)=dummy(1,1,i)/den
          m(1,2,i)=dummy(1,2,i)/den
          m(2,1,i)=dummy(2,1,i)/den
          m(2,2,i)=dummy(2,2,i)/den
      end do

      return
      end

      subroutine ztos
C*****
c      this subroutine takes the numerical z-parameters
c      and converts them to s-parameters

```

```

C*****
      common /freqs/f_min,f_max
      common /matrix/m,nop
      common /num_s/ns

      real*8 f_min,f_max,z_real,z_imag
      complex*16 m(2,2,5000),n(2,2,5000),ns(2,2,5000),
+   z0,delt_z
      integer nop

c      The characteristic impedance of the two port network is chosen
c      to be 50 Ohms for convenience.
      z0=dcmplx(50.,0.)

c      This do loop will read in the numerical Z-parameters ('n') and
c      calculate the numerical S-parameters ('ns')
      do i=1,101
          read(11,*) z_real,z_imag
          n(1,1,i)=dcmplx(z_real,z_imag)
          read(12,*) z_real,z_imag
          n(2,1,i)=dcmplx(z_real,z_imag)
          n(1,2,i)=n(2,1,i)
          read(13,*) z_real,z_imag
          n(2,2,i)=dcmplx(z_real,z_imag)
c      now the numerical S-parameters ('ns') will be calculated
          delt_z=(n(1,1,i)+z0)*(n(2,2,i)+z0)-n(1,2,i)*n(2,1,i)
          ns(1,1,i)=((n(1,1,i)-z0)*(n(2,2,i)+z0)-n(1,2,i)*n(2,1,i))/
+             delt_z
          ns(2,1,i)=2*z0*n(2,1,i)/delt_z
          ns(1,2,i)=ns(2,1,i)
          ns(2,2,i)=((n(1,1,i)+z0)*(n(2,2,i)-z0)-n(1,2,i)*n(2,1,i))/
+             delt_z
      end do

      return
      end

      subroutine data_output
C*****
c      this subroutine takes the z-parameters
c      (converted from the measured s-parameters)
c      and outputs them to the data file 'measzpar.txt'
C*****

```

```

common /matrix/ meas_z,nop
common /num_s/ns
common /meas_s/ms
common /freqs/f_min,f_max

real*8 f_min,f_max,f,smag,sphase(5000),tmpphase,phasetol
complex*16 meas_z(2,2,5000),ns(2,2,5000),ms(2,2,5000)
integer nop

c      converting the frequency bounds so that they can be
c      read in MegaHertz
f_min=f_min/1.d6
f_max=f_max/1.d6

c      This do loop writes out the measured Z-parameters to the
c      file 'measzpar.txt'
do j=1,2
  do k=1,2
    do i=1,nop
      write(30,100) dreal(meas_z(k,j,i)),
+      dimag(meas_z(k,j,i))
    end do
  end do
end do

c      'phasetol' and 'tmpphase' are used in the phase unwrapping
c      section in the next do loop.
phasetol=250
tmpphase=0.

c      This next long do loop writes out the numerical and measured
c      S-parameters to the files 31-38. Column 1 of every file is
c      the frequency in MHz, column 2 is the magnitude (S21 and S12
c      are expressed in dB), and column 3 is the phase.
do j=1,2
  do k=1,2
    do i=1,nop
      f=f_min+(i-1)*((f_max-f_min)/(nop-1))
      smag=abs(ms(k,j,i))

      sphase(i)=(180/3.1415926)*atan2(dimag(ms(k,j,i)),
+      dreal(ms(k,j,i)))

```

```

c      This next 'if' statement is so that the phase is 'unwrapped'
c      by testing whether the phase skips between -180 and 180 and
c      then forcing the phase to be continuous.

```

```

      if(i.gt.1) then
        tmpphase=sphase(i-1)
        if(sphase(i)-tmpphase.gt.phasetol) then
          sphase(i)=sphase(i)-360
        else if(sphase(i)-tmpphase.lt.-phasetol) then
          sphase(i)=sphase(i)+360
        end if
      end if

```

```

      if(k.eq.1) then
        if(j.eq.1) then
          write(31,*) f,smag,sphase(i)
        else
          write(33,*) f,20*log(smag),sphase(i)
        end if
      else
        if(j.eq.1) then
          write(32,*) f,20*log(smag),sphase(i)
        else
          write(34,*) f,smag,sphase(i)
        end if
      end if

```

```

end do

```

```

do i=1,101
  f=f_min+(i-1)*((f_max-f_min)/(101-1))
  smag=abs(ns(k,j,i))
  sphase(i)=(180/3.1415926)*atan2(dimag(ns(k,j,i)),
+    dreal(ns(k,j,i)))

```

```

c      This next 'if' statement is so that the phase is 'unwrapped'
c      by testing whether the phase skips between -180 and 180 and
c      then forcing the phase to be continuous.

```

```

      if(i.gt.1) then
        tmpphase=sphase(i-1)
        if(sphase(i)-tmpphase.gt.phasetol) then
          sphase(i)=sphase(i)-360
          write(*,*)
        else if(sphase(i)-tmpphase.lt.-phasetol) then
          sphase(i)=sphase(i)+360

```

```

        write(*,*)
        end if
    end if

    if(k.eq.1) then
        if(j.eq.1) then
            write(35,*) f,smag,sphase(i)
        else
c           write(37,*) f,smag,sphase(i)
            write(37,*) f,20*log(smag),sphase(i)
        end if
    else
c       if(j.eq.1) then
            write(36,*) f,smag,sphase(i)
            write(36,*) f,20*log(smag),sphase(i)
        else
            write(38,*) f,smag,sphase(i)
        end if
    end if
c       write(35,*) f,smag,sphase(i)
    end do
end do

close(10)
close(11)
close(12)
close(13)
close(20)
close(30)
close(31)
close(32)
close(33)
close(34)
close(35)
close(36)
close(37)
close(38)

100  format(f14.8,'      ',f14.8)
      return
      end

```

B.6 Phase Correction Program

The program `sphase` is a simple program written to help correct the phase of an S -parameter. After the program `sparconv` has been run, sometimes large sections of the phase of the S -parameters appear to be 360 degrees below the rest of the phase. The program `sphase` corrects this problem. The band of frequencies that needs correction is first determined visually. Then the beginning and ending frequencies of this band are given as input to the program `sphase` during the program's operation. Then `sphase` then simply adds 360 degrees to the phase of the S -parameter in the band of frequencies specified. The program then rewrites the entire S -parameter file with the corrected phase. The source code for this program is included in the next section.

B.7 Source Code for sphase

The following is the source code for the program sphase.

```
      program sphase
c*****
c      This program will help unwrap the phase of
c      S-parameters by adding 360 degrees to certain
c      sections of the phase.
c      This program was last modified on 5/20/99
c*****

      real*8 f(5000),smag(5000),sp(5000),f_min,f_max,
+   f_beg,f_end
      integer nop,i,ibeg,iend
      character filename*80

      nop=801

      write(*,*) 'Enter measured S-parameter filename
+   to be unwrapped'
      read(*,*) filename

      open(10,file=filename,status='unknown')

      write(*,*) 'Enter begin frequency in MHz'
      read(*,*) f_beg

      write(*,*) 'Enter end frequency in MHz'
      read(*,*) f_end

c      These do statements find the frequency at which the phase
c      modification will begin, and then it will add 360 degrees
c      to the phase until the end frequency is reached. Then
c      the rest of the S-parameters will be read in so they can
c      be rewritten in a later loop.

      readflag=0
      i=1
      do while (readflag.eq.0)
         read(10,*) f(i),smag(i),sp(i)
         if(f(i).gt.f_beg) then
            ibeg=i
            readflag=1
         end if
      end do
```

```

    i=i+1
end do
write(*,*) ibeg,f(i-1)

readflag=0
do while (readflag.eq.0)
  read(10,*) f(i),smag(i),sp(i)
  sp(i)=sp(i)+360
  if(f(i).gt.f_end) then
    iend=i
    readflag=1
  end if
  i=i+1
end do

do i=iend+1,nop
  read(10,*) f(i),smag(i),sp(i)
end do

close(10, status='delete')
open(20,file=filename,status='unknown')

```

c The S-parameters will now be re-written to the same file
c with the modified phase.

```

do i=1,nop
  write(20,*) f(i),smag(i),sp(i)
end do

```

```

close(20)
end

```

APPENDIX C

NEC INPUT CODE

C.1 NEC Input Code

As discussed in Appendix A, the program `cmst1` was used to generate an input file to be used by the program NEC. This input file, `nec.in`, contains all of the information pertaining to wire locations and radii, voltage excitations, loads, the ground plane, and frequency data.

The following pages contain the NEC input code “`nec.in`”. This NEC input file was generated to produce an open circuit located at port 1, and a voltage source applied at port 2. The output created from NEC using this input file will be used to calculate the Z -parameters of the table / antenna system using the method discussed in Chapter 3.

```

cm      NEC input file for CISPR table
ce      Written by Chris Coleman
gw      1  1  0.0000  0.0000  0.9000  0.1567  0.0000  0.9000  0.0010
gw      2  1  0.1567  0.0000  0.9000  0.3133  0.0000  0.9000  0.0010
gw      3  1  0.3133  0.0000  0.9000  0.4700  0.0000  0.9000  0.0010
gw      4  1  0.0000  0.1867  0.9000  0.1567  0.1867  0.9000  0.0010
gw      5  1  0.1567  0.1867  0.9000  0.3133  0.1867  0.9000  0.0010
gw      6  1  0.3133  0.1867  0.9000  0.4700  0.1867  0.9000  0.0010
gw      7  1  0.0000  0.3733  0.9000  0.1567  0.3733  0.9000  0.0010
gw      8  1  0.1567  0.3733  0.9000  0.3133  0.3733  0.9000  0.0010
gw      9  1  0.3133  0.3733  0.9000  0.4700  0.3733  0.9000  0.0010
gw     10  1  0.0000  0.5600  0.9000  0.1567  0.5600  0.9000  0.0010
gw     11  1  0.1567  0.5600  0.9000  0.3133  0.5600  0.9000  0.0010
gw     12  1  0.3133  0.5600  0.9000  0.4700  0.5600  0.9000  0.0010
gw     13  1  0.0000  0.7467  0.9000  0.1567  0.7467  0.9000  0.0010
gw     14  1  0.1567  0.7467  0.9000  0.3133  0.7467  0.9000  0.0010
gw     15  1  0.3133  0.7467  0.9000  0.4700  0.7467  0.9000  0.0010
gw     16  1  0.0000  0.9333  0.9000  0.1567  0.9333  0.9000  0.0010
gw     17  1  0.1567  0.9333  0.9000  0.3133  0.9333  0.9000  0.0010
gw     18  1  0.3133  0.9333  0.9000  0.4700  0.9333  0.9000  0.0010
gw     19  1  0.4700  0.0000  0.9000  0.6575  0.0000  0.9000  0.0010
gw     20  1  0.6575  0.0000  0.9000  0.8450  0.0000  0.9000  0.0010
gw     21  1  0.8450  0.0000  0.9000  1.0325  0.0000  0.9000  0.0010
gw     22  1  1.0325  0.0000  0.9000  1.2200  0.0000  0.9000  0.0010
gw     23  1  1.2200  0.0000  0.9000  1.4075  0.0000  0.9000  0.0010
gw     24  1  1.4075  0.0000  0.9000  1.5950  0.0000  0.9000  0.0010
gw     25  1  1.5950  0.0000  0.9000  1.7825  0.0000  0.9000  0.0010
gw     26  1  1.7825  0.0000  0.9000  1.9700  0.0000  0.9000  0.0010
gw     27  1  0.4700  0.1867  0.9000  0.6575  0.1867  0.9000  0.0010
gw     28  1  0.6575  0.1867  0.9000  0.8450  0.1867  0.9000  0.0010
gw     29  1  0.8450  0.1867  0.9000  1.0325  0.1867  0.9000  0.0010
gw     30  1  1.0325  0.1867  0.9000  1.2200  0.1867  0.9000  0.0010
gw     31  1  1.2200  0.1867  0.9000  1.4075  0.1867  0.9000  0.0010
gw     32  1  1.4075  0.1867  0.9000  1.5950  0.1867  0.9000  0.0010
gw     33  1  1.5950  0.1867  0.9000  1.7825  0.1867  0.9000  0.0010
gw     34  1  1.7825  0.1867  0.9000  1.9700  0.1867  0.9000  0.0010
gw     35  1  0.4700  0.3733  0.9000  0.6575  0.3733  0.9000  0.0010
gw     36  1  0.6575  0.3733  0.9000  0.8450  0.3733  0.9000  0.0010
gw     37  1  0.8450  0.3733  0.9000  1.0325  0.3733  0.9000  0.0010
gw     38  1  1.0325  0.3733  0.9000  1.2200  0.3733  0.9000  0.0010
gw     39  1  1.2200  0.3733  0.9000  1.4075  0.3733  0.9000  0.0010
gw     40  1  1.4075  0.3733  0.9000  1.5950  0.3733  0.9000  0.0010
gw     41  1  1.5950  0.3733  0.9000  1.7825  0.3733  0.9000  0.0010
gw     42  1  1.7825  0.3733  0.9000  1.9700  0.3733  0.9000  0.0010
gw     43  1  0.4700  0.5600  0.9000  0.6575  0.5600  0.9000  0.0010
gw     44  1  0.6575  0.5600  0.9000  0.8450  0.5600  0.9000  0.0010
gw     45  1  0.8450  0.5600  0.9000  1.0325  0.5600  0.9000  0.0010
gw     46  1  1.0325  0.5600  0.9000  1.2200  0.5600  0.9000  0.0010
gw     47  1  1.2200  0.5600  0.9000  1.4075  0.5600  0.9000  0.0010
gw     48  1  1.4075  0.5600  0.9000  1.5950  0.5600  0.9000  0.0010
gw     49  1  1.5950  0.5600  0.9000  1.7825  0.5600  0.9000  0.0010
gw     50  1  1.7825  0.5600  0.9000  1.9700  0.5600  0.9000  0.0010
gw     51  1  0.4700  0.7467  0.9000  0.6575  0.7467  0.9000  0.0010
gw     52  1  0.6575  0.7467  0.9000  0.8450  0.7467  0.9000  0.0010

```

gw	53	1	0.8450	0.7467	0.9000	1.0325	0.7467	0.9000	0.0010
gw	54	1	1.0325	0.7467	0.9000	1.2200	0.7467	0.9000	0.0010
gw	55	1	1.2200	0.7467	0.9000	1.4075	0.7467	0.9000	0.0010
gw	56	1	1.4075	0.7467	0.9000	1.5950	0.7467	0.9000	0.0010
gw	57	1	1.5950	0.7467	0.9000	1.7825	0.7467	0.9000	0.0010
gw	58	1	1.7825	0.7467	0.9000	1.9700	0.7467	0.9000	0.0010
gw	59	1	0.4700	0.9333	0.9000	0.6575	0.9333	0.9000	0.0010
gw	60	1	0.6575	0.9333	0.9000	0.8450	0.9333	0.9000	0.0010
gw	61	1	0.8450	0.9333	0.9000	1.0325	0.9333	0.9000	0.0010
gw	62	1	1.0325	0.9333	0.9000	1.2200	0.9333	0.9000	0.0010
gw	63	1	1.2200	0.9333	0.9000	1.4075	0.9333	0.9000	0.0010
gw	64	1	1.4075	0.9333	0.9000	1.5950	0.9333	0.9000	0.0010
gw	65	1	1.5950	0.9333	0.9000	1.7825	0.9333	0.9000	0.0010
gw	66	1	1.7825	0.9333	0.9000	1.9700	0.9333	0.9000	0.0010
gw	67	1	1.9700	0.0000	0.9000	2.1267	0.0000	0.9000	0.0010
gw	68	1	2.1267	0.0000	0.9000	2.2833	0.0000	0.9000	0.0010
gw	69	1	2.2833	0.0000	0.9000	2.4400	0.0000	0.9000	0.0010
gw	70	1	1.9700	0.1867	0.9000	2.1267	0.1867	0.9000	0.0010
gw	71	1	2.1267	0.1867	0.9000	2.2833	0.1867	0.9000	0.0010
gw	72	1	2.2833	0.1867	0.9000	2.4400	0.1867	0.9000	0.0010
gw	73	1	1.9700	0.3733	0.9000	2.1267	0.3733	0.9000	0.0010
gw	74	1	2.1267	0.3733	0.9000	2.2833	0.3733	0.9000	0.0010
gw	75	1	2.2833	0.3733	0.9000	2.4400	0.3733	0.9000	0.0010
gw	76	1	1.9700	0.5600	0.9000	2.1267	0.5600	0.9000	0.0010
gw	77	1	2.1267	0.5600	0.9000	2.2833	0.5600	0.9000	0.0010
gw	78	1	2.2833	0.5600	0.9000	2.4400	0.5600	0.9000	0.0010
gw	79	1	1.9700	0.7467	0.9000	2.1267	0.7467	0.9000	0.0010
gw	80	1	2.1267	0.7467	0.9000	2.2833	0.7467	0.9000	0.0010
gw	81	1	2.2833	0.7467	0.9000	2.4400	0.7467	0.9000	0.0010
gw	82	1	1.9700	0.9333	0.9000	2.1267	0.9333	0.9000	0.0010
gw	83	1	2.1267	0.9333	0.9000	2.2833	0.9333	0.9000	0.0010
gw	84	1	2.2833	0.9333	0.9000	2.4400	0.9333	0.9000	0.0010
gw	85	1	0.0000	1.1200	0.9000	0.1567	1.1200	0.9000	0.0010
gw	86	1	0.1567	1.1200	0.9000	0.3133	1.1200	0.9000	0.0010
gw	87	1	0.3133	1.1200	0.9000	0.4700	1.1200	0.9000	0.0010
gw	88	1	0.0000	1.2200	0.9000	0.1567	1.2200	0.9000	0.0010
gw	89	1	0.1567	1.2200	0.9000	0.3133	1.2200	0.9000	0.0010
gw	90	1	0.3133	1.2200	0.9000	0.4700	1.2200	0.9000	0.0010
gw	91	1	0.4700	1.1200	0.9000	0.6575	1.1200	0.9000	0.0010
gw	92	1	0.6575	1.1200	0.9000	0.8450	1.1200	0.9000	0.0010
gw	93	1	0.8450	1.1200	0.9000	1.0325	1.1200	0.9000	0.0010
gw	94	1	1.0325	1.1200	0.9000	1.2200	1.1200	0.9000	0.0010
gw	95	1	1.2200	1.1200	0.9000	1.4075	1.1200	0.9000	0.0010
gw	96	1	1.4075	1.1200	0.9000	1.5950	1.1200	0.9000	0.0010
gw	97	1	1.5950	1.1200	0.9000	1.7825	1.1200	0.9000	0.0010
gw	98	1	1.7825	1.1200	0.9000	1.9700	1.1200	0.9000	0.0010
gw	99	1	0.4700	1.2200	0.9000	0.6575	1.2200	0.9000	0.0010
gw	100	1	0.6575	1.2200	0.9000	0.8450	1.2200	0.9000	0.0010
gw	101	1	0.8450	1.2200	0.9000	1.0325	1.2200	0.9000	0.0010
gw	102	1	1.0325	1.2200	0.9000	1.2200	1.2200	0.9000	0.0010
gw	103	1	1.2200	1.2200	0.9000	1.4075	1.2200	0.9000	0.0010
gw	104	1	1.4075	1.2200	0.9000	1.5950	1.2200	0.9000	0.0010
gw	105	1	1.5950	1.2200	0.9000	1.7825	1.2200	0.9000	0.0010
gw	106	1	1.7825	1.2200	0.9000	1.9700	1.2200	0.9000	0.0010

gw	107	1	1.9700	1.1200	0.9000	2.1267	1.1200	0.9000	0.0010
gw	108	1	2.1267	1.1200	0.9000	2.2833	1.1200	0.9000	0.0010
gw	109	1	2.2833	1.1200	0.9000	2.4400	1.1200	0.9000	0.0010
gw	110	1	1.9700	1.2200	0.9000	2.1267	1.2200	0.9000	0.0010
gw	111	1	2.1267	1.2200	0.9000	2.2833	1.2200	0.9000	0.0010
gw	112	1	2.2833	1.2200	0.9000	2.4400	1.2200	0.9000	0.0010
gw	113	1	0.0000	0.0000	0.9000	0.0000	0.1867	0.9000	0.0010
gw	114	1	0.0000	0.1867	0.9000	0.0000	0.3733	0.9000	0.0010
gw	115	1	0.0000	0.3733	0.9000	0.0000	0.5600	0.9000	0.0010
gw	116	1	0.0000	0.5600	0.9000	0.0000	0.7467	0.9000	0.0010
gw	117	1	0.0000	0.7467	0.9000	0.0000	0.9333	0.9000	0.0010
gw	118	1	0.0000	0.9333	0.9000	0.0000	1.1200	0.9000	0.0010
gw	119	1	0.1567	0.0000	0.9000	0.1567	0.1867	0.9000	0.0010
gw	120	1	0.1567	0.1867	0.9000	0.1567	0.3733	0.9000	0.0010
gw	121	1	0.1567	0.3733	0.9000	0.1567	0.5600	0.9000	0.0010
gw	122	1	0.1567	0.5600	0.9000	0.1567	0.7467	0.9000	0.0010
gw	123	1	0.1567	0.7467	0.9000	0.1567	0.9333	0.9000	0.0010
gw	124	1	0.1567	0.9333	0.9000	0.1567	1.1200	0.9000	0.0010
gw	125	1	0.3133	0.0000	0.9000	0.3133	0.1867	0.9000	0.0010
gw	126	1	0.3133	0.1867	0.9000	0.3133	0.3733	0.9000	0.0010
gw	127	1	0.3133	0.3733	0.9000	0.3133	0.5600	0.9000	0.0010
gw	128	1	0.3133	0.5600	0.9000	0.3133	0.7467	0.9000	0.0010
gw	129	1	0.3133	0.7467	0.9000	0.3133	0.9333	0.9000	0.0010
gw	130	1	0.3133	0.9333	0.9000	0.3133	1.1200	0.9000	0.0010
gw	131	1	0.4700	0.0000	0.9000	0.4700	0.1867	0.9000	0.0010
gw	132	1	0.4700	0.1867	0.9000	0.4700	0.3733	0.9000	0.0010
gw	133	1	0.4700	0.3733	0.9000	0.4700	0.5600	0.9000	0.0010
gw	134	1	0.4700	0.5600	0.9000	0.4700	0.7467	0.9000	0.0010
gw	135	1	0.4700	0.7467	0.9000	0.4700	0.9333	0.9000	0.0010
gw	136	1	0.4700	0.9333	0.9000	0.4700	1.1200	0.9000	0.0010
gw	137	1	0.6575	0.0000	0.9000	0.6575	0.1867	0.9000	0.0010
gw	138	1	0.6575	0.1867	0.9000	0.6575	0.3733	0.9000	0.0010
gw	139	1	0.6575	0.3733	0.9000	0.6575	0.5600	0.9000	0.0010
gw	140	1	0.6575	0.5600	0.9000	0.6575	0.7467	0.9000	0.0010
gw	141	1	0.6575	0.7467	0.9000	0.6575	0.9333	0.9000	0.0010
gw	142	1	0.6575	0.9333	0.9000	0.6575	1.1200	0.9000	0.0010
gw	143	1	0.8450	0.0000	0.9000	0.8450	0.1867	0.9000	0.0010
gw	144	1	0.8450	0.1867	0.9000	0.8450	0.3733	0.9000	0.0010
gw	145	1	0.8450	0.3733	0.9000	0.8450	0.5600	0.9000	0.0010
gw	146	1	0.8450	0.5600	0.9000	0.8450	0.7467	0.9000	0.0010
gw	147	1	0.8450	0.7467	0.9000	0.8450	0.9333	0.9000	0.0010
gw	148	1	0.8450	0.9333	0.9000	0.8450	1.1200	0.9000	0.0010
gw	149	1	1.0325	0.0000	0.9000	1.0325	0.1867	0.9000	0.0010
gw	150	1	1.0325	0.1867	0.9000	1.0325	0.3733	0.9000	0.0010
gw	151	1	1.0325	0.3733	0.9000	1.0325	0.5600	0.9000	0.0010
gw	152	1	1.0325	0.5600	0.9000	1.0325	0.7467	0.9000	0.0010
gw	153	1	1.0325	0.7467	0.9000	1.0325	0.9333	0.9000	0.0010
gw	154	1	1.0325	0.9333	0.9000	1.0325	1.1200	0.9000	0.0010
gw	155	1	1.2200	0.0000	0.9000	1.2200	0.1867	0.9000	0.0010
gw	156	1	1.2200	0.1867	0.9000	1.2200	0.3733	0.9000	0.0010
gw	157	1	1.2200	0.3733	0.9000	1.2200	0.5600	0.9000	0.0010
gw	158	1	1.2200	0.5600	0.9000	1.2200	0.7467	0.9000	0.0010
gw	159	1	1.2200	0.7467	0.9000	1.2200	0.9333	0.9000	0.0010
gw	160	1	1.2200	0.9333	0.9000	1.2200	1.1200	0.9000	0.0010

gw	161	1	1.4075	0.0000	0.9000	1.4075	0.1867	0.9000	0.0010
gw	162	1	1.4075	0.1867	0.9000	1.4075	0.3733	0.9000	0.0010
gw	163	1	1.4075	0.3733	0.9000	1.4075	0.5600	0.9000	0.0010
gw	164	1	1.4075	0.5600	0.9000	1.4075	0.7467	0.9000	0.0010
gw	165	1	1.4075	0.7467	0.9000	1.4075	0.9333	0.9000	0.0010
gw	166	1	1.4075	0.9333	0.9000	1.4075	1.1200	0.9000	0.0010
gw	167	1	1.5950	0.0000	0.9000	1.5950	0.1867	0.9000	0.0010
gw	168	1	1.5950	0.1867	0.9000	1.5950	0.3733	0.9000	0.0010
gw	169	1	1.5950	0.3733	0.9000	1.5950	0.5600	0.9000	0.0010
gw	170	1	1.5950	0.5600	0.9000	1.5950	0.7467	0.9000	0.0010
gw	171	1	1.5950	0.7467	0.9000	1.5950	0.9333	0.9000	0.0010
gw	172	1	1.5950	0.9333	0.9000	1.5950	1.1200	0.9000	0.0010
gw	173	1	1.7825	0.0000	0.9000	1.7825	0.1867	0.9000	0.0010
gw	174	1	1.7825	0.1867	0.9000	1.7825	0.3733	0.9000	0.0010
gw	175	1	1.7825	0.3733	0.9000	1.7825	0.5600	0.9000	0.0010
gw	176	1	1.7825	0.5600	0.9000	1.7825	0.7467	0.9000	0.0010
gw	177	1	1.7825	0.7467	0.9000	1.7825	0.9333	0.9000	0.0010
gw	178	1	1.7825	0.9333	0.9000	1.7825	1.1200	0.9000	0.0010
gw	179	1	1.9700	0.0000	0.9000	1.9700	0.1867	0.9000	0.0010
gw	180	1	1.9700	0.1867	0.9000	1.9700	0.3733	0.9000	0.0010
gw	181	1	1.9700	0.3733	0.9000	1.9700	0.5600	0.9000	0.0010
gw	182	1	1.9700	0.5600	0.9000	1.9700	0.7467	0.9000	0.0010
gw	183	1	1.9700	0.7467	0.9000	1.9700	0.9333	0.9000	0.0010
gw	184	1	1.9700	0.9333	0.9000	1.9700	1.1200	0.9000	0.0010
gw	185	1	2.1267	0.0000	0.9000	2.1267	0.1867	0.9000	0.0010
gw	186	1	2.1267	0.1867	0.9000	2.1267	0.3733	0.9000	0.0010
gw	187	1	2.1267	0.3733	0.9000	2.1267	0.5600	0.9000	0.0010
gw	188	1	2.1267	0.5600	0.9000	2.1267	0.7467	0.9000	0.0010
gw	189	1	2.1267	0.7467	0.9000	2.1267	0.9333	0.9000	0.0010
gw	190	1	2.1267	0.9333	0.9000	2.1267	1.1200	0.9000	0.0010
gw	191	1	2.2833	0.0000	0.9000	2.2833	0.1867	0.9000	0.0010
gw	192	1	2.2833	0.1867	0.9000	2.2833	0.3733	0.9000	0.0010
gw	193	1	2.2833	0.3733	0.9000	2.2833	0.5600	0.9000	0.0010
gw	194	1	2.2833	0.5600	0.9000	2.2833	0.7467	0.9000	0.0010
gw	195	1	2.2833	0.7467	0.9000	2.2833	0.9333	0.9000	0.0010
gw	196	1	2.2833	0.9333	0.9000	2.2833	1.1200	0.9000	0.0010
gw	197	1	2.4400	0.0000	0.9000	2.4400	0.1867	0.9000	0.0010
gw	198	1	2.4400	0.1867	0.9000	2.4400	0.3733	0.9000	0.0010
gw	199	1	2.4400	0.3733	0.9000	2.4400	0.5600	0.9000	0.0010
gw	200	1	2.4400	0.5600	0.9000	2.4400	0.7467	0.9000	0.0010
gw	201	1	2.4400	0.7467	0.9000	2.4400	0.9333	0.9000	0.0010
gw	202	1	2.4400	0.9333	0.9000	2.4400	1.1200	0.9000	0.0010
gw	203	1	0.0000	1.1200	0.9000	0.0000	1.2200	0.9000	0.0010
gw	204	1	0.1567	1.1200	0.9000	0.1567	1.2200	0.9000	0.0010
gw	205	1	0.3133	1.1200	0.9000	0.3133	1.2200	0.9000	0.0010
gw	206	1	0.4700	1.1200	0.9000	0.4700	1.2200	0.9000	0.0010
gw	207	1	0.6575	1.1200	0.9000	0.6575	1.2200	0.9000	0.0010
gw	208	1	0.8450	1.1200	0.9000	0.8450	1.2200	0.9000	0.0010
gw	209	1	1.0325	1.1200	0.9000	1.0325	1.2200	0.9000	0.0010
gw	210	1	1.2200	1.1200	0.9000	1.2200	1.2200	0.9000	0.0010
gw	211	1	1.4075	1.1200	0.9000	1.4075	1.2200	0.9000	0.0010
gw	212	1	1.5950	1.1200	0.9000	1.5950	1.2200	0.9000	0.0010
gw	213	1	1.7825	1.1200	0.9000	1.7825	1.2200	0.9000	0.0010
gw	214	1	1.9700	1.1200	0.9000	1.9700	1.2200	0.9000	0.0010

gw	215	1	2.1267	1.1200	0.9000	2.1267	1.2200	0.9000	0.0010
gw	216	1	2.2833	1.1200	0.9000	2.2833	1.2200	0.9000	0.0010
gw	217	1	2.4400	1.1200	0.9000	2.4400	1.2200	0.9000	0.0010
gw	218	1	0.4700	1.1200	0.9500	0.4888	1.1200	0.9500	0.0010
gw	219	1	0.4888	1.1200	0.9500	0.5075	1.1200	0.9500	0.0010
gw	220	1	0.5075	1.1200	0.9500	0.5263	1.1200	0.9500	0.0010
gw	221	1	0.5263	1.1200	0.9500	0.5450	1.1200	0.9500	0.0010
gw	222	1	0.5450	1.1200	0.9500	0.5638	1.1200	0.9500	0.0010
gw	223	1	0.5638	1.1200	0.9500	0.5825	1.1200	0.9500	0.0010
gw	224	1	0.5825	1.1200	0.9500	0.6013	1.1200	0.9500	0.0010
gw	225	1	0.6013	1.1200	0.9500	0.6200	1.1200	0.9500	0.0010
gw	226	1	0.6200	1.1200	0.9500	0.6388	1.1200	0.9500	0.0010
gw	227	1	0.6388	1.1200	0.9500	0.6575	1.1200	0.9500	0.0010
gw	228	1	0.6575	1.1200	0.9500	0.6763	1.1200	0.9500	0.0010
gw	229	1	0.6763	1.1200	0.9500	0.6950	1.1200	0.9500	0.0010
gw	230	1	0.6950	1.1200	0.9500	0.7138	1.1200	0.9500	0.0010
gw	231	1	0.7138	1.1200	0.9500	0.7325	1.1200	0.9500	0.0010
gw	232	1	0.7325	1.1200	0.9500	0.7513	1.1200	0.9500	0.0010
gw	233	1	0.7513	1.1200	0.9500	0.7700	1.1200	0.9500	0.0010
gw	234	1	0.7700	1.1200	0.9500	0.7888	1.1200	0.9500	0.0010
gw	235	1	0.7888	1.1200	0.9500	0.8075	1.1200	0.9500	0.0010
gw	236	1	0.8075	1.1200	0.9500	0.8263	1.1200	0.9500	0.0010
gw	237	1	0.8263	1.1200	0.9500	0.8450	1.1200	0.9500	0.0010
gw	238	1	0.8450	1.1200	0.9500	0.8638	1.1200	0.9500	0.0010
gw	239	1	0.8638	1.1200	0.9500	0.8825	1.1200	0.9500	0.0010
gw	240	1	0.8825	1.1200	0.9500	0.9013	1.1200	0.9500	0.0010
gw	241	1	0.9013	1.1200	0.9500	0.9200	1.1200	0.9500	0.0010
gw	242	1	0.9200	1.1200	0.9500	0.9388	1.1200	0.9500	0.0010
gw	243	1	0.9388	1.1200	0.9500	0.9575	1.1200	0.9500	0.0010
gw	244	1	0.9575	1.1200	0.9500	0.9763	1.1200	0.9500	0.0010
gw	245	1	0.9763	1.1200	0.9500	0.9950	1.1200	0.9500	0.0010
gw	246	1	0.9950	1.1200	0.9500	1.0138	1.1200	0.9500	0.0010
gw	247	1	1.0138	1.1200	0.9500	1.0325	1.1200	0.9500	0.0010
gw	248	1	1.0325	1.1200	0.9500	1.0513	1.1200	0.9500	0.0010
gw	249	1	1.0513	1.1200	0.9500	1.0700	1.1200	0.9500	0.0010
gw	250	1	1.0700	1.1200	0.9500	1.0888	1.1200	0.9500	0.0010
gw	251	1	1.0888	1.1200	0.9500	1.1075	1.1200	0.9500	0.0010
gw	252	1	1.1075	1.1200	0.9500	1.1263	1.1200	0.9500	0.0010
gw	253	1	1.1263	1.1200	0.9500	1.1450	1.1200	0.9500	0.0010
gw	254	1	1.1450	1.1200	0.9500	1.1638	1.1200	0.9500	0.0010
gw	255	1	1.1638	1.1200	0.9500	1.1825	1.1200	0.9500	0.0010
gw	256	1	1.1825	1.1200	0.9500	1.2013	1.1200	0.9500	0.0010
gw	257	1	1.2013	1.1200	0.9500	1.2200	1.1200	0.9500	0.0010
gw	258	1	1.2200	1.1200	0.9500	1.2388	1.1200	0.9500	0.0010
gw	259	1	1.2388	1.1200	0.9500	1.2575	1.1200	0.9500	0.0010
gw	260	1	1.2575	1.1200	0.9500	1.2763	1.1200	0.9500	0.0010
gw	261	1	1.2763	1.1200	0.9500	1.2950	1.1200	0.9500	0.0010
gw	262	1	1.2950	1.1200	0.9500	1.3138	1.1200	0.9500	0.0010
gw	263	1	1.3138	1.1200	0.9500	1.3325	1.1200	0.9500	0.0010
gw	264	1	1.3325	1.1200	0.9500	1.3513	1.1200	0.9500	0.0010
gw	265	1	1.3513	1.1200	0.9500	1.3700	1.1200	0.9500	0.0010
gw	266	1	1.3700	1.1200	0.9500	1.3888	1.1200	0.9500	0.0010
gw	267	1	1.3888	1.1200	0.9500	1.4075	1.1200	0.9500	0.0010
gw	268	1	1.4075	1.1200	0.9500	1.4263	1.1200	0.9500	0.0010

gw	269	1	1.4263	1.1200	0.9500	1.4450	1.1200	0.9500	0.0010
gw	270	1	1.4450	1.1200	0.9500	1.4638	1.1200	0.9500	0.0010
gw	271	1	1.4638	1.1200	0.9500	1.4825	1.1200	0.9500	0.0010
gw	272	1	1.4825	1.1200	0.9500	1.5013	1.1200	0.9500	0.0010
gw	273	1	1.5013	1.1200	0.9500	1.5200	1.1200	0.9500	0.0010
gw	274	1	1.5200	1.1200	0.9500	1.5388	1.1200	0.9500	0.0010
gw	275	1	1.5388	1.1200	0.9500	1.5575	1.1200	0.9500	0.0010
gw	276	1	1.5575	1.1200	0.9500	1.5763	1.1200	0.9500	0.0010
gw	277	1	1.5763	1.1200	0.9500	1.5950	1.1200	0.9500	0.0010
gw	278	1	1.5950	1.1200	0.9500	1.6138	1.1200	0.9500	0.0010
gw	279	1	1.6138	1.1200	0.9500	1.6325	1.1200	0.9500	0.0010
gw	280	1	1.6325	1.1200	0.9500	1.6513	1.1200	0.9500	0.0010
gw	281	1	1.6513	1.1200	0.9500	1.6700	1.1200	0.9500	0.0010
gw	282	1	1.6700	1.1200	0.9500	1.6888	1.1200	0.9500	0.0010
gw	283	1	1.6888	1.1200	0.9500	1.7075	1.1200	0.9500	0.0010
gw	284	1	1.7075	1.1200	0.9500	1.7263	1.1200	0.9500	0.0010
gw	285	1	1.7263	1.1200	0.9500	1.7450	1.1200	0.9500	0.0010
gw	286	1	1.7450	1.1200	0.9500	1.7638	1.1200	0.9500	0.0010
gw	287	1	1.7638	1.1200	0.9500	1.7825	1.1200	0.9500	0.0010
gw	288	1	1.7825	1.1200	0.9500	1.8013	1.1200	0.9500	0.0010
gw	289	1	1.8013	1.1200	0.9500	1.8200	1.1200	0.9500	0.0010
gw	290	1	1.8200	1.1200	0.9500	1.8388	1.1200	0.9500	0.0010
gw	291	1	1.8388	1.1200	0.9500	1.8575	1.1200	0.9500	0.0010
gw	292	1	1.8575	1.1200	0.9500	1.8763	1.1200	0.9500	0.0010
gw	293	1	1.8763	1.1200	0.9500	1.8950	1.1200	0.9500	0.0010
gw	294	1	1.8950	1.1200	0.9500	1.9138	1.1200	0.9500	0.0010
gw	295	1	1.9138	1.1200	0.9500	1.9325	1.1200	0.9500	0.0010
gw	296	1	1.9325	1.1200	0.9500	1.9513	1.1200	0.9500	0.0010
gw	297	1	1.9513	1.1200	0.9500	1.9700	1.1200	0.9500	0.0010
gw	298	1	0.4700	1.1200	0.9000	0.4700	1.1200	0.9167	0.0010
gw	299	1	0.4700	1.1200	0.9167	0.4700	1.1200	0.9333	0.0010
gw	300	1	0.4700	1.1200	0.9333	0.4700	1.1200	0.9500	0.0010
gw	301	1	1.9700	1.1200	0.9000	1.9700	1.1200	0.9167	0.0010
gw	302	1	1.9700	1.1200	0.9167	1.9700	1.1200	0.9333	0.0010
gw	303	1	1.9700	1.1200	0.9333	1.9700	1.1200	0.9500	0.0010
gw	304	1	1.2017	2.2200	1.0000	1.2383	2.2200	1.0000	0.0010
gw	305	1	1.2017	2.2200	1.0000	1.1651	2.2200	1.0000	0.0010
gw	306	1	1.1651	2.2200	1.0000	1.1285	2.2200	1.0000	0.0010
gw	307	1	1.1285	2.2200	1.0000	1.0920	2.2200	1.0000	0.0010
gw	308	1	1.0920	2.2200	1.0000	1.0554	2.2200	1.0000	0.0010
gw	309	1	1.0554	2.2200	1.0000	1.0188	2.2200	1.0000	0.0010
gw	310	1	1.0188	2.2200	1.0000	0.9822	2.2200	1.0000	0.0010
gw	311	1	0.9822	2.2200	1.0000	0.9456	2.2200	1.0000	0.0010
gw	312	1	0.9456	2.2200	1.0000	0.9090	2.2200	1.0000	0.0010
gw	313	1	0.9090	2.2200	1.0000	0.8724	2.2200	1.0000	0.0010
gw	314	1	0.8724	2.2200	1.0000	0.8359	2.2200	1.0000	0.0010
gw	315	1	0.8359	2.2200	1.0000	0.7993	2.2200	1.0000	0.0010
gw	316	1	0.7993	2.2200	1.0000	0.7627	2.2200	1.0000	0.0010
gw	317	1	0.7627	2.2200	1.0000	0.7261	2.2200	1.0000	0.0010
gw	318	1	0.7261	2.2200	1.0000	0.6895	2.2200	1.0000	0.0010
gw	319	1	0.6895	2.2200	1.0000	0.6529	2.2200	1.0000	0.0010
gw	320	1	0.6529	2.2200	1.0000	0.6163	2.2200	1.0000	0.0010
gw	321	1	0.6163	2.2200	1.0000	0.5798	2.2200	1.0000	0.0010
gw	322	1	0.5798	2.2200	1.0000	0.5432	2.2200	1.0000	0.0010

gw	323	1	0.5432	2.2200	1.0000	0.5066	2.2200	1.0000	0.0010
gw	324	1	0.5066	2.2200	1.0000	0.4700	2.2200	1.0000	0.0010
gw	325	1	1.2383	2.2200	1.0000	1.2749	2.2200	1.0000	0.0010
gw	326	1	1.2749	2.2200	1.0000	1.3115	2.2200	1.0000	0.0010
gw	327	1	1.3115	2.2200	1.0000	1.3480	2.2200	1.0000	0.0010
gw	328	1	1.3480	2.2200	1.0000	1.3846	2.2200	1.0000	0.0010
gw	329	1	1.3846	2.2200	1.0000	1.4212	2.2200	1.0000	0.0010
gw	330	1	1.4212	2.2200	1.0000	1.4578	2.2200	1.0000	0.0010
gw	331	1	1.4578	2.2200	1.0000	1.4944	2.2200	1.0000	0.0010
gw	332	1	1.4944	2.2200	1.0000	1.5310	2.2200	1.0000	0.0010
gw	333	1	1.5310	2.2200	1.0000	1.5676	2.2200	1.0000	0.0010
gw	334	1	1.5676	2.2200	1.0000	1.6041	2.2200	1.0000	0.0010
gw	335	1	1.6041	2.2200	1.0000	1.6407	2.2200	1.0000	0.0010
gw	336	1	1.6407	2.2200	1.0000	1.6773	2.2200	1.0000	0.0010
gw	337	1	1.6773	2.2200	1.0000	1.7139	2.2200	1.0000	0.0010
gw	338	1	1.7139	2.2200	1.0000	1.7505	2.2200	1.0000	0.0010
gw	339	1	1.7505	2.2200	1.0000	1.7871	2.2200	1.0000	0.0010
gw	340	1	1.7871	2.2200	1.0000	1.8237	2.2200	1.0000	0.0010
gw	341	1	1.8237	2.2200	1.0000	1.8602	2.2200	1.0000	0.0010
gw	342	1	1.8602	2.2200	1.0000	1.8968	2.2200	1.0000	0.0010
gw	343	1	1.8968	2.2200	1.0000	1.9334	2.2200	1.0000	0.0010
gw	344	1	1.9334	2.2200	1.0000	1.9700	2.2200	1.0000	0.0010
ge	-1								
fr	0	101	0	0	50.00	1.00			
ld	4	302	1	1		50.		0	
ld	4	299	1	1	9999999999.			0	
ex	0	304	1	0		1.			
gn	1								
xq									
en									

BIBLIOGRAPHY

BIBLIOGRAPHY

- [1] C. R. Paul, *Introduction to Electromagnetic Compatibility*. New York: John Wiley & Sons, Inc., 1992.
- [2] International Electrotechnical Commission, Genève, Suisse, *CISPR 25: Limits and Methods of Measurement of Radio Disturbance Characteristics for the Protection of Receivers Used on Board Vehicles*, first ed., 1995.
- [3] Hewlet-Packard Company, Santa Rosa, California, *HP 8510C Network Analyzer System Operating and Programming Manual*, second ed., January 31 1994.
- [4] Gerald J. Burke, *Numerical Electromagnetics Code - NEC - 4 Method of Moments Part I: User's Manual*. Lawrence Livermore National Laboratory, January 1992.
- [5] Gerald J. Burke, *Numerical Electromagnetics Code - NEC - 4 Method of Moments Part II: Program Description - Theory*. Lawrence Livermore National Laboratory, January 1992.
- [6] D. M. Pozar, *Microwave Engineering*. Reading, Massachusetts: Addison-Wesley Publishing Company, 1990.
- [7] S. Ramo, J. R. Whinnery, and T. Van Duzer, *Fields and Waves in Communication Electronics*. New York: John Wiley & Sons, Inc., Second ed., 1984.